6-2002

Synthesis, Characterization and Applications of some Conducting Polymers

Fatma Yousif Mohamed Balhey

Synthesis, Characterization and Applications of some Conducting Polymers

A Thesis Submitted to

The Deanship of Graduate Studies of the
United Arab Emirates University

By

Fatma Yousif Mohammed Balhay

In Partial fulfilment of the degree of

MSc

In

Materials Science and Engineering

June-2002

Supervision Committee Members

Dr. Ahmed Galal Helmy
Assistant Professor of Physical Chemistry
And Materials Chemistry
Department of Chemistry,
College of Science,
United Arab Emirates University

Dr. Kamal Mohammed Sayed khalil
Assistant Professor of Physical Chemistry
And Materials Chemistry
Department of Chemistry,
College of Science,
United Arab Emirates University

Examination Committee Members

Dr. Mamdouh Ahmed Abdel Rehim
Associate Professor of Physical Chemistry
Faculty of Science
University of Cairo

Dr. Naser Naim Qamhieh
Assistant Professor of Physics
College of Science
United Arab Emirates University

TABLE OF CONTENT

Acknowledgement

First of all, thanks To Allah who gave me help, strength and patient until I finished this master degree research. The effort involved in the writing and production of this research was with the guidance of my project supervisors Dr. Ahmed Galal Helmy and Dr. Kamal Khalil. I gratefully acknowledge the advice, dedication, and professionalism exhibited by them. Many thanks go to the Deanship of graduate studies Dr. Hadif Alowais, for his support and help. Also, I would like to thanks the Deanship of the college of science for the help I had been given from all science departments. Central Laboratory Unit (CLU) thanks for the time you spent on my surface measurements. Furthermore, I thank the United Arab Emirates University, which offered me the chance to enrol in the Master Program. I would like to thank all my friends at the college for their great friendship.

Finally, I would like warmly to introduce a special thanks to every member of my family especially my father and mother for their invaluable support through out my studies.

Abstract

Conducting polymers emerged as a new class of materials by the end of the sixties. Since then many efforts have been made to put these materials to industrial use. Among the achievements are their applications in the semiconductor industry, medical field, chemical and biological sensors, etc. A different track that alleviated the prospects of the application of conducting polymers is the modification of the polymer film, namely through the inclusion of metallic moieties for specific target usage. In this thesis the candidate aimed to synthesis well established and extensively studied class of electrically conductive polymer, 3-methylthiophene. The polymer was then subjected to a modification by an inorganic component. The work was intended to examine the evolution of several properties upon the inorganic component inclusion within the polymer film matrix. Basically, one of the achieved goals is the hybridisation of the two phases in a semi-quantitative protocol. Conducting polymer films were electro-synthesized and the film thickness was varied depending on the amount of charge used. The modification of the polymer films was achieved by the application of an inorganic layer by dip-coating the film-covered substrate in an electrolyte prepared via sol- gel process.

The electrical properties of the prepared films were examined by running electrochemical impedance spectroscopy experiments. The experimental data, thus obtained were then fitted using numerical/graphical methods of some equivalent circuits. The films were tested in contact with organic and aqueous medium. The data were compared and analysed using the

suggested equivalent circuit models. The inorganic film material, the polymer films, and the "modified" organic-inorganic film hybrids were further investigated using thermo-gravimetric, Fourier Transform infrared spectroscopic, scanning electron microscopy, and x-ray diffraction analyses.

The hybrid films possessed improved electrical properties, namely increased capacitance. The film hydrophilic property affected the electronic/ionic conduction when examining the film in water vs. acetonitrile. A proposed model in which the inorganic layer provides a surplus of charge storage at the film/electrolyte boundaries to high capacitance "inner" organic layer is suggested. This model is more accepted especially in the case where the polymer film is less conductive and when the ionic diffusion is restricted. Unique hybrid film morphologies were found to depend on the thickness of the polymer film and the time needed to deposit the inorganic layer. Phase separation between the organic polymer film and the inorganic layer was realized when inorganic deposition time was minimum. Inorganic particle size ranged between 20 nm and few μm. Thermal gravimetric analysis proved that the inclusion of the inorganic layer stabilized the thermal degradation of the film. The presence of the iron-doped silica based inorganic moieties was confirmed from the EDXA and XRD measurements. On the molecular level, infrared spectroscopy data showed silicon and iron oxide vibrations and confirming the inclusion of the inorganic layer within the polymer matrix.

LIST OF TABLES

TABLE **Page**

LIST OF FIGURES

List of abbreviations and symbols

-	AcN	Acetonitrile
-	C_f	Capacitance
-	CPE	Constant phase element
-	CV	Cyclic voltammetric
-	C_{dl}	Double layer capacitance
-	CME	Chemically modified electrode
-	DTA	Differential Thermal Analysis
-	DSC	Differential Scanning Calorimetric
-	E_{appl}	Applied potential
-	ECD	Electrochemical devices
-	EDS	Electron Diffraction Spectroscopy
-	EDXA	Energy Dispersive X-Ray Analysis
-	EIS	Electrochemical Impedence Spectroscopy
-	FTIR	Fourier- transform infra-red spectroscopy
-	f	Frequency
-	μ	Charge mobility
-	NMR	Nuclear magnetic resonance
-	n	Number of charge carrier
-	PMT	Poly (3-methylthiophene)
-	PEDOT	Poly(3,4-ethylenedioxythiophene)
-	Q_c	Electro polymerization charge
-	R_{elec}	Electrolytic resistance
-	R_{pol}	Polymer resistance
-	R_s	Total resistance

-	SEM	Scanning Electron Microscopy
-	SRFTIR	Surface reflectance Fourier-transfom infra red Spectroscopy
-	TBAHFP	Tetra-butyle ammonium hexa-fluorophosphates
-	TEOS	Tetra ethyl ortho silicate
-	TGA	Thermal Gravimetric Analysis
-	T_g	Glass transition temperature
-	UV	Ultra-Violet
-	XPS	X-Ray photo electron spectroscopy
-	XRD	X-Ray diffraction

INTRODUCTION

1.1 General Introduction

Interest in π-conjugated polymers has continued during the last decades [1-7]. The extensive delocalization of π-electrons is well known to be responsible for the range of remarkable characteristics that these polymers tend to exhibit. These properties include non-linear optical behaviour, electronic conductivity, and exceptional mechanical properties [8,9,10] such as tensile strength and resistance to severe environments. Polymers composed of aromatic and heteroaromatic ring structures have been particularly outstanding from a materials perspective [4]. Applications in advanced aerospace technology have provided a powerful impetus for the development of specialized polyheteroaromatics. For instance, the United States Air Force Wright Laboratory has for nearly thirty years been engaged in an intense effort to develop polymers and molecular composites suitable for aircraft structure [1]. Much of their early work was based on fused heteroaromatic polymers, known as "ladder polymers." Later investigations were directed to rigid rod polymers based on the polybenzobisazole family [11-15], for example the poly-[benzobisazole-phenylene] structures shown in Figure 1.

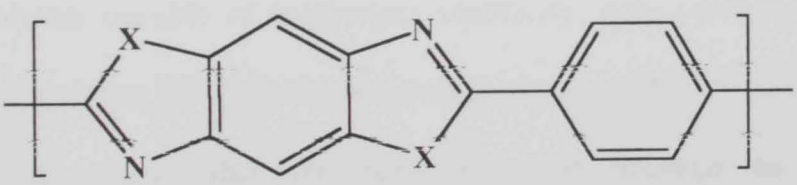

Figure 1. Poly-[benzobisazole-phenylene]
(X = NH, O, S.)

The most important aspect of conjugated polymers from an electrochemical perspective is their ability to act as electronic conductors. Not surprisingly π-electron polymers have been the focus of extensive research [16], ranging from applications of "conventional" polymers (*e.g.*, poly (thiophene), poly (aniline), poly (pyrrole)) in charge storage devices such as batteries and super-capacitors, to new polymers with specialized conductivity properties such as low band-gap and intrinsically conducting polymers. Moreover, many successful commercial applications of these polymers have been available for more than fifteen years, including electrolytic capacitors, "coin" batteries, magnetic storage media, electrostatic loudspeakers, and anti-static bags. It has been estimated [6] that the annual global sales of conducting polymers in the year 2000 will surpass one billion US dollars. Therefore, these materials have considerable commercial potential both from the continued development of well-established technologies to the introduction of other generations that includes, but not limited to, conducting organic polymer/inorganic hybrids presented in this thesis.

1.2 Theory of Electronic Conduction

The first polymer capable of conducting electricity, poly (acetylene), was first reported by Shirakawa [17], who reported its preparation accidentally. Heeger and Chiang [18] discovered that the polymer would undergo an increase in conductivity by twelve orders of magnitude upon oxidative doping. This important discovery attracted the attention of polymer and electrochemical scientists and engineers. Since then, extensive and intensive work started in

different disciplines and the strive was, and continues to be, a material that pocesses the processibility, environmental stability, and weight advantages of a fully organic polymer with the useful electrical properties of a metal.

The essential structural characteristic of all conjugated polymers is their quasi-infinite π-system extending over a large number of recurring monomer units. This feature results in materials with directional conductivity, strongest along the axis of the chain [19]. The simplest possible form is of course the archetype poly (acetylene) -(-CH-)$_x$- shown in Figure 2. Poly (acetylene) is unstable to be of any practical value, however, its structure is the foundation for all conjugated polymers. Owing to its structural and electronic simplicity, poly (acetylene) is well suited to *ab initio* and semi-empirical calculations and has therefore played a critical role in the elucidation of the theoretical aspects of conducting polymers.

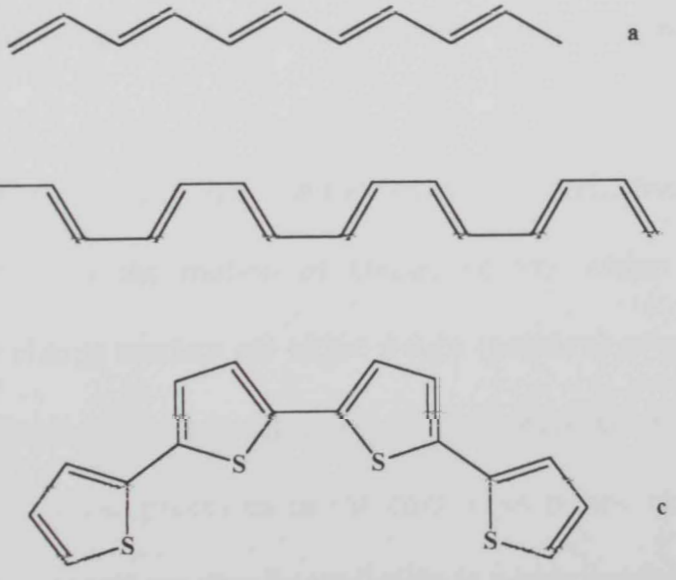

Figure 2. Conjugated Polymer Structure: (a) trans- and (b) cis-polyacetylene, and (c) polythiophene

Electronically conducting polymers are extensively conjugated molecules, and it is believed that they possess a spatially delocalized band-like electronic structure [7, 20]. These bands originated from the splitting of interacting molecular orbitals of the constituent monomer units in a manner evocative of the band structure of solid-state semiconductors (cf. Figure 3).

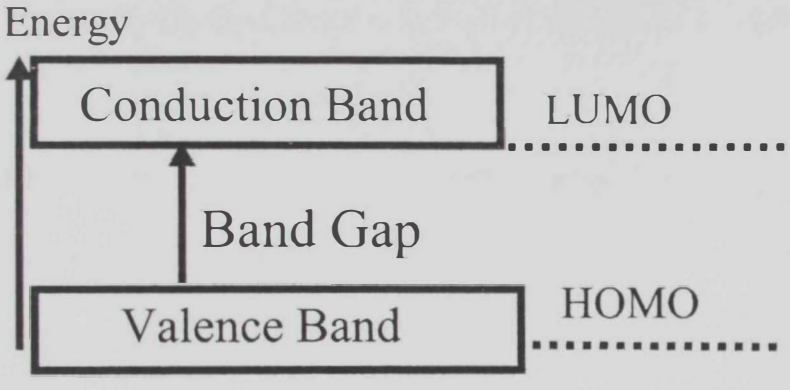

Figure 3. Band structure in electronically conducting polymer

It is well established [16, 21] that, the mechanism of conduction in this class of polymers is based on the motion of charge defects within the conjugated framework. The charge carriers are either p-type (positive) or n-type (negative), and resulted of oxidizing or reducing the polymer, respectively. The following overview describes these processes in the context of p-type carriers bearing in mind that similar concepts are equally applicable to n-type carriers.

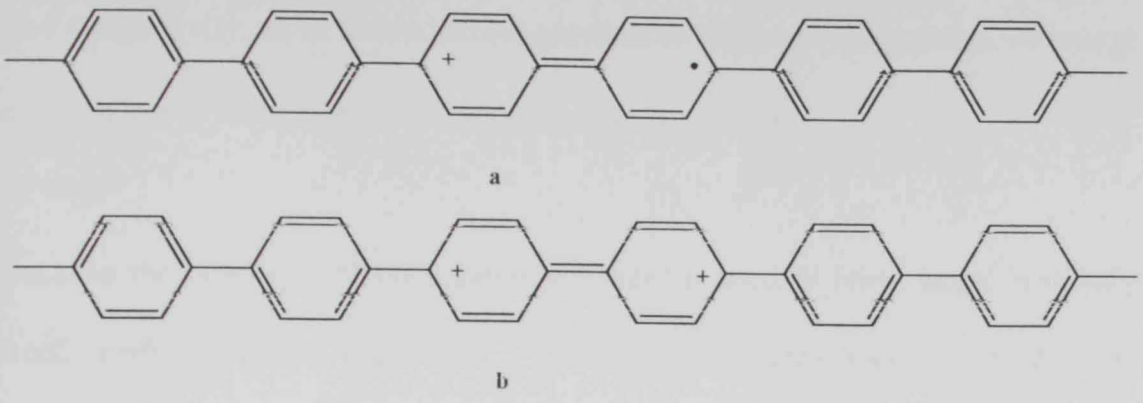

Figure 4. Positively Charged Defects on Poly (p-phenylene). a: polaron, b: bipolaron

Oxidation of the polymer initially generates radical cation that pocesses both spin and charge. According to solid-state physics terminology, this species is referred to as polaron and comprises both the hole-site and the structural distortion that accompanies it. This illustration is depicted in Figure 4a. The cation and radical are a bound species. Further increase in the distance between the cation and radical would necessitate the creation of additional higher energy species that has a quinoid configuration. Theoretical analyses [22, 23] have demonstrated that two nearby polarons combine to form the lower energy bipolaron shown in Figure 4b. One bipolaron is more stable than two polarons despite the coulombic repulsion of the two ions. Since the defect is simply a boundary between two moieties of equal energy, the infinite conjugation chain on either side, it can migrate in either direction without affecting the energy of the backbone, provided that there is no significant energy barrier to the process. It is this charge carrier mobility that leads to the high conductivity of these polymers.

The conductivity, σ, of a conducting polymer is related to the number of charge carriers, n, and their mobility, μ, according to the relation:

$$\sigma \propto n\mu \qquad (1)$$

Because the band gap of conjugated polymers is usually fairly large, n is very small under ambient conditions. Consequently, conjugated polymers are insulators in their neutral state and no intrinsically conducting organic polymer would be identified. A polymer can be made conductive by oxidation (p-doping) and/or, less frequently, reduction (n-doping) of the polymer either by chemical or electrochemical means, generating the mobile charge carriers described earlier.

1.3 Chemically Modified Surfaces and Catalysis

The interest in these polymers has been prompted by their applicability in the area of chemically modified electrodes [24-26]. One goal of coating electrodes with electroactive polymers is the development of new materials with enhanced catalytic properties. Most of the work published to date has been devoted to systems where the polymer itself is inert and serves only as a support for the electrocatalytic metal sites [27]. The electrocatalyst site acted as mediator that facilitated the transfer of electrons across the polymer/substrate interface. Electrocatalysis in general is of great economic importance and the aim of these modified electrodes is to drive electrochemical reactions selectively and/or at modest potentials. The electrocatalytic reduction of O_2 is one example that has been of particular interest [28-32] for fuel cell applications. Embedding electrocatalytic transition metal species in a polymer modified electrode matrix is

a means to endow the electrode with the chemical, electrochemical, optical, and other properties of the immobilized molecule [26]. Additional advantages include: (i) control of the reaction rate by the applied potential or current, (ii) close proximity of electrocatalytic sites to the electrode, (iii) high concentration of active centers despite low amount of material required, (iv) cooperative effects due to the proximity of other catalytic sites, and (v) easy removal of the catalyst from the substrate.

The rate of electron exchange between the solid substrate, at which the polymeric film is grown, and the catalyst sites is important with respect to electrocatalysis. Thus, as the electron transfer rate increases the reaction rate increases. As indicated in the preceding sections that electronically conducting polymers exhibit rapid electron transport through its unique delocalized electronic structure, on the other hand redox polymers have a somewhat slow rate of electron transport by self-exchange through a potential gradient. Polymer films that combine the aforementioned properties would be desirable. Deronzier and Moutet [33] combined redox-active centers with conjugated polymeric systems. Similar attempts were also cited in the literature [34] with little success in noticeably improving the rate of charge transfer. The present work embodies the introduction of an inorganic moiety within the extended π-system of the conjugated organic polymer film. This system could be described as an organic-conjugated-polymer/inorganic hybrid. Recent review articles illustrated the concept of polymer hybrids through the attachment of a redox site to the organic moiety [35-

38] and the inorganic nano-size inclusion within the conducting polymer backbone [39].

Impedance spectroscopy has lately proven a valuable technique for determining important characteristics of electrochemically active polymer materials, such as polyacetylene (PA), polypyrrole (PPy), and the like [40]. Indeed, analysis of impedance data affords to obtain, in a single experiment, information on charge transfer resistances, double layer and limiting (at low frequency) capacitances, diffusion coefficients and, provided the reaction mechanism is known, exchange current densities. This technique has demonstrated its capability on many instances. It has been applied in many fields ranging from metal or semiconductor, electrode- electrolyte interface, electrode /layer/ electrolyte system, porous electrodes, solid electrolytes [41].

Conducting polymers are fascinating new materials having a lot of properties of scientific and technological interest [42]. They have been formed from acetylene, pyrrole, thiophene, and various benzene derivatives [43]. Electrically conducting polymers are attracting considerable attention at present in view of the possibility of exploiting these materials in applications [44] such as rechargeable batteries, photovoltaic devices, electrochromic light modulators, and polymer light-emitting diodes [45]. Polypyrrole, polythiophene and polyaniline were utilized for construction of different sensor devices [46]. Polyacetylene represents the first synthesized electronically conductive polymer. However, metallic conductivity in this polymer has been reported only in 1977 when it was

doped with iodine and other molecular acceptors [40]. Conducting polymers can be prepared either by chemical or electrochemical polymerisation from a monomer solution containing one of the aforementioned compounds.

Polymer modified electrodes have been the subject of considerable interest. The combination of different materials may take the form of particulates in a polymer matrix, metal/polymer/metal sandwiches, composites of one polymer within another or bilayers of two segregated polymers [47]. Sargent et al. [48] found that the electrochemical modification of conducting polymer electrodes using biochemical reagents is a simple step that can be used to generate useful analytical signals. The basis for using conducting polymers for sensing purposes lies in their ability to be reversibly oxidized and/or reduced through the application of electrical potential. Several techniques have been used to protect metals from corrosion. Among them, polymer coatings may be the most widely used method. In general, good corrosion protection requires that the coatings have good adhesion to the metal substrates. The present work embodies:

- The preparation of the polymer.
- Its modification with an in organic material (towards the formation of an organic/inorganic composite).
- The characterization of the resulting composite material using electrochemical, spectroscopic, surface and thermal techniques.
- And its possible applications as a catalytic surface.

1.4 Electrochemical synthesis of conducting polymers

Electropolymerization has proved to be of great utility in the production of conductive aromatic polymers [49]. The first conducting polymer, $(SN)_x$, was proposed in 1973 by Walatka [50]. Since then, new materials have been chemically synthesized like: [50] polyacetylene, poly-*p*-phenylene, polypyrrole, polyaniline, polythiophene, polyazulene, polypyrene, polycarbazole, polyindole, polyisothianaphthalene, etc. Electrochemically synthesized aromatic conducting polymers are mostly amorphous. The amorphous form may be caused by wide distributions of polymer length and standard potentials of the redox sites. It does not mean that there is no structure: Teragishi et al. reported that polyaniline films frequently show morphological features such as fibrils, granules and powder, depending on the thickness and the electrochemical and solution conditions [51]. Also, Arbizzani et al, reported that the polymers electrosynthesized starting from 3-methylthiophene and 3,3`-bithiophene show different optical properties owing to their different conjugation length [52]. It is well known that electrochemically synthesized conjugated polymers can be transformed into highly conductive polyions by oxidizing or reducing reactions, which by analogy with the common semiconductor terminology are sometimes referred to as p-doping or n-doping processes [53]. Since these processes can be driven electrochemically, conjugated polymers such as polythiophene, polypyrrole and their derivatives may find applications as reversible positive electrodes in rechargeable lithium batteries. The electrochemical reactions imply that the charge that is removed from the

polymer chain is balanced by a dopant counterion from the electrolytic solution. Doping can be achieved either by exposure to dopant vapour or solution, e.g. potassium naphthalide solution, or electrochemically [49].

The general reaction pathway involves successive additions of monomer radical-cations to oligomer radical-cations, deprotonation to form a neutral (n+1) oligomer and reoxidation back to a radical cation. The overall reaction involves the removal of 2.25 to 2.5 electrons per repeat unit, giving an oxidized polymer with a cationic centre for every 2-4 repeat units, and counter-ions included from the electrolyte to achieve charge neutrality. Thus, the deposited layer is conductive and polymerisation can proceed even when the anode is covered with polymer. The oxidized polymer can be reduced to the neutral state with loss of the counter-ion. On reoxidation either the same or different counter-ions can be included. Thus these polymers display both electronic and ionic conduction effects [49].

Electrochemical polymerization process is normally carried out in a single compartment electrochemical cell by adopting a standard three electrodes configuration typical electrochemical bath consists of a monomer and a supporting electrolyte dissolved in appropriate solvent. Electrochemical polymerisation process can be carried out either potentiostatically (i.e. constant voltage condition) or galvanostatically (i.e. constant current condition) by using a suitable power supply. Potentiostatic conditions are recommended to obtain thin films while galvanostatic conditions are recommended to obtain thick films [54].

When using electrochemical polymerization process, three things must be taken into account: (i) choice of monomers, (ii) choice of the solvent and supporting electolyte, and (iii) electrodes. The compounds that possess relatively lower anodic oxidation potential and are susceptible to electrophilic substitution reaction can produce conducting polymers by electrochemical technique. Since the electrochemical polymerization reaction proceeds via radical cation intermediates, nucleopilic character of the solvent and electrolyte imposes certain restrictions on their choice. Aprotic solvents (such as acetonitrile, benzonitrile, etc.) with poor nucleophilic character are preferably used for this reason. The choice of supporting electrolyte depends upon the solubility, degree of dissociation and nucleophilicity criteria. Quaternary ammonium salts of the type R_4NX (where R=Alkyl,Aryl radical and $X=Cl^-$, Br^-, I^-, ClO_4^-, BF_4^-, PF_6^-, $CF_3SO_3^-$, $CH_3C_6H_4SO_3^-$) are soluble in aprotic solvent and are highly dissociated in them. Such salts are, therefore, commonly used as supporting electrolytes in electrochemical polymerisation of conducting polymers.

A standard three electrodes system comprises of a working electrode, counter electrode and reference electrode. The working electrode acts as a substrate for electro-deposition of polymers. It is necessary that the electrode should not oxidise concurrently with the aromatic monomer. For this reason, inert electrodes such as Pt, Au, SnO_2 substrates, ITO and stainless substrates are used. A counter electrode that is a metallic foil of Pt, Au and Ni, is used sometimes. A reference electrode like saturated calomel electrode (SCE), Ag/AgCl electrode etc,

can be used. The electrochemical polymerization technique has several features that can be mentioned as follows: (i) simple and a single-stage process, (ii) the resulting polymer is self-doped and the basic structure is not isolated, (iii) relatively low cost.

It was reported by Bull et al. [55] that polypyrrole could be conveniently synthesized using platinum and tantalum as electrodes. The results indicate that poly (pyrrole) films are porous to solvent and electrolyte ions, and this porosity is responsible for the apparent reversible electrochemical behavior previously observed with many redox couples at poly (pyrrole) on Pt. These electrochemically conducting films do exhibit electron transfer reactions with solution species, although less reversibly than that at naked or film-covered Pt. The films are unstable to oxidative conditions such as potentials >0.6 vs. SCE or the presence of halogens.

1.5 Properties of conducting polymers

The results described by Brillas et al. [42], Cordruwisch et al. [46], Bull et al. [55], Athawale et al. [56], Chidsey et al. [57], and Kelaidopoulou et al. [58] proved that the electrical properties and the morphology of the prepared conducting polymer film are affected by the nature of electrolyte employed, the type of the solvent used, the concentration of monomer, the amount of current or potential applied to the cell, and the temperature maintained during the course of the electro-synthesis.

Poly (*N*-vinylcarbazole), (PVCz), that displays interesting electrical properties has already been intensively studied mainly due to its wide field of applications. The switching mechanism of polymer films from a non-conducting to a conducting state is of primary important in all cases, so that the film oxidation process is a fundamental question. Indeed, the oxidation of the polymer produces cationic radicals in the film that generates an electronic conductivity inside the polymer matrix. The displacement of ions across the polymer/solution interface ensures global electro-neutrality. Anions have to migrate within the polymer film due to the change in the redox state of the PVCz film. So it is well known that the anions play a main role in the formation of a conducting polymer since they contribute to the electro-activity level [59]. The results of Lee et al [60] indicate that *p*-terphenyl is polymerized more efficiently than biphenyl and the poly (phenylene) (PPP) film prepared from *p*-terphenyl shows more reversible doping and dedoping properties than that from biphenyl.

Among the conducting class of polymers, polyaniline (Pan) is unique because of its high electrical conductivity and good environmental stability and also that it can be synthesized with relative ease. As a result poly (aniline) has been studied extensively. However, it was found to exhibit limited solubility in common organic solvents. This problem has been overcome to some extent by using substituted derivatives of aniline such as anisidine, toluidine, *N*-methyl or *N*-ethyl aniline, etc. The polymers of the substituted derivatives of aniline exhibit greater solubility but the conductivity is found to be slightly lower than that of

pure polyaniline. Hence, the conductivity in these polymers can be varied either by changing the oxidation state by applying potential or by doping it with different acids [56a]. Athawale et al. [56b] found that the substituted derivatives of poly (aniline) have certain advantages i.e. they are easily processible and bear good mechanical strength compared to pure poly (aniline). Among the substituted derivatives two types are observed; one is ring substituted and the other are *N*-alkyl and aryl substituted derivatives. The *N*-substituted derivatives exhibit an additional property of having conductivity comparable to that observed for poly (aniline). These *N*-aryl substituted polymers represent a new class of conducting polymers intermediate between poly (aniline) and poly (phenylene). Usually, they are synthesized in aqueous media using protonic acids such as $HClO_4$, H_2SO_4, HCl etc. However, such a media poses a serious problem of over oxidation of the polymer or its decomposition. These limitations can be overcome to a certain extent by synthesizing the polymer in a nonaqueous media, also, the processibility of the polymer is enhanced. Fiordiporti and Pistoia [40] reported that charge transfer resistances are rather low at intermediate PAn oxidation levels in agreement with the metallic behavior reported at these potentials when an impedance study has been carried out in aqueous acidic and in neutral organic solutions on PAn films prepared with the cyclic voltammetry technique. For the capacitance associated with the polymer, large values have been found which vary as a function of the film potential and the electrolyte used. Polymer degradation

does not occur at high potentials in organic solutions, this testifying that such a reaction is caused by aqueous electrolytes.

Switching poly (pyrrole) from its reduced (insulating) state to its oxidized (electronically conducting) state simplistically involves the removal of electrons from a delocalized π-system and some research groups [61] have suggested that conductance is due to the movement of polarons and bipolarons (a polaron is a radical cation and the associated local modifications in the geometry of the poly (pyrrole) chain). The formulation of any theory for the conduction mechanism requires information about the number of electrons required for the switching process (along with other physical-chemical properties).

Amongst the conjugated polymers, the poly (thiophene), (PTh), and their derivatives are well-known candidates for their good electronic conductivity and stability. In order to obtain suitable physicochemical properties of PTh, different chemical and electrochemical methods are employed [49]. Most of the conducting polymers produced so far by electrochemical technique exhibit poor mechanical strength that unfortunately forbids their usage in commercial products. It has been experimentally demonstrated that the co-polymerization is one of the most effective methods to impart the mechanical strength to the known brittle polymers.

1.6 Chemically modified electrodes

A chemically modified electrode (CME) is one whose surface is purposely altered with material that reacts selectively and reversibly with a chosen analyte. Such a material might be an adsorbed ligand with which a metal ion binds [62].

The electrochemical modification of conducting polymer electrodes using biochemical reagents is a simple step that can be used to generate useful analytical signals. The basis for using conducting polymers for sensing purposes lies in their ability to be reversibly oxidized and/or reduced through the application of electrical potential. Conducting electro-active polymers (CEPs) that contain bioactive molecules, e.g. enzymes, antibodies, cells, and DNA have been used extensively in biosensor applications [48]. In another study [58], it was found that platinum particles dispersed in a poly (2-hydroxy-3-aminophenazine) film (pHAPh/Pt) provide a better catalyst than smooth Pt for the electro-oxidation of methanol and formic acid in perchloric acid aqueous solutions. The catalytic activity of the Pt particles is further enhanced when Sn is co-deposited in the polymer film. Polymer coatings on electrode surface have been employed: (1) to incorporate electro-catalysts, (2) to stabilize the substrate from attack, (3) and as analytical probes and reference electrodes [55].

The corrosion of metals is an enormous problem throughout the world. Several techniques have been used to protect metals from corrosion. Among them, polymer coatings may be the most widely used method. In general, good corrosion protection requires that the coatings have good adhesion to the metal substrates [63].

In the early period of the research on CPEs, it has been realized that the electrochemical behavior of redox, ion exchange and conducting polymers may considerably depend on the physiochemical properties of the polymer phase.

Many experimental observations on polymer modified electrodes, such as the variation of the rate of charge transport, cyclic voltammetric peak-shape effects, the non-Nernstian thermodynamics, ion-exchange properties have been explained in terms of polymer-polyelectrolyte models [64].

Catalysis of electrochemical reactions is one of the major motivations for the rapidly increasing interest in modified electrodes. Comparing monolayer derivatized electrodes covered by a redox polymer film equivalent to several monolayers of active catalyst, it was anticipated that the second could be more effective than the first for the same attached catalytic system. This should be valid for redox as well as for chemical catalysis, one result of this being the possibility of redox catalysis at redox polymer film electrode, while this type of process is likely to be of low efficiency, if any, at mono-layer derivatized electrodes. This prediction was based on a model of electro-catalytic reactions at redox polymer electrodes in which the rate-limiting process was assumed to be the electro-catalytic reaction itself, rather than either the diffusion of the substrate in the film from the solution toward the electrode or the propagation of electrons through the film from the electrode toward the solution [65].

1.7 Characterization of the conducting polymer film

There are a number of very different features about polymers that make their characterization different from that of small molecules. When a newly synthesized polymer requires characterization or laboratory wants to characterize a competitive polymeric product, there are a number of steps that should be

followed. First, the viscosity, the molecular weight, and perhaps the molecular weight distribution should be obtained on a newly synthesized material to determine if in fact the material is polymeric. Then an infra-red (IR) spectrum and possibly a nuclear magnetic resonance (NMR) spectrum are obtained in order to identify functional groups or make a complete identification in the case of a known polymer. Thermal analytical data can also aid in the identification and characterization of the material. DTA or DSC can be used to obtain a melting point, a glass transition temperature (T_g), and a measure of the thermal stability of the polymer. Thermogravimetric analysis (TGA) can also yield information on the thermal stability of the polymer as well as determine the presence of volatile components such as solvents, residual monomers, or oligomers. X-ray diffraction (XRD) can be used to help identify the chemical structure of the polymer as well as provide information on the preferred conformation of the polymer chains in the crystalline regions [66].

There are many physical properties and tests that can be conducted on polymers. The tests are usually designed to obtain fundamental property information or information about the final end-use performance or behavior of the product. Important special properties of coatings are their ability to adhere to a surface and their surface smoothness. Microscopy and surface energy techniques are helpful in characterizing these properties [66].

When used to study electrochemical systems, electrochemical impedance spectroscopy (EIS) can give accurate, error-free kinetic, and mechanistic

information using a variety of Techniques and output formats. For this reason, EIS is becoming a powerful tool in the study of corrosion, semiconductors, batteries, electroplating, and electro-organic synthesis. Tanguy et al. [67] reported that impedance spectroscopy was used to study the redox mechanism of poly (3-methylthiophene). It has been demonstrated that, like other conducting polymers, the redox process involves two types of doping. A fast doping occurs at the surface of aggregates of compact chains and it does not require the penetration of counter-ions between the chains. The second type of doping is a bulk phenomenon being equally important as the first but its kinetic is limited by the diffusion of counter-ions between the chains and, as a result, it appears slower than the capacitive phenomenon. Sargent et al. [48] used the same technique as well to study the mechanisms of antibody-antigen (Ab-Ag) interactions at conducting poly (pyrrole) electrodes. The effect of the variation in ion exchange, solution composition, and the condition of the synthesis have been used to study the capacitive behavior of antibody-containing poly (pyrrole) electrodes in the presence of the antigen. The theory of charge generation and transportation in the heterogenous polymeric domains is proposed as the predominant basis for the analytical signals observed at these electrodes. The significant difference in the impedance response at different potentials confirmed that the Ab-Ag interaction was largely influenced by the applied potential.

In cyclic voltammetry the applied potential is varied with time in a symmetrical saw-tooth wave form, while the resulting current is detected and recorded over the

entire cycle of forward and reverse sweeps [62]. Panero et al. [53] determined the kinetic parameters of the process of oxidation (p-doping) of polypyrrole in electrochemical cells containing a solution of lithium perchlorate in propylene carbonate using cyclic voltammetry, frequency response analysis, and galvanostatic pulse transients. The results are interpreted on the basis of models developed for intercalation electrodes, and the validity of the three techniques is discussed in relation to the geometry and morphology of the polymer electrode [53]. Nunziante and Pistoia [68] used repeated cyclic voltammetry scans between –0.2 and + 0.8 V vs SCE to study poly (aniline) films in acidic solutions on Pt substrates. The polymer yield (film thickness) depends on several factors, such as: aniline (An) and acid concentration, nature of the acid and scan rate.

1.8 Applications of conducting polymers

The investigations on electro-polymerized conducting polymers during the last years have shown the possibilities for various applications of these new materials [46] including applications as photo-refractive materials, as chemosensory materials, and in electro-luminenscent devices. In all of these applications, the nature of the electronic interaction between the metal and the conjugated backbone is of central importance that is influenced by the bonding between the metal and the backbone [69].

1.8.1 Electrochromic display

Owing to their environmental stability, low cost and easieness of preparation, conducting polymers have played the major role in electronics and

opto-electronics. Among the opto-electronic applications, is the fabrication of large area electrochromic devices (ECD's). ECD's are used in commercial sign boards, arrival/departure time tables in airports and railway stations, calculators, computers, clocks, electrochromic windows to control solar energy and any other piece of equipment that utilizes the liquid crystal display (LCD) [54].

1.8.2 The solid-state electrochromic cell

A solid-state electro-chromic cell similar to that used for characterizing conducting polymers is applicable for commercial purposes. The large area of laminated solid state electro-chromic devices were fabricated from poly (aniline) and solid polymer electrolytes, prepared by mixing protonic acids or alkali metal salts with either PEO or PEI and PAN based membrane [54].

Pinto et al. [47] reported that the performance of pyrrole and thiophene polymer electrodes in lithium cells has been examined in lithium perchlorate-propylene carbonate electrolyte by cyclic voltammetry. However, polypyrrole has worse mechanical properties (toughness, adherence) than other polymers such as PTh that, on the other hand, may be a prospective candidate as a positive electrode in lithium batteries. The lower price of the monomer as well as the higher redox potential, are advantages in comparison with PPy. Arbizzani et al. [52] found that the differences in the optical properties of 3-methylthiophene-based polymers make it possible to design a variable light transmission electro-chromic device with two regio-chemically and conformationally different polymers, poly(3-

methylthiophene) and poly(3,3`-dimethyl-2,2`-bithiophene), operating in complementary mode in the visible region.

A new concept of hybrid super-capacitors based on both conducting polymers and activated carbons has been developed and tested with a polythiophene derivative and several activated carbons by Laforgue et al. [70]. The results obtained with 4 cm^2 laboratory test cells have been confirmed at larger scale (industrial prototypes) in terms of energy. However, the lack of pressure in the modules limited the power of the devices.

1.8.3 Electrochemical applications of silica-based organic-inorganic hybrid materials

Organic-inorganic hybrid materials represent an important class of synthetic engineering materials that showed promising properties. A comprehensive overview was presented on the implication of silica-based organic-inorganic hybrid materials in electrochemical science [71]. Components of these materials possess unique properties and display new properties as a result of the nature and degree of interfacial interaction between them. It involves composite materials of both class I (weak bonds between the organic and inorganic components) and class II (strong chemical bonds). Starting with a description of the common designs of electrodes modified with these hybrids, the review then reports their applications in the various fields of electrochemistry, illustrating the diversity of the organically modified silicates used for this purpose. The mild chemical conditions allowed by the sol-gel process provide very versatile access to

these electrochemical devices. They have found many applications in electroanalysis, including preconcentration associated with voltammetric detection, permselective coatings, electrochemical sensors, electrocatalysis, and detectors for chromatography. They were also applied as redox and conducting polymers, as solid polymer electrolytes for batteries, for the design of spectroelectrochemical and electro-chemiluminescence devices, and in the field of electrochemical biosensors.

The sol-gel process, which is mainly based on inorganic polymerization reactions, is a chemical synthesis method initially used for the preparation of inorganic materials such as glass and ceramics. Mild synthetic conditions allow effective mixing of the organic and inorganic phases that lead to new morphological and unique properties. There are different methods that can be used for the synthesis of hybrid materials via the sol-gel process. These methods are based on their macromolecular structures and phase correlation [72]:

1- Hybrid networks synthesized by using low molecular weight organoalkoxysilanes as one or more of the precursors to introduce the Si-C bond.

2- Co-condensation of functionalized organic species with metal alkoxides and establishing covalent bonding.

3- Infiltration of performed oxide gels with polymerizable organic monomers/polymer or vise versa, entrap organic molecules as guest within inorganic gel matrix as host.

4- In situ formation of the inorganic species within a polymer matrix, especially for inorganic particles,

5- Interpenetrating networks and simultaneous formation of organic and inorganic phases.

6- Direct deposition of the sol-gel (inorganic-containing component) onto a polymeric matrix (such as conducting polymer in this work).

The properties of the resulting product depend on the properties of the individual components as well as the factors such as phase's size, shape and interfacial properties. For instance, inorganic materials such as glass and ceramics are hard but not impact resistant, whereas organic polymers are flexible, and, conductive in this present work. In this respect, two major classes of these materials could be indentified [73]: (i) Class I; in which organic and inorganic components are linked through covalent bond, and (ii) Calss II; in this case the material does not contain covalent bond between organic and inorganic components.

Recent work showed interest in exploiting the properties of hybrid poly (aniline)-silica materials [74,75]. In this study, the authors explored the idea of using the heterogeneous porosity of inorganic (sol-gel silica) and organic (poly (vinylidene fluoride)) films as a template for the preparation of polyaniline composites. The large size pore distribution (similar to ca. 2.5-800 nm) in both template matrices results in a part of the polyaniline growing more ordered than in films synthesized without spatial restriction. Small-angle X-ray scattering and

scanning electron microscopy experiments were done to determine the extreme values of the pore diameters. Using other experimental techniques, including cyclic voltammetry, UV-Vis-NIR spectroscopy, electrochemical impedance and chronopotentiometry, the authors concluded that the electrochemical properties of poly (aniline), such as oxidation and reduction charges, diffusion coefficient and charge-discharge capacity, are improved in these composites. Similar synthesis work included poly(pyrrole) composites as well [76]. The electrochemical behavior of the exchange process for dopant anions in this polypyrrole (PPy)-silica glass composite film in acetonitrile solution was analyzed by cyclic voltammetry. Several conducting polymers such as poly (3,4-ethylenedioxythiophene) (PEDOT) have been also used to prepare novel conducting composite material [77, 78]. The conducting composite material has been prepared by using conducting PEDOT and silica network produced by sol-gel process. The doped PEDOT exhibited excellent conductivity and transparency due to the low band-gap in nature, and silica network provided good mechanical properties and adhesion to the surface of silica glass. In order to utilize the advantages of these materials as well as to serve convenient process, the conducting composite of PEDOT and silica were produced by the in-situ sol-gel process of tetraethylorthosilicate. Physical properties were monitored with varying reaction conditions and the excellent conductive coating materials exhibiting: 100 S/cm conductivity, 80% transparency, and 9 H pencil hardness were prepared.

The advance of materials chemistry has influenced the design of analytical sensors, especially those using spectroscopic or electrochemical methods for generating the signal. New methods of immobilizing enzymes, chromophores, and electron-transfer catalysts have resulted from initiatives in materials science. Systems based on sol-gel chemistry are especially noteworthy in this regard, but other important materials for chemical and biochemical sensors include zeolites, organic polymers, and various conducting composites. Applications cited include determinations of inorganic ions, gases, neurotransmitters, alcohols, carbohydrates, amino acids, proteins, and DNA [79].

An overview is presented dealing with the use of pure, chemically modified and sol-gel-derived silicates for designing electrode materials that are then exploited in various electroanalytical applications [80]. The exploration of the potential consequences of such inorganic solids when used in electrochemical environments has intensified since 1995. This review focuses on recent advances achieved with silica-modified electrodes (SiO_2-MEs) in the fields of electroanalysis. After a description of the attractive properties of silica-based materials for the electrochemical community, an outline of the preparation methods for SiO_2-MEs is given, and their relevance to various areas of electroanalysis is discussed.

AIM OF THESIS

Conducting polymers is still gaining an extended popularity in terms of research and exploitation of new venues for the application of such materials. On the other hand, nano-materials are counted as one of the new eras of advancement in science and technology. Hybrid materials made of the combination of the above two materials constitute a cornerstone for new applications. However, several hybrid materials based on conducting polymers did not receive extensive attention in terms of determining their electrical and physicochemical properties. In this thesis, the candidate will attempt to achieve the following goals:

- To synthesis of a known class of conducting polymers, poly(3-methylthiophene), using electrochemical methods.
- To change of synthesis conditions namely, the thickness of the film will also be intended.
- To use the sol gel technique to prepare an inorganic module film and to characterize its morphological, thermal and compositional aspects.
- To prepare a hybrid organic-polymer/inorganic materials and to characterize their properties using different techniques.
- To apply the electrochemical impedance spectroscopy technique to determine the electronic properties of the films before and after modification.
- To use surface techniques such as scanning electron microscopy coupled with elemental analysis means, such as energy dispersive x-ray analysis to

interaction and chemical composition of the resulting film with the nano-inorganic particles.

- To determine, on the molecular level, the structure of the polymer film, especially after inorganic particles inclusion.
- To measure the effect of metal inclusion (basically silicon and iron) on the thermal stabilization imparted to the organic polymer layer.
- To use x-ray diffraction analysis to determine the structural aspects of the metal oxides within the film.

EXPERIMENTAL SECTION

Experimental

2.1 Materials and Reagents

2.1.1 Metal Substrates

Two types of metal substrates were used for polymer film deposition: Platinum (99.998%, puratronic) and graphite rods (spectroscopic grade, 99.9995%), both from Alfa Aesar (MA, USA). Platinum has the dimension of 3.0 cm long and 1.2 mm diameter and was used for the growth of polymer films prepared for surface measurements. The second type of platinum was imbedded within Teflon housing and had an apparent surface area of 0.3 cm^2, this type of substrates was used for polymer films characterized by electrochemical impedance spectroscopy. Graphite rods were 6.15 mm in diameter and a length of 3 mm was used to deposit the polymer film.

2.1.2 Reagents and Solutions Preparation

3-Methylthiophene (MT), tetra-butyl ammonium tetra-fluoroborate (TBATFB), acetonitrile (AcN), sodium chloride, tetra-ethyl orthosilicate (TEOS), formamide, nitric acid, ethanol, and ferric nitrate used for polymer film growth, sol-gel preparation and polymer characterization in this study were high purity grade reagents. All chemicals purchased were used as received and were supplied by Aldrich Chem. Co. (Milwaukee, WI. USA).

Test solutions were prepared by dissolving a pre-weighed sample or from stock and diluted using dry acetonitrile or de-ionized water supply. Water was

first distilled then de-ionized using "*Nano-Pure*" Millipore water purification system. The conductivity of water used in this study is 18.3 μS.

Solvents used in the electropolymerization were distilled, purified according to standard methods [81], and kept over molecular sieves type A4 for at least 48 hours prior to use.

2.1.3 Electrode Mounting and Electrochemical Cells

Electrochemical polymerizations were carried out with three-electrode system cell where the working electrode was a platinum disc (wire or sheet, whenever stated) or graphite rod. All the potentials in the polymerization, the voltammetric studies, and the electrochemical impedance spectroscopic (EIS) measurements were referenced to an Ag/AgCl electrode (saturated). The auxiliary electrode was a 2 x 2 cm^2 platinum sheet or 10 cm (length) x 1.5 mm (diameter) platinum wire purchased from Alfa Aesar. All electrodes were polished prior to the electropolymerization step according to the following steps: the electrode was mechanically polished using metallurgical papers of different grades 600-1200μm. Following this, the surface was treated by rubbing it with filter paper. Finally, the surface was polished with fine tissue using a slurry of alumina/water (10 μm) until no visible scratches were observed. Prior to immersion in the cell, the substrate was rinsed with distilled water, dried, and it was then thoroughly degreased in methanol. Finally, the solid substrate was rinsed with conductive water, solvent employed in the next experiment, dried, and immediately put in use. For the purpose of specimens preparation for the scanning electron microscope (SEM) and

surface reflectance Fourier-transform infra red spectroscopy (SRFTIRS) experiments, platinum wires or graphite rods were employed. Care was taken into account to avoid touching the substrate surface by hands.

All electrochemical measurements were performed in a conventional 100-mL flat bottom (Pyrex) glass cell. It was fitted with top cover Teflon lid with five inlet joints as shown in Figure 5. The central opening was used to introduce the solid substrate onto which the polymer is deposited (joint inlet A). The second inlet (B) was used to introduce the reference electrode bridge tube. The tube tip was fitted with a vicor tip and a shrinkable Teflon tube to minimize diffusion. The tip of the reference electrode bridge was always adjusted as near as possible to the surface of the working electrode (solid substrate on which polymer was deposited) by manipulating the joint position. The remaining inlet (C) in the lid was used to introduce the platinum counter electrode.

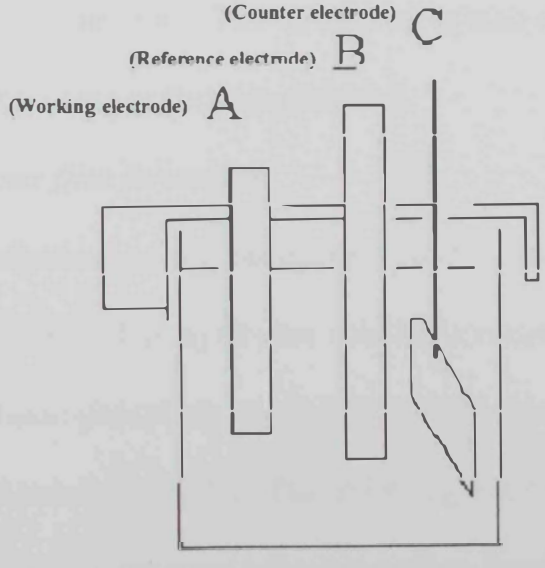

Figure 5. Electrochemical cell used for the synthesis of the polymer film

2.2 Equipment, Instrumentation, and Experimental set-up

2.2.1 Electrochemical Equipments

An EG & G potentiostat/galvanostat model 371A (Princeton Applied Research, USA) controlled by an IBM computer and *SoftCorr* software was used for the polymer film formation. The polymer film formed was examined using a Gamry CMS system equipped with a PC and a Gamry control/analysis-software (Gamry, Inc., USA).

Polymer film formation was accomplished using a repeated cycles voltammetric program. The instrument was programmed to allow the application of an initial potential (E_1) at which the solid substrate surface was maintained within a delay time (t_1). The potential was then swept to the second potential value (E_2), and finally to the final potential (E_3). The scan rate for the potential sweeps was 100 mV/s and the number of repeated cycles was as indicated in the results and discussion section. The number of cycles used to graft the polymer film affected the thickness of the film obtained.

2.2.2 Polymer film formation

The electrosynthesis of the conducting polymer film was achieved using the EG & G potentiostat. The synthesis solution consisted of 0.1 M tetrabutyl ammonium hexafluorophosphate (TBAHFP), 0.05 M methyl thiophene (MT) dissolved in dry acetonitrile (AcN). The following potential program was used for the polymer grafting over the solid substrate surface (working electrode):

Table 1. Electrochemical parameters for polymer film formation

E_1 = -0.5 V,	t_1 = 60 s,	scan rate (1) = 100 mV/s
E_2 = 1.75 V,	t_2 = pass,	scan rate (2) = 100 mV/s
E_3 = -0.5 V,	t_3 = pass,	scan rate (3) = 100 mV/s

The applied potential was modulated as a triangular wave.

2.2.3 Sol-gel preparation of the Fe_2O_3/SiO_2 coating film

Polymer films modification was achieved using Fe_2O_3/SiO_2 and was carried out by dip coating of the substrate with Silica sol-gel containing 10 atom % Fe. Preparation of the 10% Fe_2O_3/SiO_2 sol was carried out from tetraethyl orthosilicate (TEOS), formamide (CH_3CONH_2), ethanol (C_2H_5OH), 0.1 N nitric acide (HNO_3) aqueous solution. The Mixing molar ration of TEOS : CH_3CONH_2 : C_2H_5OH : $HNO_3(aq)$ was 1 : 1 : 4 : 4.5. A calculated amount of Iron(III)nitrate, $Fe(NO_3)_3.6H_2O$, was add to the above solution. The mixture was stirred for 2 h at room temperature and used for the dip coating process.

2.2.3.1 Preparation of a module film from the coating material

Since the physical surface areas of the test electrodes are very small, it is rather impractical to carry out any bulk characterization for the coating material in such way. Therefore, a module film was prepared by dip coating of a glass-slide substrate with the prepared sol mixture. The module film was dried at 60°C for 24 hours, and then was used for SEM microscopy. TGA sample from the module film "coating-layer" was obtained by scratching the dry film with a hard metallic tool.

A Calcined module film was obtained by calcinations of another module film at 350°C for 60 min, and used for SEM microscopic investigations.

2.2.3.2 Preparation of a bulk sample from the coating material

Bulk sample of the 10% Fe_2O_3/SiO_2 material was obtained by allowing a small portion (few ml) of the prepared coating sol – placed in a glass watch - to dry at room at 60°C for 24 h period. The dry bulk thus obtained was used for further FTIR and TGA characterization work.

2.2.4 Inorganic hybrid component application to the polymer film

The grafting of the polymer film over the substrate was then followed by the application of the inorganic component to the polymer. A typical reaction mixture for this preparation consisted of: 44.6 mL TEOS, 7.96 mL formamide, 11.21 mL ethanol, 3.6 mL of 0.1 M nitric acid, and 4.04 g of iron (III) nitrate nona-hydrate. The aforementioned chemicals were mixed in 150 mL beaker and were steadily stirred for two hours. A clear solution was thus obtained. The solid substrate coated with polymer was then dipped in the sol-gel resulted solution. The solid substrate was then heated in a conventional oven for 30 minutes at 60 °C. The coated-polymer with a dried sol-gel layer was then inserted into a firing autoclave for 10-15 minutes as stated at 350 °C.

The reaction mixture described above underwent a sol- gel process with the TEOS inorganic precursor to produce the hybrid materials as it was coated at the polymer film. In general, the sol-gel procedure consists of the steps shown in Figure 6 [82].

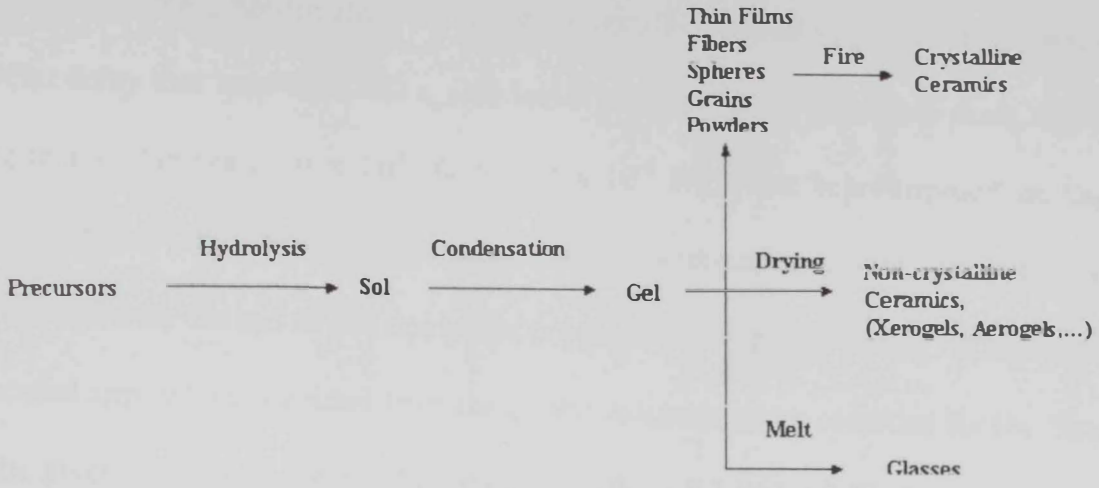

Figure 6. General steps in the sol-gel synthesis of ceramic materials

2.3 Polymer/hybrid film characterization

2.3.1 EIS measurements

The EIS measurements on polymer/hybrid films were performed at room temperature in a 0.1 M TBAHFP test solution. Some experiments were carried out in 0.1 M NaCl. A three-electrodes electrochemical cell, with a saturated Ag/AgCl reference electrode and a platinum counter electrode, was also used for all measurements. The exposed sample area was 0.282 cm^2 in case of platinum substrate-covered with polymer film and 1.0 cm^2 for the case of using graphite substrate.

The EIS measurements were carried out with the (Gamry) CMS 100 electrochemical impedance system. The measurements were performed under potentiostatic control at different applied potentials [83]. The test conditions are listed in Table 2.

After the determination of the open circuit potential (E_{open}) from the open circuit delay that lasts for 1200 s, sine wave voltages (10 mV) peak to peak, at the frequencies between 5.0×10^{3} Hz to 1.0×10^{-2} Hz, were superimposed on the applied direct (and constant) potential. All the measurements were automatically controlled with the aid of the computer program provided by Gamry. The direct potential applied was decided from the cyclic voltammogram recorded for the film in the given electrolyte, i.e. 0.1 M TBAHFP/AcN or 0.1 M $NaCl/H_2O$.

Table 2. EIS test conditions

Reference Electrode	Ag/AgCl
Counter Electrode	Platinum
Electrolyte	TBAHFP/AcN or $NaCl/H_2O$
Electrolyte Concentration	0.1 M
Tested Area	0.282 or 1.0 cm^2
Frequency Range	10^{-2} - 5000 Hz
AC Potential	10 mV
DC Potential	-0.5 - +1.2 V

2.3.2 Surface Instrumentation and Measurements

Polymer and hybrid films were characterized using scanning electron microscope (SEM) equipped with an energy dispersive x-ray analyzer (EDXA), surface reflectance Fourier-transform (infra red) spectroscopy (SRFTIRS), x-ray diffraction (XRD) and x-ray photoelectron spectroscopy (XPS).

A Jeol Model JSM-5600 SEM equipped with EDXA capability was used for surface morphological determination. The instrument is fully computerized with 18 - 300,000 times magnification power, with guaranteed resolution of 3.5

nm, acquisition of both secondary and back-scattered electron images. For some experiments, the samples were coated with a thin film of gold to eliminate the effect of charging during measurements. A Jeol JFC-1200 fine coater was used for this purpose and a current of 20 mA was applied for 150 s coating period.

SRFTIRS experiments were achieved using a Nicolet Magna-IR spectrometer, Nic-Plan IR-microscope and a Spectra Tech stage controller. All results were analyzed using an Omnic software and library.

For XRD experiments, a Philips analytical x-ray instrument equipped with a diffract meter type PW1840 was used. The instrument is equipped with a Cu anode, with a generator tension of 40 kV, a generator current of 30 mA. The receiving slit was set at 0.2. Other conditions for the experiment-setup are listed in table 3.

The three-electrode electrochemical cell used for the preparation of samples for surface analysis was identical to that used for electrochemical characterizations. Saturated Ag/AgCl reference electrode and a platinum sheet counter electrode were use. The working electrode was in the form of a graphite rod or a platinum wire with nominal surface area about 1.0 or 5.0 cm^2 according to the cell used. The electrochemical cell was a pyrex glass cylinder with a flat circular piece of glass fused on each end. Two small holes on the top of the cylinder connected with two plastic tubes were used to accommodate the gas bubbler. A platinum sheet counter electrode of large area was housed inside the chamber. A cavity was left at the top of the chamber to be filled with the testing

solution and to insert the reference electrode. The cavity is connected to the working electrode throw a Luggin capillary tube. Polymer film formation was carried out in 0.05 M MT, and 0.1 M TBAHFP in AcN. EG & G potentiostat/Galvanostat was used for polymer film formation in all cases for subsequent surface measurements.

2.3.3 X-ray diffraction

X-ray diffraction analyses were performed on polymer films grafted onto platinum substrates. The polymer films were formed by cyclic voltammetric technique for 20 cycles. Experiments were performed on polymer films immersed in the sol-gel prepared solution for 60 seconds and on as prepared films (without silica coatings). Films were then peeled out of the surface of the platinum substrate using a sharp lab knife, dried and introduced into the diffractometer. Test conditions are listed as indicated in Table 3.

Table 3. Test conditions for X-Ray Diffraction experiments

Diffractometer type	PW1840
Tube anode	Cu
Generator tension	40 KV
Generator current	30 mA
Wavelength α_1	1.54056 A°
Wavelength α_2	1.54439 A°
Intensity ratio(α_1/α_2)	0.500
Monochromator used	No
Full scale of recorder	10 Kcount/s
Time constant of recorder	0.5
Start angle	2.010° (2θ)

2.3.4 Scanning electron microscopy (SEM)

Samples investigated by SEM were prepared as previously described in the preceding section. Except that, polymer films prepared with different thickness and different dipping time in the sol-gel solution were examined. Thus, the polymer film was first prepared using different number of cycles, ca. 5 to 20 cycles, and dipping time 15 – 300 seconds in the sol-gel solution. The films were dried under vacuum then forwarded immediately to the SEM chamber over the graphite or platinum substrates. Information regarding the elemental composition of the films was obtained from the EDXA measurements performed at the different films prepared.

2.3.5 FT-IR spectroscopy

The effect of loading the polymer films with inorganic silicon-containing layer was examined using IR spectroscopic technique. Again, sample preparation was achieved as previously indicated for the x-ray diffraction samples. Some experiments were performed on the as-grown films without peeling it from the solid substrate using the SRFTIRS technique. Moreover, some experiments were also conducted using TGA coupled to FTIR measurements in order to identify the different thermal transitions of the samples under investigations.

2.4 Thermal gravimetric analysis

Thermal gravimetric analyses were performed using a 2950 TA instrument (Princeton, USA). Heating rate was typically 5-10 °C/minute and inert gas used

was either purified nitrogen or helium. The TGA instrument was interfaced with an FTIR system that allowed monitoring the gas outlet analysis.

Samples for thermal gravimetric analyses were prepared using the previously mentioned protocols and were scrubbed off the substrate surface thoroughly using a sharp laboratory knife. Samples were desiccated prior to mounting on the TG instrument pan for weighing. Typical start up masses ranged between 8.0 mg to 50.0 mg for the tested samples. Figure7, shows the deposition of the module film on glass substrate that was used for further characterization.

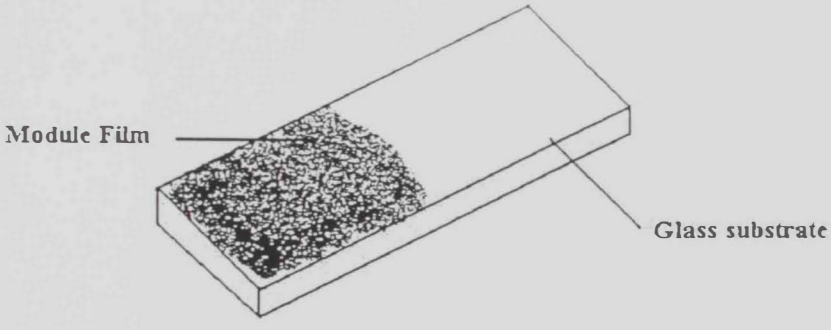

Figure 7. Module film deposition on glass substrate

RESULTS & DISCUSSION

The results and discussion section is divided into four sections. The first section deals with the preparation, and electrochemical characterization (namely, electrochemical impedance measurements, EIS) of poly(3-methylthiophene) (PMT) synthesized under different preparative conditions and tested in different environments. The second section, deals with modification and testing of the electrochemically prepared organic polymer films by the inclusion of an inorganic-containing moiety via the sol-gel technique. The third phase of the work was devoted towards the surface and spectral characterization of the polymer films. The fourth part of the work deals with thermal and x-ray diffraction analyses of the films.

3.1 Potential dependence of impedance spectrum

The potential dependence of impedance spectrum for PMT coated Pt surface is shown in figure 8a. The results are presented in the form of Nyquist diagrams, giving the imaginary part as a function of the real part of the impedance. The value of applied potentials to the polymer film, were selected within a relatively wide range, ca. between –0.5 V and +1.2 V (vs. Ag/AgCl). It is important to notice that the polymer film starts to develop electronic/ionic conductivity as the potential approaches the first oxidation peak [84], ca. around 0.6 V. The measured values of direct current (d.c.) electronic conductivity σ in PMT clearly indicated that electronic transport is fast in this system [85]. It is well established though, that the main carriers for charge transport are bipolarons in poly(thiophene) systems [86, 87]. Moreover, it has been found that the fast electronic transport for

the film is associated to the state of polymer at low spin content [88]. The value of potential at which the maximum value of σ occurs, does correspond to the maximum spin content of the polymer [89]. In this consideration, the estimation of the polymer resistance, R, is based upon the fact that the film is a semi-infinite system [90]. The EIS data of figure 8a are for a film with an estimate thickness of 100 – 150 nm if we consider that deposition takes place with 1.0 $mC.cm^{-2}$ of PMT when a total deposition charge mounts to approximately 100 $mC.cm^{-2}$. In examining the impedance spectra for this film, the electronic resistance of PMT, estimated from Ohm's law (ca. in the order of 1.0×10^{-3} Ω), will be neglected. Thus, the differences in the EIS data of PMT doped with PF^{6-} (HFP), reveals mainly the onset of the capacitive behavior that deviates by the departure from the constant phase element (CPE) with a slope approximately equal to 45°, as the frequency decreases. This observation is in good agreement with the results described previously in the literature for poly(pyrrole) in similar potential ranges [91, 92]. According to the model described by Pickup [91, 92], the ionic resistance, R_{ion}, of the polymer film was obtained from the difference between the real axis intercept of the low frequency vertical segment and the real axis intercept at high frequency. As could be noticed the intercept of the impedance spectra with the real axis in the high frequency-region, is about the same for the potential range displayed ($+0.4\ V < E_{appl.} \leq +1.2\ V$). The electrolytic resistance, $R_{elec.}$, is estimated from the high frequency intercept [93]. The direct current resistance of the

polymer, R_{pol}, is relatively lower than that of the electrolytic solution, R_{elec}. The later is estimated in the range 10 Ω – 60 Ω. In the potential range in which the films acquire a high level of doping, R_{pol}, is < 10 Ω. The presence of relatively small anionic species, in this case PF^{6-}, allows their uptake by the polymeric film during the oxidation process [94]. As the applied potential to the polymer film, E_{appl}, shifts towards more positive values, ionic transport vs. electronic transport within the film is privileged. This is clearly noticed in the change in the slope of the impedance curve, cf. figure 8a. An explanation for this trend is caused by the increase in the anion uptake by the film as the applied potential increases. Moreover, the increase of charge delocalization in the oxidized polymeric chains combined with a consequent diminution of solvation energy for the doping anions adds to the previously mentioned effect. As the applied potential shifts towards more positive values (ca. E_{appl} > +0.8 V), a noticeable increase in the high-frequency semicircle amplitude with no appearance of initial capacitive behavior in the low-frequency region is observed, cf. figure 8b. With the relatively small number of cycles used to graft the film, the surface roughness is not expected to be high for the given thickness of the film. Therefore, a depression in the semi-circle in the range of frequency between 10 Hz and 5 kHz, that represents the roughness at the polymer/electrolyte interface [95], is not quite pronounced.

Figures 8-11 show characteristic diagrams obtained on four samples of PMT of different thickness. Again, the diagrams shown in figures 8-11 were recorded during the oxidation process (i.e. the potential at the polymer surface was

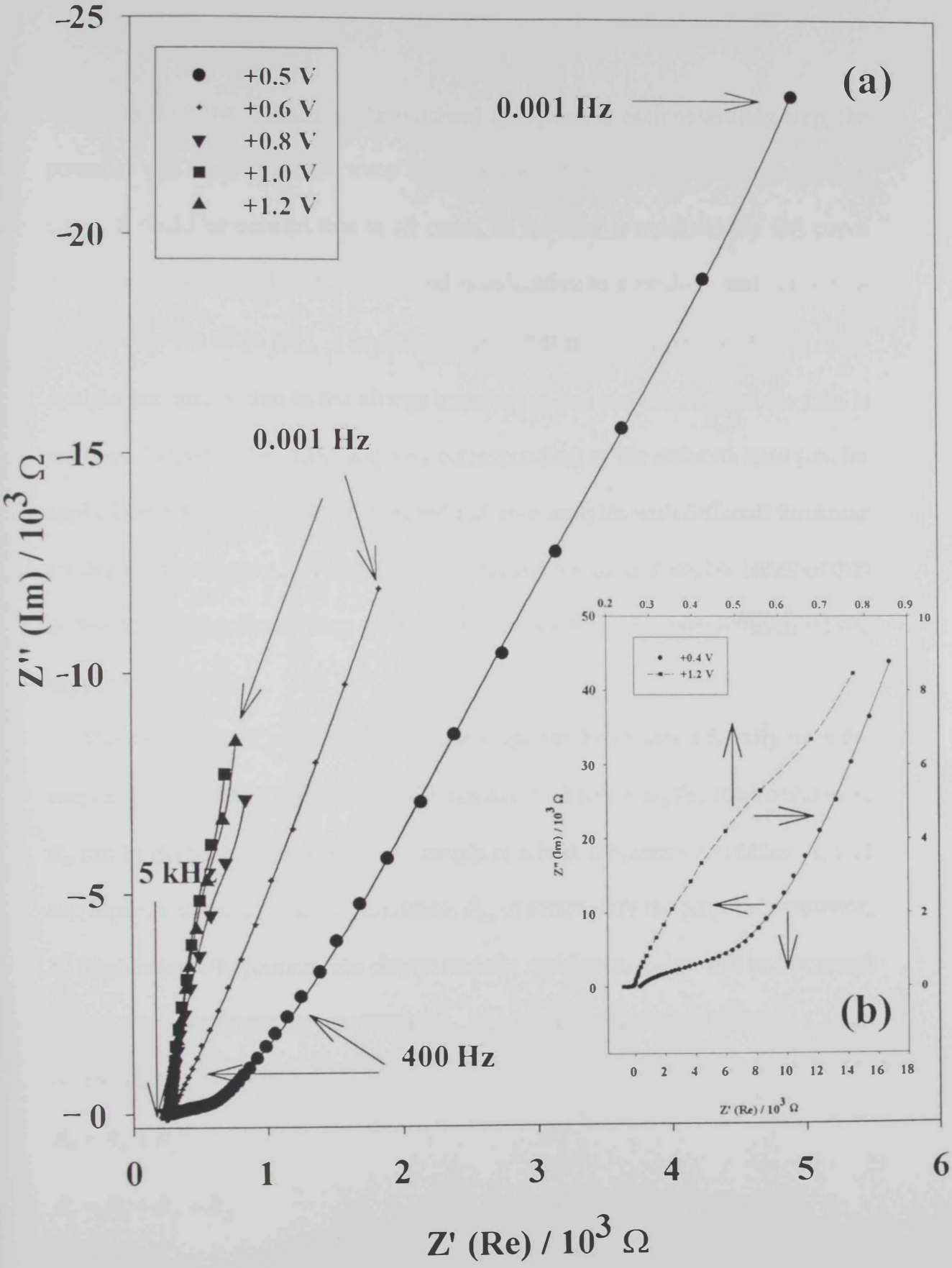
+0.5 V
+0.6 V
+0.8 V
+1.0 V
+1.2 V
(a)
0.001 Hz
0.001 Hz
5 kHz
400 Hz
Z'' (Im) / 10^3 Ω
Z' (Re) / 10^3 Ω
+0.4 V
+1.2 V
(b)
Z'' (Im) / 10^3 Ω
Z' (Re) / 10^3 Ω

Figure 8

increased from the reduced to the oxidized state) and at each measuring step, the potential was maintained for some time, ca. for the polymer to reach equilibrium state. It could be noticed that in all cases, as the film is oxidized the EIS curve display almost vertical part. This trend is indicative to a predominant capacitive behavior for the films [96]. The diffusion part that is usually represented by a 45° straight line and is due to the charge transport is not identified when the film is oxidized (doped). The EIS diagrams corresponding to the reduced state (ca. for applied potential of –0.5 V) of different polymer samples with different thickness are depicted in figure 12. The diagrams displayed represent complex behavior that is due to the superimposition of a low frequency transport phenomenon on the capacitive effect.

The capacitance C_f of the oxidized electrode can be obtained directly from the vertical part of the impedance (cf. figures 8-11). Moreover, the total resistance, R_s, can be derived. This resistance consists of a high frequency resistance, R_0 that corresponds to the electrolyte resistance, R_u, in series with the polymer resistance, R_p (that eventually contains the charge transfer resistance, R_{ct}, as will be discussed later). The low frequency resistance, R_p', associated with the capacitance, C_f, can be deduced as follows:

$$R_0 = R_u + R_p \qquad (1)$$

$$R_s = R_u + R_p + R_p' \qquad (2)$$

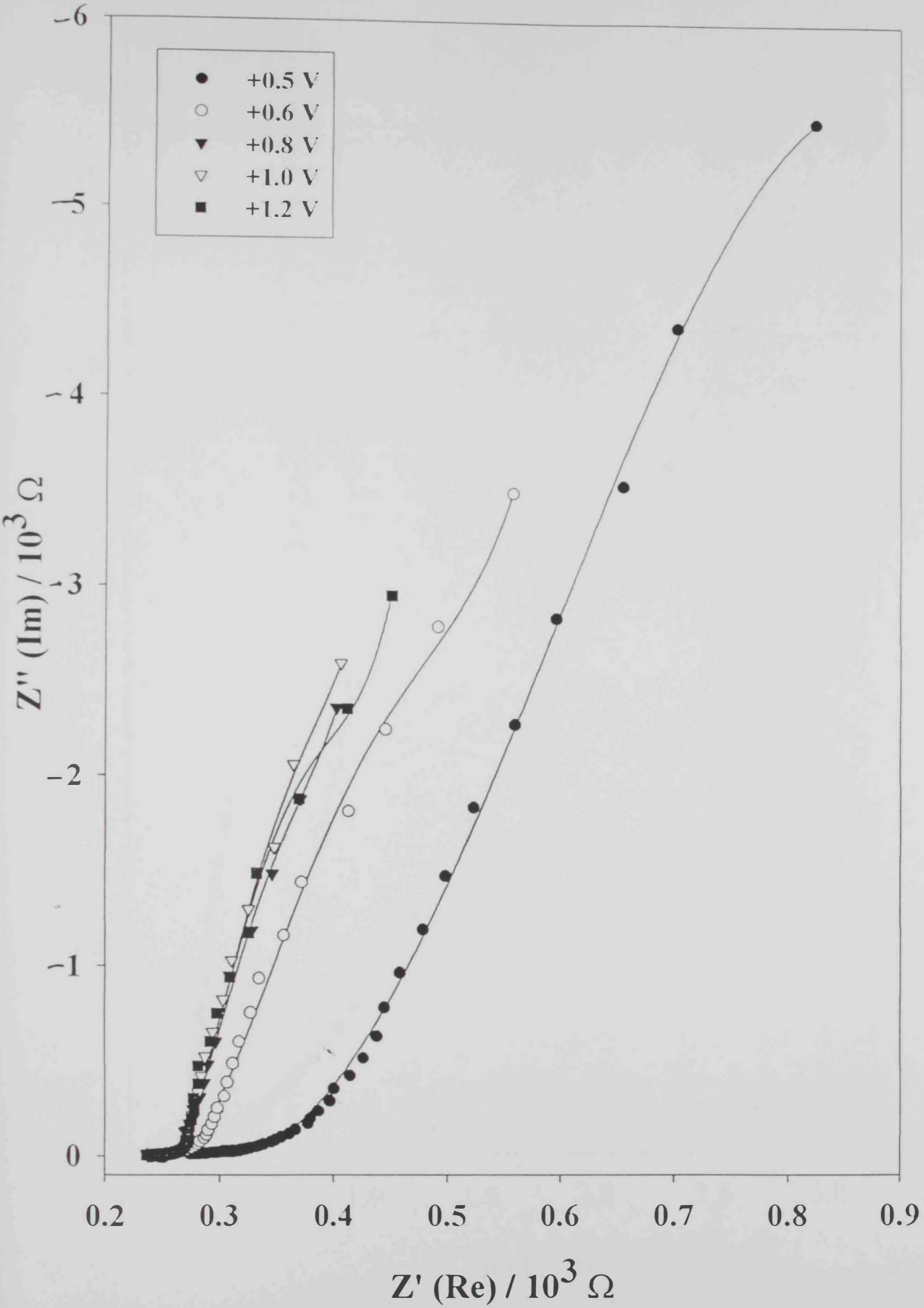
+0.5 V
+0.6 V
+0.8 V
+1.0 V
+1.2 V
Z'' (Im) / 10^3 Ω
Z' (Re) / 10^3 Ω
0
1
2
3
4
5
6
0.2
0.3
0.4
0.5
0.6
0.7
0.8
0.9

Figure 9

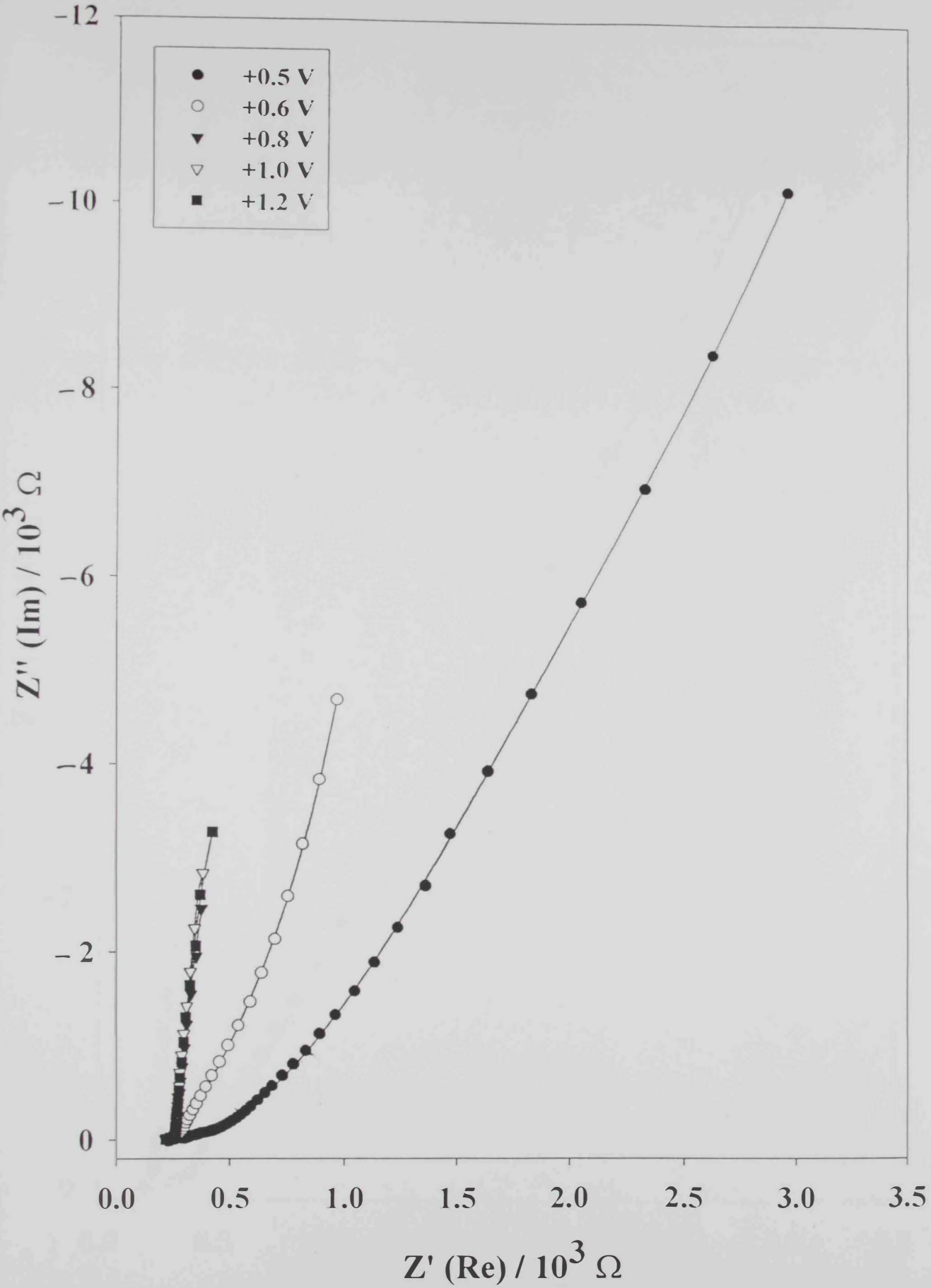
+0.5 V
+0.6 V
+0.8 V
+1.0 V
+1.2 V
-12
-10
-8
-6
-4
-2
0
Z'' (Im) / 10^3 Ω
0.0
0.5
1.0
1.5
2.0
2.5
3.0
3.5
Z' (Re) / 10^3 Ω

Figure 10

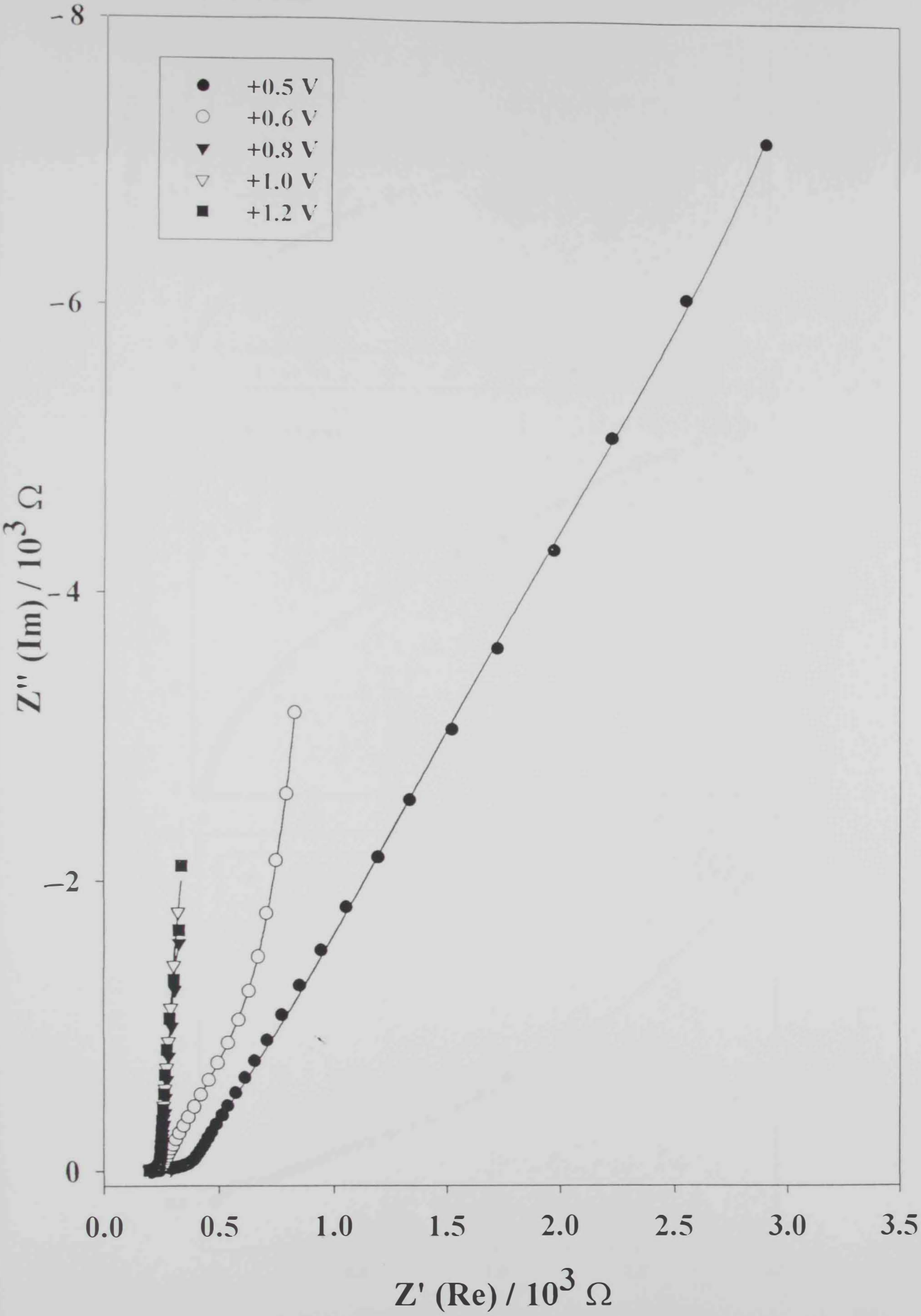
+0.5 V
+0.6 V
+0.8 V
+1.0 V
+1.2 V
-8
-6
-4
-2
0
Z'' (Im) / 10^3 Ω
0.0
0.5
1.0
1.5
2.0
2.5
3.0
3.5
Z' (Re) / 10^3 Ω

Figure 11

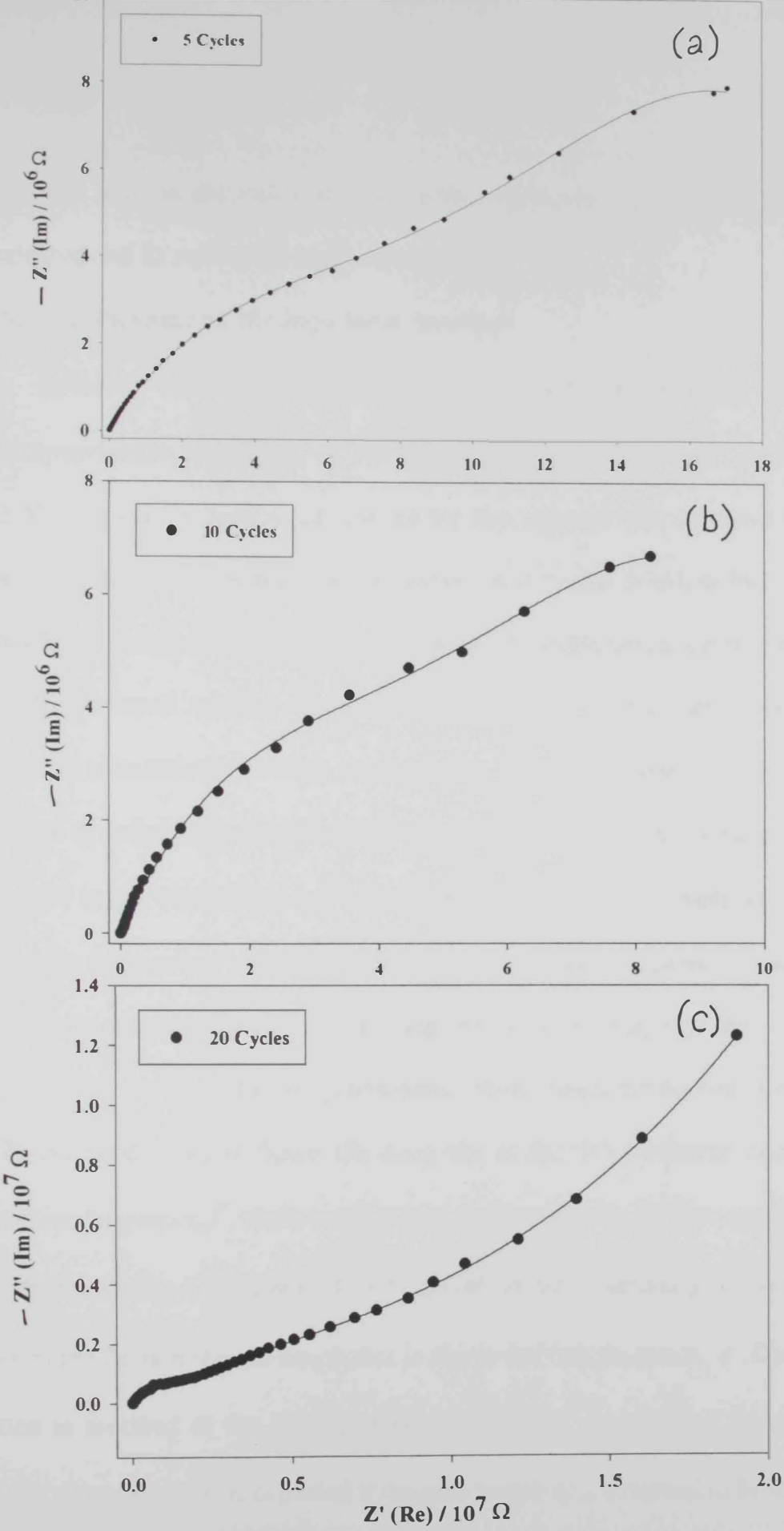
5 Cycles
(a)
− Z'' (Im) / 10^6 Ω
10 Cycles
(b)
− Z'' (Im) / 10^6 Ω
20 Cycles
(c)
− Z'' (Im) / 10^7 Ω
Z' (Re) / 10^7 Ω

Figure 12

Equation 1 is used to determine the electrolytic resistance, R_u, when the film is fully oxidized and its resistance could be neglected.

3.2 Effect of thickness on the impedance spectrum

The influence of the film thickness, ℓ, expressed by the overall electropolymerization charge, Q_c, ca. between 200 – 1500 mC.cm^{-2} and with $E_{appl.}$ = +1.2 V, is given in figures 12 and 13 for the reduced and oxidized films, respectively. Each measurement was carried out on a freshly prepared PMT-film. The impedance spectra exhibit the same characteristic shape typical for conducting polymer film-covered surfaces for all thickness studied. It typically shows the asymmetrical metal/film/electrolyte configuration. At high frequencies (ca. >100 Hz.) a small ill-defined capacitive semicircle is identified followed by a linear part of 45° phase angle, that merges into a pure capacitive line of 90° phase angle at a characteristic frequency, f^*, that will be termed the transition frequency. Medium and low frequency ranges are of primary importance because of their dependence upon different synthetic and testing conditions. Thus, except for the film prepared using 20 cycles, the data of figure 13a show that as the film thickness increases, the transition frequency, f^*, shifts towards lower values and the 45° line is enlarged as the film thickness, ℓ, increases. This behavior can be explained in terms of the increase of the finite diffusion length that is due to the film thickness, ℓ. The later definition is ascribed as the homogeneous model [97]. In terms of the porous model, the same behavior is expected if the pore length ℓ_p is assumed to be equal

(a)
5 Cycles
10 Cycles
15 Cycles
20 Cycles
−Z'' (Im) / 10³ Ω
Z' (Re) / 10³ Ω
0
2
4
6
8
0.2
0.3
0.4
0.5
0.6
0.7
0.8
0.9
(b)
f / Hz
(1/λ²) / nm x 10⁻⁴
E_appl = +1.2 V

Figure 13

or proportional to the film thickness. Figure 13b depicts the plot of the transition frequency, f^*, vs. $1/\ell_p^2$, where f^* was obtained graphically from the intercept of the 45° and the 90° phase angle lines of the Nyquist diagrams of figure 13a [98]. Departure from the intercept with the origin could be attributed to the high level of inaccuracy in estimating the film thickness.

3.3 Testing the polymer film in different solvents/electrolytes

The Bode-|Z| diagrams obtained for several PMT films in 0.1 M TBAHFP/AcN, in 0.1 M $NaCl/H_2O$ with different thickness and at different applied potentials are presented in Figures 14-17, respectively. As can be noticed in Figures 14 (a-d), at a given potential the impedance, Z, values gradually decrease as the film thickness increases when testing the polymer formed with different number of cycles in 0.1 M TBAHFP. Generally, this trend was also observed when comparing the effect of applying different potentials for the same film thickness. Thus, when the applied potential is shifted in the positive direction, a progressive decrease in Z resulted. Faradaic impedance results for several conducting polymers as well, such as poly(pyrrole), poly(aniline) and poly(acetylene) were reported earlier in the literature [99-104]. The data obtained in the aforementioned literature have been explained in terms of different "equivalent circuits." The choice of the circuit depended on the film thickness, the applied potential and the nature of polymer. Electrochemical impedance plots often contain several time constant and usually a portion of one or more of their

semicircles are seen (in a typical Nyquist diagrams). Figures 14 (a-d) illustrate an important fact, the "fully" reduced film at ca. –0.5 V and that "fully" oxidized at ca. +1.2 V exhibited an ordered and well-defined log |Z| vs. log *f* trend as the film thickness increases. However, the film at the interstitial doping zone, i.e. at $E_{appl.}$ between 0.0 V and 0.6 V (vs. Ag/AgCl) showed irregular behavior. The voltammetric results indicated the presence of a dark-blue oxidized PMT films at potentials higher than +0.6 V (where full oxidation occurs and large amounts of PF_6^- accumulated as doping anions) [105,106]. The presence of the film reddish color of its reduced form at potentials lower than +0.6 V indicates that the polymer contains a low percentage of PF_6^-. In the potential range +0.6 V to +0.8 V, where the film starts to oxidize, or more correctly when the polymer is partially oxidized, a mixture of the film oxidized and reduced states coexist [107]. This observation has been previously confirmed from chronoamperometric measurements reported earlier [85]. This is in agreement with the cyclic voltammetric (CV) results of figure 18. Figures 15 (a-d), on the other hand, show the same experiments as in figures 14 (a-d) for PMT films grafted with different thickness and tested in 0.1 M $NaCl/H_2O$ as the electrolytic medium. The following observations are concluded by comparing the data in figures 14 (a-d) with those in figures 15 (a-d): (i) for all film thickness studied, the log |Z| vs. log *f* displays a peculiar behavior for films tested with E_{appl} =+0.4 V, and confirming the presence of two time constants; (ii) the distinct doping level for reduced and oxidized films, when 0.0 V > $E_{appl.}$> +0.6 V displays quite similar log |Z| vs. log *f* curves in the case of films tested in

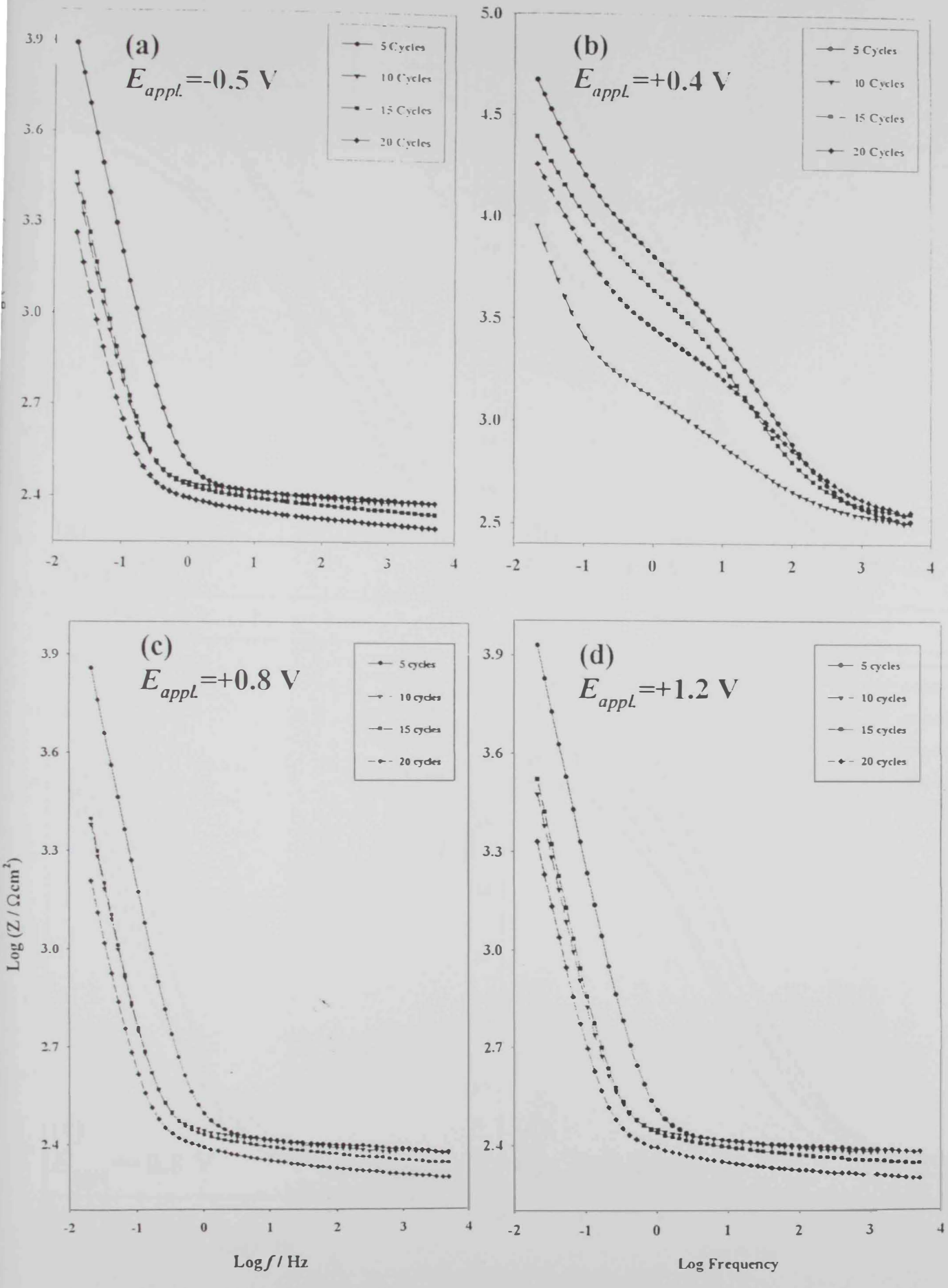
(a)
$E_{appl.}$=-0.5 V
5 Cycles
10 Cycles
15 Cycles
20 Cycles
(b)
$E_{appl.}$=+0.4 V
5 Cycles
10 Cycles
15 Cycles
20 Cycles
(c)
$E_{appl.}$=+0.8 V
5 cycles
10 cycles
15 cycles
20 cycles
(d)
$E_{appl.}$=+1.2 V
5 cycles
10 cycles
15 cycles
20 cycles
Log (Z / Ωcm²)
Log ƒ / Hz
Log Frequency

Figure 14

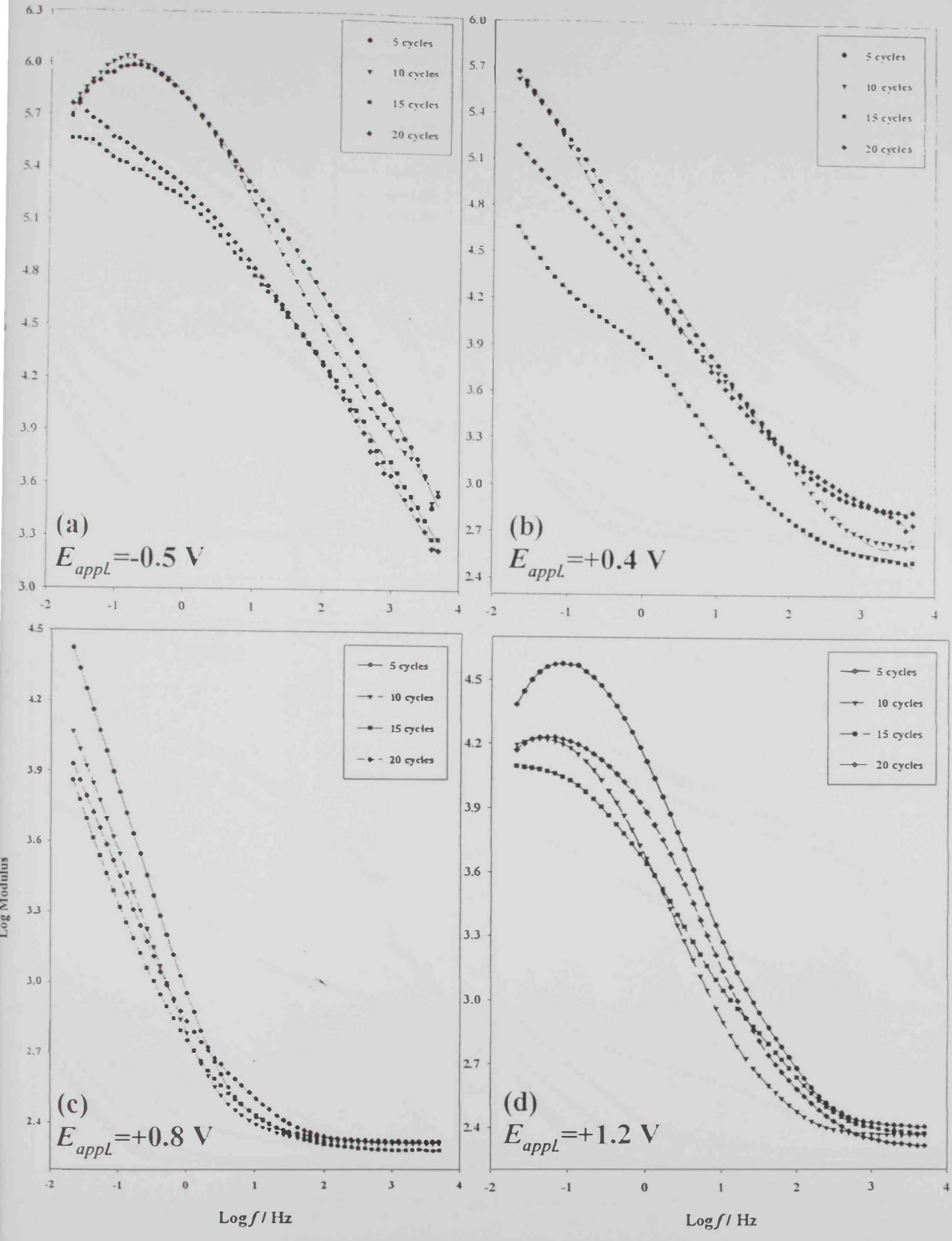
5 cycles
10 cycles
15 cycles
20 cycles
(a)
$E_{appl.}$=-0.5 V
(b)
$E_{appl.}$=+0.4 V
(c)
$E_{appl.}$=+0.8 V
(d)
$E_{appl.}$=+1.2 V
Log Modulus
Log ƒ / Hz
Log ƒ / Hz

Figure 15

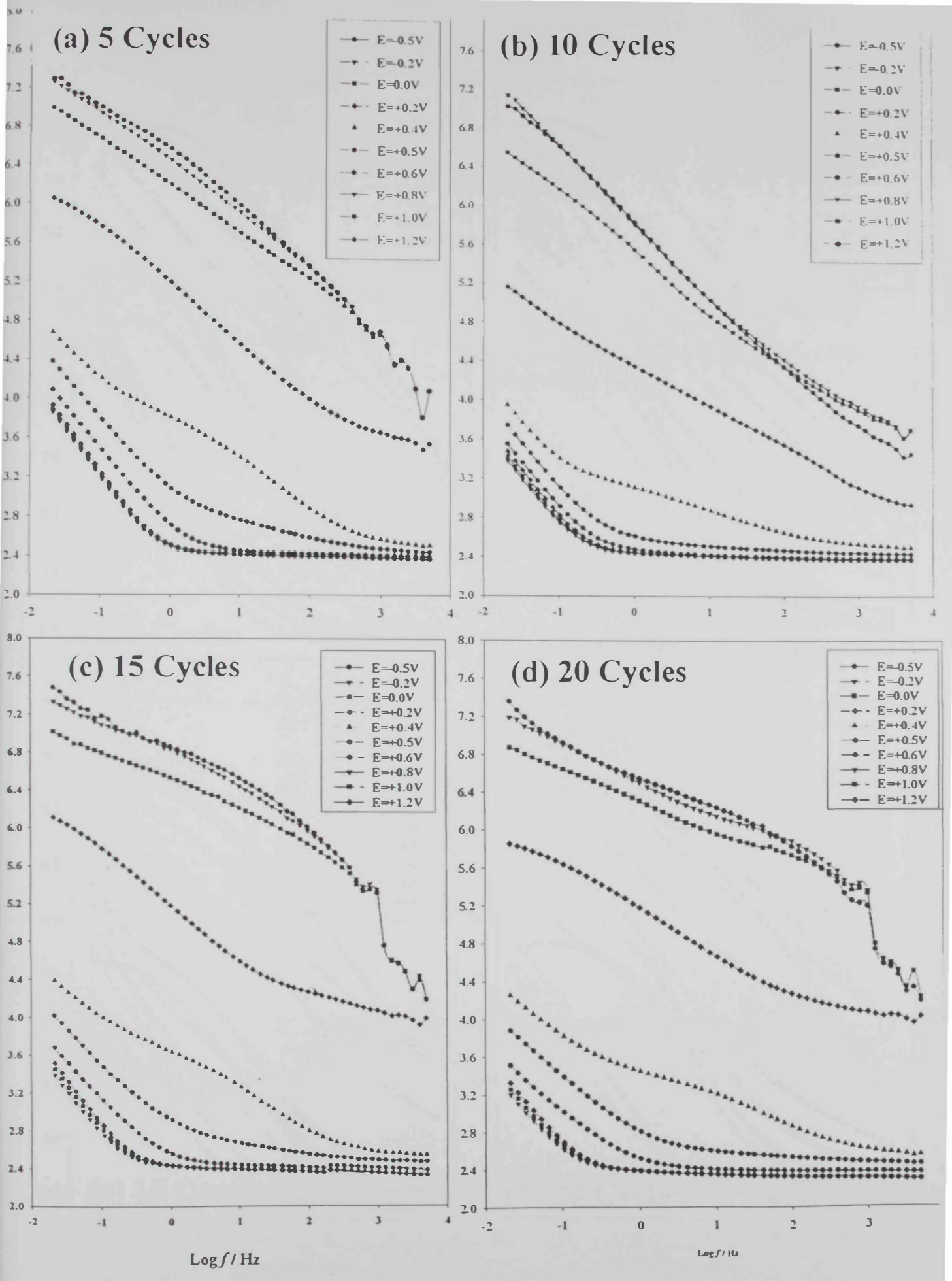
(a) 5 Cycles
(b) 10 Cycles
(c) 15 Cycles
(d) 20 Cycles
E=-0.5V
E=-0.2V
E=0.0V
E=+0.2V
E=+0.4V
E=+0.5V
E=+0.6V
E=+0.8V
E=+1.0V
E=+1.2V
Log f / Hz

Figure 16

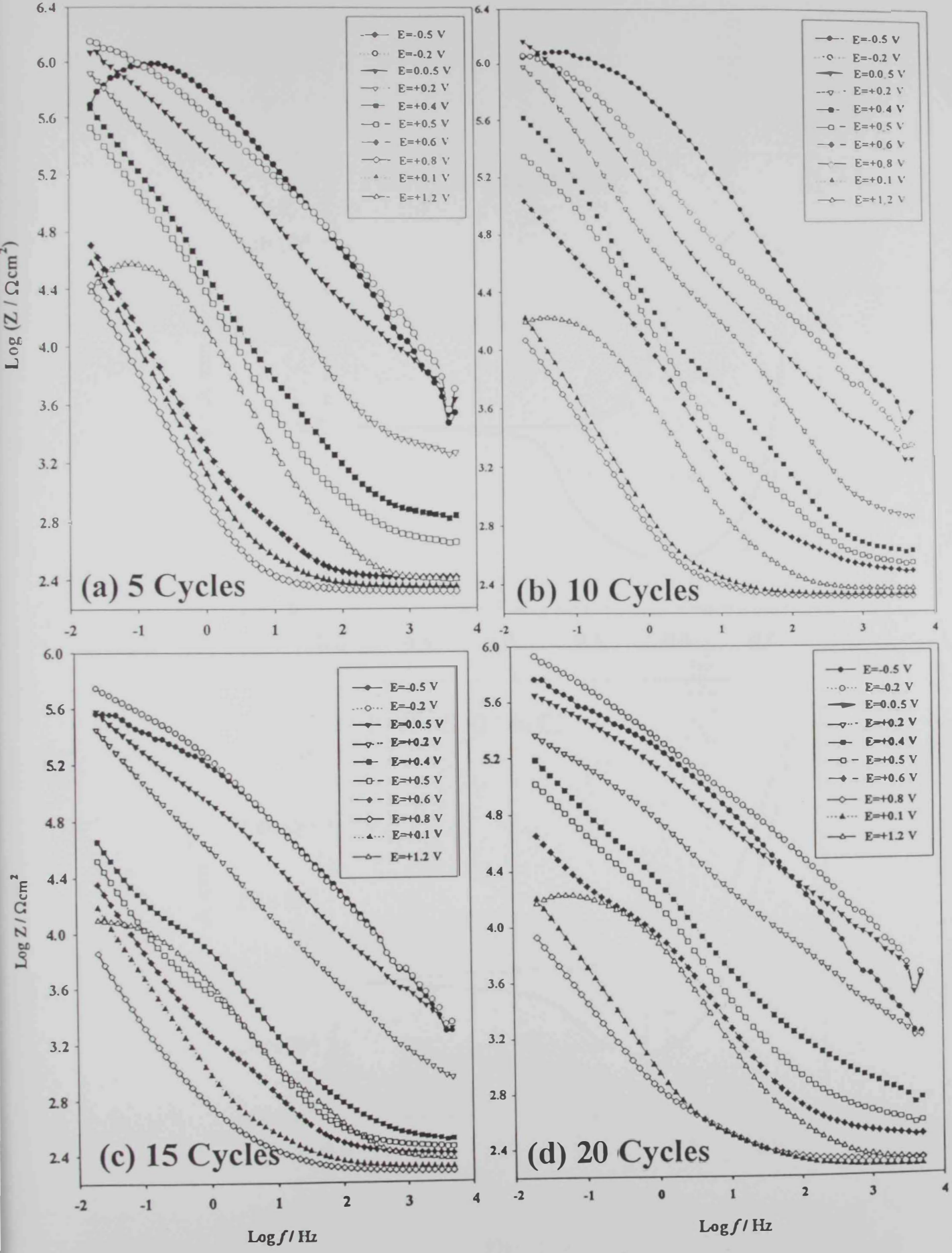
(a) 5 Cycles
(b) 10 Cycles
(c) 15 Cycles
(d) 20 Cycles
E=-0.5 V
E=-0.2 V
E=0.0.5 V
E=+0.2 V
E=+0.4 V
E=+0.5 V
E=+0.6 V
E=+0.8 V
E=+0.1 V
E=+1.2 V
Log (Z / Ωcm²)
Log Z / Ωcm²
Log f / Hz

Figure 17

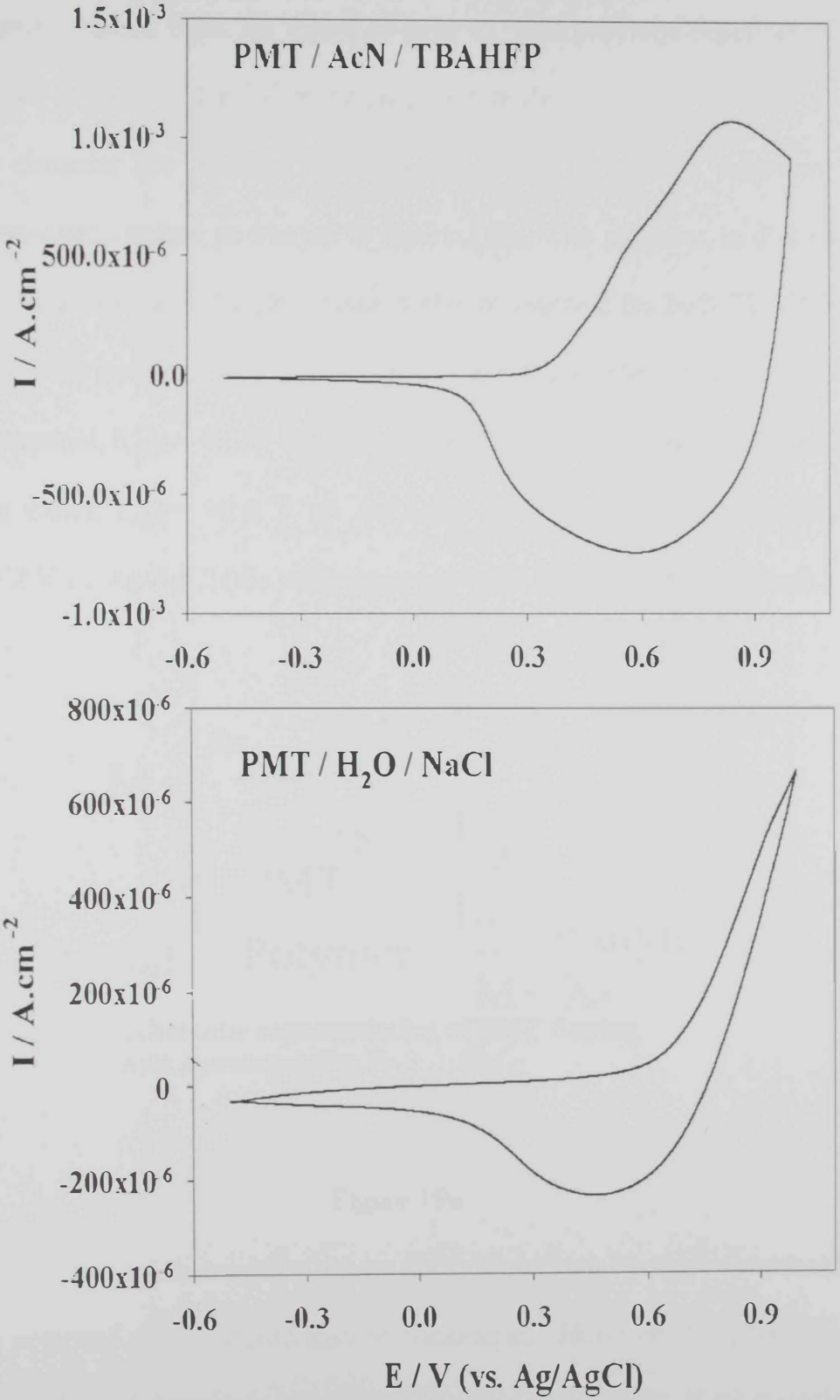
PMT / AcN / TBAHFP
1.5x10-3
1.0x10-3
500.0x10-6
0.0
-500.0x10-6
-1.0x10-3
I / A.cm-2
-0.6
-0.3
0.0
0.3
0.6
0.9
PMT / H2O / NaCl
800x10-6
600x10-6
400x10-6
200x10-6
0
-200x10-6
-400x10-6
I / A.cm-2
-0.6
-0.3
0.0
0.3
0.6
0.9
E / V (vs. Ag/AgCl)

Figure 18

TBAHFP, while films tested in NaCl showed only similar behavior for highly reduced and oxidized films, ca. figure 15 (a & d). The previous observations can be explained in terms of the following proposed model:

We may consider the polymer film deposited onto a metallic substrate as a metal/polymer/electrolyte as shown in figure 19a. The polymer in this case is ionically conductive and the electrolyte is electro-inactive for both TBAHFP and NaCl within the potential window studied. We will consider the three values of applied potential, $E_{appl.}$= -0.5 V vs. Ag/AgCl (PMT is in the reduced, electronically insulating state), $E_{appl.}$= +0.6 V vs. Ag/AgCl (PMT is partially oxidized), and $E_{appl.}$= +1.2 V vs. Ag/AgCl (the value beyond which PMT is over-oxidized).

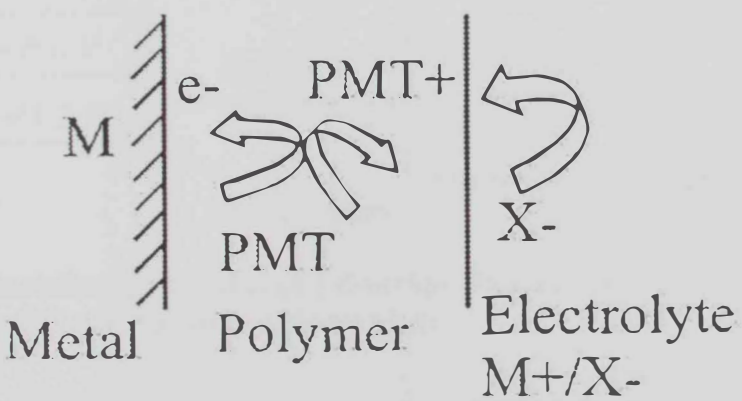

Schematic representation of PMT doping with counter-anion X-

Figure 19a

The electric potential distribution across the system (metal/polymer/electrolyte) at the three potential values should also be considered. However, the potential drop across the polymer/electrolyte interface is of prime importance, if we consider the

metallic nature of the metal/polymer interface. The system will be also considered at equilibrium and electronic charge passage is negligible. The potential drop, ($E_{polymer} - E_{electrol.}$), is defined by the ion-exchanging equilibrium between the polymer and the electrolyte, and is also known as "Donan potential" ΔE_D [108]. The value of ΔE_D is a function of the activities, a, of the exchanging ionic species i of charge z_i in the polymer and electrolytic phases [109], thus:

$$\Delta E_D = \frac{RT}{z_i F} \ln\left(\frac{a_i^{polymer}}{a_i^{electrol}}\right) \qquad (3)$$

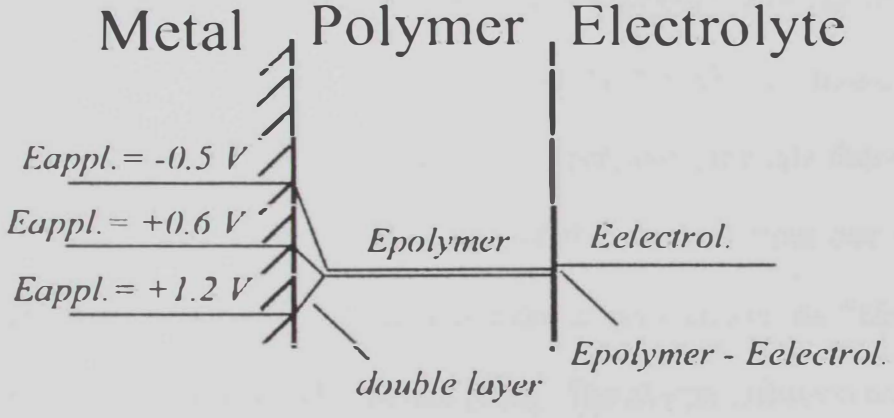

Electrical potential (E) distribution across the Metal/Polymer/Electrolyte

Figure 19b

In equation (3), R, T, and F have their conventional meanings. Many factors contribute to the charge exchange at the polymer/electrolyte interface, and therefore, affect the EIS spectra (cf. figures 14 and 15). Among those factors are the hydrophobic nature of the polymer, the film morphology, the level of doping

within the film, the applied potential, the size of ions in contact with the polymer surface, etc. PMT can be considered as an anion exchanger in the oxidized state (cf figure 19a). At equilibrium, and with an electrolyte with adequate concentration, the value of ΔE_D should not exceed ~10 mV. The final established potential drop across this interface would also depend on the chemical potentials of the anions/cations exchange between the polymer and electrolyte. Thus, a positive or negative interfacial electrical potential drop will be established. We will also consider the electron transfer between the metallic substrate and the conducting polymer film almost constant throughout the rest of this investigation. We will now pay more attention towards the charge transport across the conducting polymer. In the case of redox polymers, the rate-determining step for the charge transport is the transition of the electron from one redox site to a neighboring one [109]. This transition is also known as "electron-hopping" process that is diffusional in nature [110]. The charge diffusion coefficients are of the order of $D_e \sim 10^{-10}$–10^{-13} $cm^2.s^{-1}$. In the case of aqueous electrolyte (ca. 0.1 M NaCl), its conductivity is in the order of $\sim 10^{-1}$ $S.cm^{-1}$. Thus, if the mobility of the counter-ions in the polymer film is lower than in the aqueous phase by several orders of magnitude, the counter-ion transport coupled to the electron transport will not limit the charge-hopping process significantly. A "Warburg"-type diffusional impedance is normally used to describe the charge-hopping process [110]. In the case of PMT, a typical conducting polymer, the electronic conductivity is a function of the concentration of polarons and bipolarons [111].

Furthermore, conductivity depends to a big extent on the chemical structure of the polymer film and its morphology. The rate-determining step in the case of PMT would be the electron movement from one polymer chain to another [112]. This electron exchange processes between large conjugated organic systems are known to be fast [113]. This clearly explains the relative high conductivity of this class of polymers. In this case we will consider the PMT as similar to a redox polymer, but with relatively high ionic and low electronic conductivities. It might be possible at this stage to separate the double layer charging of the metal-polymer interface from the interfacial oxidation-reduction of the polymer redox sites and the associated diffusion-type electron transport across the film [114]. When the PMT is oxidized, its electronic conductivity will surpass that of the mobile counter-ions. Therefore, electrical field is established within the polymer film, and the ions migrate to reach an equilibrium. The polymer film behaves in this case as a porous metal with pores of limited depth and size [115]. The structure of the double layer, nature of solvent, size of doping ions, and their solvation (etc.) should affect the electrical characteristics of the film and therefore, yield a distinct behavior for the film in TBAHFP/AcN vs. $NaCl/H_2O$.

Both figures 16 (a-d) and 17 (a-d) show that, at low potentials (ca. between -0.5 V and +0.2 V vs. Ag/AgCl), the equivalent circuit may be related to a "modified" Randles circuit (ca. figures 20a and 20b), although in the low-frequency region the 45° Warburg line and the finite-diffusion line normal to the x-axis can hardly be distinguished (in the corresponding Z' vs. Z" plots of figures 16 and 17, that is not

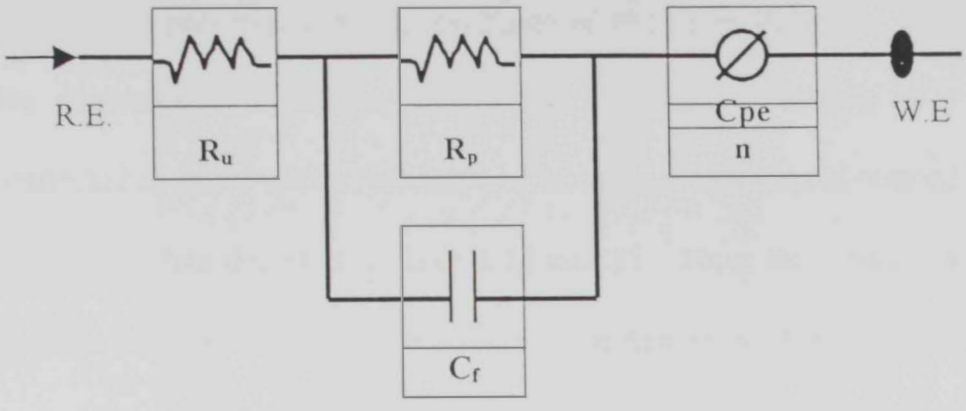

Figure 20a

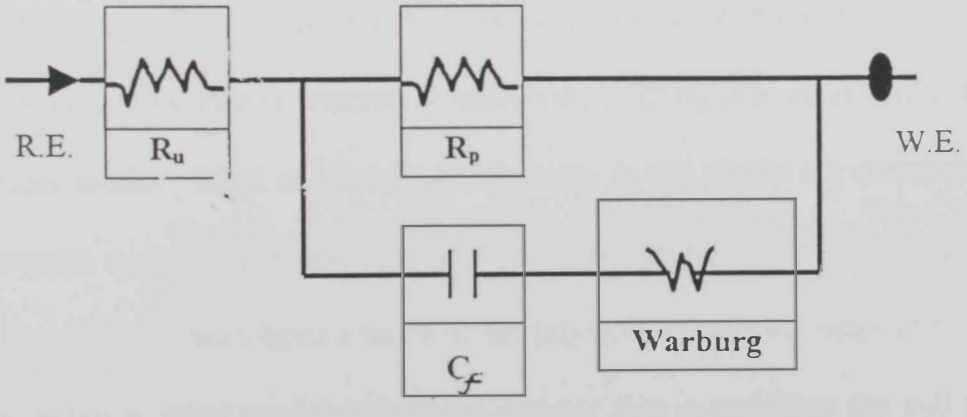

Figure 20b

shown). Thicker films (ca. higher than 100 μm) display the impedance loci related to diffusion with better resolution [116]. As the applied potential reaches the oxidation values for the polymer film, the resistance of PMT film decreases, and the semicircles decreases in "diameter" since the film tend to behave as a capacitance connected in series with a resistance. The same observation is noticed in the log |Z| vs. log *f* plots depicted in figures 16 and 17. Thus, the capacitive behavior of the films start as the applied potential approaches 0.6 V - 0.8 V. Thus, the slope starts to inflect at $E_{appl.}$ = +0.2 V and more than one time constant appears as $E_{appl.}$ = +0.4 V in the case of films tested in TBAHPF. On the other hand, the films tested in NaCl displayed a unique behavior at $E_{appl.}$ = +0.8 V, the onset of film oxidation in aqueous medium. It is important to notice that the impedance values reached by all films for all thickness studied and at all the potentials used are relatively lower when the electrolytic medium used was TBAHFP/AcN when compared to $NaCl/H_2O$. Again, the later is attributed to the hydrophobic nature of the film that would not allow adequate ion migration to the polymer matrix.

Equivalent circuits. EIS data is commonly analyzed by fitting it to an equivalent electrical circuit model. Most of the circuit elements in the model are common electrical elements such as resistors, capacitors, and inductors. To be useful, the elements in the model should have a basis in the physical electrochemistry of the system. For instance, most models contain a resistor that exemplifies the cell's solution resistance [117]. Table 4 lists the common circuit elements used

throughout the analysis in this work, the equation for their current versus voltage relationship, and their impedance.

Component	Current vs. Voltage	Impedance
Resistor	$E = IR$	$Z = R$
Inductor	$E = L\, di/dt$	$Z = j\omega L$
Capacitor	$I = C\, dE/dt$	$Z = 1/j\omega C$

Table 4. Common Electrical Elements Used in this Work

From Table 4 we notice that the impedance of a resistor is independent of frequency and has only a real component. Because there is not imaginary impedance, the current through a resistor is always in phase with the voltage. Whereas the impedance of an inductor increases as the frequency increases. Inductors have only an imaginary impedance component. As a result, an inductor's current is phase-shifted 90° with respect to the voltage. In general, the impedance versus frequency behavior (sometimes termed the Bode plot) of a capacitor is opposite to that of an inductor. A capacitor's impedance decreases as the frequency is raised. Capacitors also have only an imaginary impedance component. The current through a capacitor is phase shifted –90° with respect to the voltage. Since no previous faradaic impedance studies have been reported for PMT modified using the sol-gel technique to include an inorganic moiety to form hybrid material, this work describes the testing of several circuits in attempting to fit the experimental data obtained for its oxidized and reduced forms. This part of

the work starts with analysis of the unmodified PMT in two electrolytic media, as mentioned previously, then compared to that of the modified PMT with a sol-gel layer that basically contains silicon and doped with iron. The candidate found that the equivalent circuits depicted respectively in figures 20a and 20b could describe the behavior of all films adequately. In these circuits: (i) resistors simulate the resistive behavior of metal substrate, polymer film and electrolytic solution (R); (ii) capacitors simulate the capacitive behavior of the polymer film, metal substrate/film interface, and film/electrolyte interface (C); (iii) transmission lines simulating the diffusion impedance, also known as "Warburg impedance" (W); (iv) constant phase elements (CPE), as defined in equation (4) [118], where A is the frequency independent constant, ω the angular frequency and n_{CPE} is a dimensional factor (between 0.5 and 1.0). The above assignment is similar to those mentioned previously in the literature [119, 120].

$$Z_{CPE} = A_{CPE}(j\omega))^{-n}_{CPE} \qquad (4)$$

The reason of using more than one equivalent circuit is attributed to the fact that, the shape of the impedance diagram for PMT changed significantly from anodic to cathodic ($E_{appl.}$) that is commensurate to the variation of the properties of the polymers as a function of the oxidation state. A typical diagram is shown in figure 21 for PMT in TBAHFP/AcN. This representation provides a model to compare between the experimental data and the calculated fitted curve in all cases studied. Experimental data are represented by dots while simulated one by the solid lines.

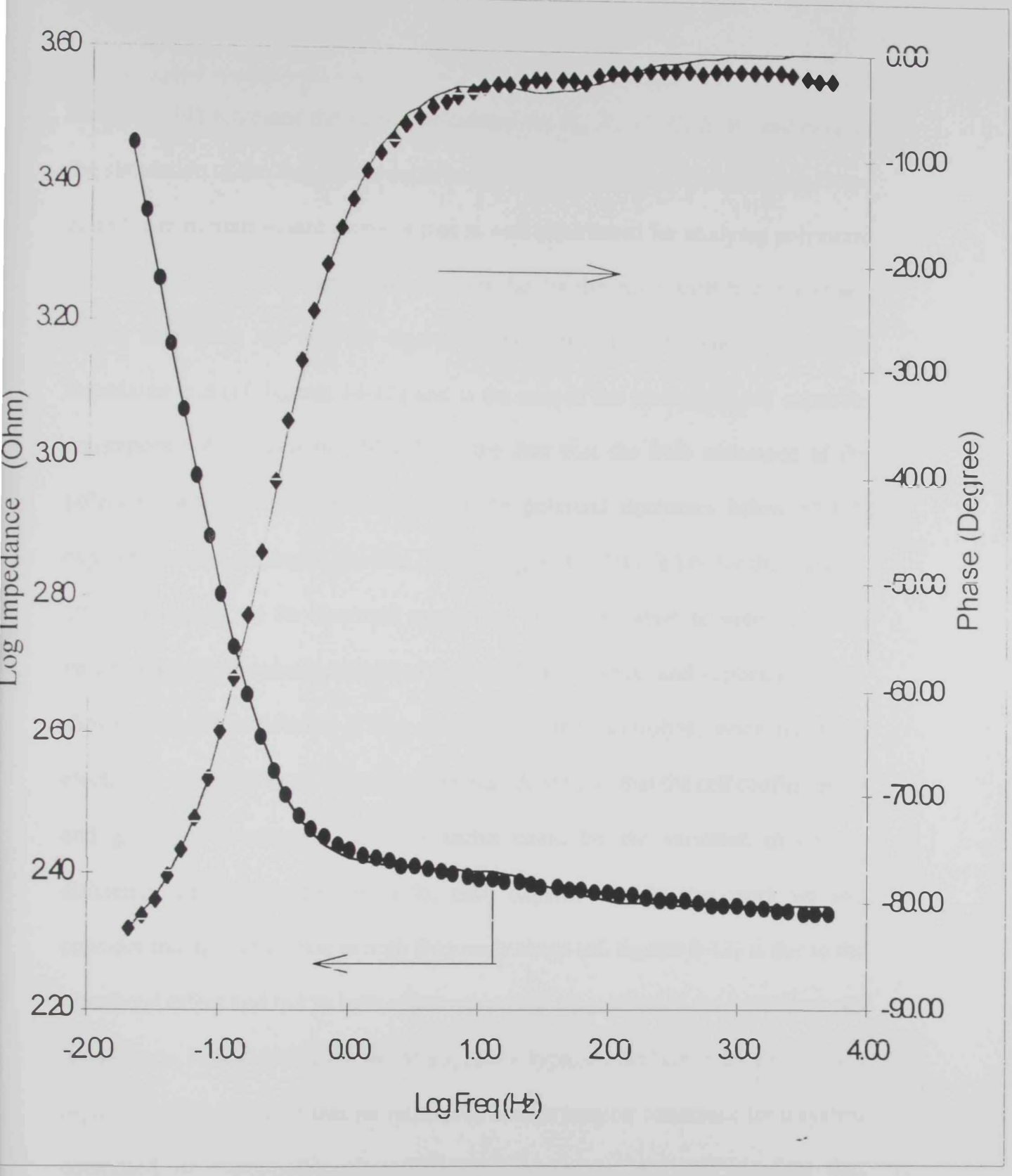
3.60
3.40
3.20
3.00
2.80
2.60
2.40
2.20
Log Impedance (Ohm)
0.00
-10.00
-20.00
-30.00
-40.00
-50.00
-60.00
-70.00
-80.00
-90.00
Phase (Degree)
-2.00
-1.00
0.00
1.00
2.00
3.00
4.00
Log Freq (Hz)

Figure 21

Tables (5-14) represent the values calculated for R_u, R_p, C_f, CPE, W, and n_{CPE} in the simulation of the impedance experiments. The candidate followed a non-linear complex minimum square protocol that is well established for studying polymeric systems [121]. R_u is almost entirely responsible for the initial shift from the origin on the impedance real axis (cf. figures 8-13) or the end of the curve at the high impedance end (cf. figures 14-17) and is the sum of the electrolyte and substrate resistances. As shown in tables 5-12, the fact that the bulk resistance of the polymer does explicitly decrease when the potential decreases below +0.4 V explains that the doping of the film (i.e. at $E_{appl.} > +0.4$ V) is a key for the apparent effect of doping on its electrical properties. It is important to notice that the variation of the R_u values, calculated for each film thickness and applied potential, shows that this resistance is not only due to the electrolyte, since the same electrolyte was used in all the measurements. Assuming that the cell configuration and geometry is constant, another factor could be the variation in current efficiency during film formation for each experiment. In this work we will consider that the semicircle at high frequency range (cf. figures 8-13) is due to the interfacial effect and not to bulk effects since the magnitude of the resistance and capacitance values evaluated would suggest a typical interface behavior. It was reported in the literature that no interfacial charge transfer resistance for a system composed of metal/polymer/metal [122]. Moreover, we will consider that semicircle at high frequency is due to ion transfer at the polymer/electrolyte interface. Therefore, R_p, is the charge transfer resistance associated with the

interface between polymer and electrolyte while *CPE* is the constant phase element equivalent to the double layer capacitance produced by charge accumulation at the interface (C_f). The later consideration assumes a flat configuration for the film (i.e. surface roughness is not taken into account). In fact the value of *CPE* is much larger than that of C_f. In the fitting calculation, it was possible to verify that there is a decrease in the semicircle height (i.e. that corresponds to the maximum at the imaginary axis) that leads to set $n_{CPE} \leq 1.0$. The later is considered as an ideal value, however, this value showed a variation with the condition of the film under consideration.

Examination of tables 5-12 would lead to the following conclusions: (i) the value of R_u displayed a common behavior for all "unmodified" polymeric films studied. For films studied with an applied potential, ($E_{appl.}$) between –0.5 V and 0.0 V, R_u increases and then starts to decrease as the applied potential is ramped to more positive values. In this case, the film is switched from a relative doping to a merely insulating one. As the applied potential approaches the oxidation value for the polymer, R_u starts to decrease indicating that the film is completely switching to the full doped and conducting state. Moreover, a relative slight increase in the value of R_u is noticed as the thickness of the film increases (cf. tables 5-8). On the other hand, R_u values are relatively lower for all potential ranges studied. This could be explained in terms of the conduction mechanism that involves ionic diffusion within the film that is much easier accessed in case of using AcN rather that H_2O as a solvent. (ii) For all fits, the charge transfer resistance that is

included in the value of the polarization resistance, R_p, was found to be relatively high. This indicates that a charge transfer process at the polymer/electrolyte interface (that includes the double layer) is not significant at the relatively lower end of the frequency. It will be however difficult to obtain a full description of the behavior of charge transfer within the double layer at the polymer/solution interface. It is obvious from the above discussion that the electron transport through the polymer chains is accompanied by ionic migration. The transport of the ions through the double layer and particularly at the polymer/solution interface may be modeled as the charge/discharge of a capacitor. Since the surface of the polymer is irregular and binding sites of ions to the polymer possess different energies, a capacitive component and a constant phase elements are associated with the charge transfer resistance [123 - 127]. Again the values of R_p generally decrease as the applied potential increases. While no appreciable changes in the values of R_p were noticed in the case of films tested in TBAHFP/AcN with change in thickness, films tested in aqueous solutions displayed progressive decrease in the R_p values with film thickness (ca. when comparing films formed with 5 or 10 cycles with those formed with 15 or 20 cycles, respectively). The charge transfer resistance component, R_{ct}, of the polarization resistance, R_p, is inversely proportional to the rate of electron transfer. Thus, R_{ct} can be used as a measure of the facility of the kinetic process of the charge transfer [128]. When R_{ct} decreases, the charge transfer rate constant tends to increase. An analysis of the data displayed in tables 5-12 shows initially high values of R_p that is followed by a

noticeable decrease that reaches its lowest value as the film approaches its redox potential (E_{ox}). The fact that the maximum value of electron transfer is reached as the film-potential approaches its E_{ox} value indicates that a high ionic uptake predominates the charge diffusion and can be rather described in terms of variation in *CPE* and the *Warburg* component for relatively low applied potentials and thicker films in the aqueous medium. It is crucial to indicate at this point that, R_{ct} values cannot be considered solely to evaluate the film conductivity with the change of the applied potential to the film. Other factors, such as film channeling, morphology, synthesis-electrolyte memory effect, type of monomer, film modification, etc. would affect such variation in R_{ct}. (iii) It is clear that the *CPE* is associated with the film capacitance, C_f. The value of *CPE*, however, is proportional to the sample thickness. As could be noticed from the data presented in tables5-12, the value of *CPE* increases while that of C_f decreases with thickness. Film capacitance C_f, however, is relatively larger in the case of films analyzed in aqueous solutions. The variation in the values of *CPE* and C_f is also more pronounced in the case of films tested in $NaCl/H_2O$. This is the second evidence to prove the effect of hydrophobicity of the film and its capacitive properties that has a major contribution on the applicability of these films in rechargeable batteries. The polymer film possibly reaches a maximum C_f value as its approaches E_{ox} and in some cases when exceeding its redox potential value[129]. The variation of the double layer capacitance produced by charge accumulation at the polymer/solution interface is related to the charge compensation taking place

Table 5. EIS fitting data of polymer coated over Pt surface for 5 cycles and tested in TBAHFP / AcN

E / V	R_u / Ω.cm^2 x 10^3	R_p / Ω.cm^2 X 10^6	C_f / F.cm^2 x 10^{-6}	CPE / $\Omega^{-1}.s^n$ x 10^{-3}	n
-0.5	1.244	0.271	4.266	2.014	0.612
-0.2	6.237	6.811	8.112	2.788	0.584
0.0	6.415	1.845	6.471	4.101	0.562
0.2	2.332	0.230	3.647	3.089	0.555
0.4	0.303	0.151	7.746	0.130	0.565
0.5	0.241	0.166	309.9	0.0140	0.643
0.6	0.251	0.00130	461.3	0.0205	0.900
0.8	0.208	0.0746	10.38	0.0739	0.866
1.0	0.187	0.114	973.9	0.0930	0.592
1.2	0.172	0.105	895.6	0.104	0.643

Table6. EIS fitting data of polymer coated over Pt surface for 10 cycles and tested in TBAHFP / AcN

E / V	R_u / Ω.cm^2 x 10^3	R_p / Ω.cm^2 x 10^6	C_f / F.cm^2 x 10^{-6}	CPE / $\Omega^{-1}.s^n$ x 10^{-4}	n
-0.5	1.571	5.186	0.482	1.257	0.649
-0.2	2.347	18.94	0.466	0.883	0.559
0.0	2.663	9.242	2.054	0.773	0.562
0.2	1.347	0.431	5.649	0.0124	0.632
0.4	0.731	0.368	4.619	0.0457	0.512
0.5	0.260	0.128	13.700	0.0209	0.584
0.6	0.234	0.00584	21.180	0.0867	0.536
0.8	0.206	0.0464	31.970	0.00760	0.551
1.0	0.198	0.0535	29.330	0.00829	0.790
1.2	0.183	0.395	25.300	0.00564	0.534

Table 7. EIS fitting data of polymer coated over Pt surface for 15 cycles and tested in TBAHFP / AcN

E / V	R_u / Ω.cm^2 x 10^3	R_p / Ω.cm^2 x 10^6	C_f / F.cm^2 x 10^{-6}	CPE / $\Omega^{-1}.s^n$ x 10^{-4}	n
-0.5	4.105	4.276	0.829	0.124	0.521
-0.2	5.741	21.15	0.512	0.344	0.614
0.0	6.443	8.321	1.278	0.891	0.553
0.2	6.831	0.672	3.331	2.294	0.541
0.4	0.329	0.120	1.316	3.794	0.530
0.5	0.281	0.0794	26.62	5.032	0.592
0.6	0.238	0.00386	13.77	7.759	0.831
0.8	0.124	0.0559	8.076	8.489	0.545
1.0	0.109	0.0757	9.667	7.632	0.799
1.2	0.147	0.0721	2.311	6.273	0.555

Table 8. EIS fitting data of polymer coated over Pt surface for 20 cycles and tested in TBAHFP / AcN

E / V	R_u / Ω.cm² x 10^3	R_p / Ω.cm² x 10^6	C_f / F.cm² x 10^{-6}	CPE / $\Omega^{-1}.s^n$ x 10^{-4}	n
-0.5	5.305	3.214	2.118	0.423	0.523
-0.2	5.866	15.47	1.863	0.761	0.611
0.0	6.217	7.881	2.394	0.790	0.556
0.2	6.555	0.371	3.407	2.368	0.544
0.4	0.163	0.161	6.527	4.733	0.522
0.5	0.303	0.0291	1.234	9.448	0.525
0.6	0.238	0.00386	0.838	9.759	0.732
0.8	0.157	0.0436	4.833	9.796	0.855
1.0	0.155	0.0630	4.264	9.965	0.839
1.2	0.163	0.0569	3.632	8.932	0.933

Table 9. EIS fitting data of polymer coated over Pt surface for 5 cycles and tested in NaCl / H_2O

E / V	R_u / Ω.cm² x 10^3	R_p / Ω.cm² x 10^6	C_f / F.cm² x 10^{-6}	CPE / $\Omega^{-1}.s^n$ x 10^{-3}	n	W x 10^{-1} F.cm²	C_c x 10^{-6} F.cm²
-0.5*	3.156	2.014	-	-	-	8.821	5.121
-0.2*	4.781	2.014	-	-	-	8.821	5.121
0.0*	5.498	1.913	-	-	-	4.245	9.007
0.2	1.519	0.0375	16.86	8.347	0.544	-	-
0.4	0.623	0.0593	28.54	0.987	0.522	-	-
0.5	0.457	0.0404	24.33	0.671	0.525	-	-
0.6	0.242	0.00316	164.0	0.0319	0.732	-	-
0.8	0.210	0.0336	410.9	0.0204	0.855	-	-
1.0	0.219	0.0383	181.2	0.0140	0.839	-	-
1.2	0.188	0.0284	10.97	0.0246	0.933	-	-

* Used model in figure 20b.

Table 10. EIS fitting data of polymer coated over Pt surface for 10 cycles and tested in NaCl / H_2O

E / V	R_u / Ω.cm² x 10^3	R_p / Ω.cm² x 10^5	C_f / F.cm² x 10^{-6}	CPE / $\Omega^{-1}.s^n$ x 10^{-3}	n
-0.5	1.453	8.849	0.251	2.741	0.523
-0.2	3.392	5.331	1.540	2.777	0.558
0.0	6.108	9.007	2.933	2.004	0.599
0.2	0.448	3.726	14.96	1.824	0.631
0.4	0.303	3.487	18.21	0.504	0.600
0.5	0.320	1.634	20.71	6.427	0.593
0.6	0.305	0.0164	33.85	8.323	0.726
0.8	0.302	0.0438	128.4	17.03	0.763
1.0	0.208	0.132	426.0	10.24	0.606
1.2	0.197	0.121	36.06	18.13	0.527

Table 11. EIS fitting data of polymer coated over Pt surface for 15 cycles and tested in NaCl / H_2O

E / V	R_u / Ω.cm^2 x 10^{-3}	R_p / Ω.cm^2 x 10^{5}	C_f / F.cm^2 x 10^{-6}	CPE / $\Omega^{-1}.s^n$ x 10^{-3}	n	W x 10^{-1} F.cm^2	C_c x 10^{-6} F.cm^2
-0.5*	3.470	3.998	-	-	-	4.035	58.00
-0.2*	1.720	6.998	-	-	-	1.035	5.800
0.0	5.769	0.217	7.363	7.482	0.524	-	-
0.2	0.432	0.0326	27.95	0.255	0.506	-	-
0.4	0.299	0.0309	30.09	0.428	0.569	-	-
0.5	0.289	0.0128	36.71	0.0489	0.657	-	-
0.6	0.230	0.00748	746.4	0.0743	0.548	-	-
0.8	0.185	0.0979	1936.0	0.0706	0.551	-	-
1.0	0.196	0.0739	515.6	0.0870	0.544	-	-
1.2	0.149	0.0606	42.61	0.0418	0.573	-	-

* Used model in figure 20b.

Table 12. EIS fitting data of polymer coated over Pt surface for 20 cycles and tested in NaCl / H_2O

E / V	R_u / Ω.cm^2 x 10^{-3}	R_p / Ω.cm^2 x 10^{5}	C_f / F.cm^2 x 10^{-6}	CPE / $\Omega^{-1}.s^n$ x 10^{-3}	n	W x 10^{-1} F.cm^2	C_c x 10^{-6} F.cm^2
-0.5*	1.124	6.998	-	-	-	4.035	5.800
-0.2*	1.729	6.388	-	-	-	5.035	2.580
0.0*	1.734	0.641	0.593	8.523	0.549	-	-
0.2	1.364	0.270	8.283	0.433	0.507	-	-
0.4	0.469	0.0546	31.70	0.654	0.559	-	-
0.5	0.355	0.0389	25.67	0.892	0.612	-	-
0.6	0.292	0.00569	19.66	0.924	0.608	-	-
0.8	0.196	0.0601	129.5	0.0131	0.537	-	-
1.0	0.182	0.136	91.46	0.0323	0.705	-	-
1.2	0.158	0.189	17.46	0.0243	0.592	-	-

* Used model in figure 20b.

within the electrical double layer during the oxidation of the polymer. However, we would expect the results reported in this work to be relatively higher than those reported in the literature [101], due to the relative thickness of the film and the different method used for film formation. Polymer films produced by evaporation, however, possess more surface heterogeneities that affect the value of *CPE*. Another factor that should have a remarkable effect on shaping the values obtained for *CPE* is the swelling of the film caused by the solvent/electrolyte intervention. Again, the impedance (Z) can be represented by the *CPE* or the W component. This will depend on the applied potential, the thickness of the film and polymer modification. Thus, in the regions where the semi-circle radius is very small (i.e. for "fully" oxidized films), *CPE* can be associated to the capacitance of the spatial charge layer formed in the polymer/electrolyte interface. We will consider the transmission lines represented by the Warburg element, and the resistance/capacitance assembly to describe the diffusion through the polymer [130]. This case is usually true when diffusion takes place in a medium where the interface precludes the flow of the species and is represented by a hyperbolic tangent function [117, 119, 131]. Z is estimated from equation (5) [119], where the components of the hyperbolic tangent function $T(Y_o$ and $B)$ are used to calculate the diffusion coefficient according to equation (6). The data for the diffusion coefficients estimated from equations 5 and 6 are depicted in table 15.

$$Z_{(T)} = \frac{1}{Y_o(j\omega)^{1/2}} \tanh B(j\omega)^{1/2} \qquad (5)$$

$$D = \left(L^2 / B^2\right) \qquad (6)$$

Where, L is the thickness of the film and other elements of the equations as previously described. It is important to take into account that the diffusion coefficient, D, is a combination of the ionic diffusion coefficient, D_i, and the electronic diffusion coefficient component, D_e [132]. Therefore, the ratio of D_i/D_e depends on the conductive nature of the film. Thus, as the polymer film approaches its "fully" conductive state (i.e. when $E_{appl.} > 0.4$ V) $D_e >> D_i$. The film thickness, on the other hand, will still play a major role in controlling the D_e values, namely when the morphology of the different layers of the film start to differ considerably. The variation displayed in the capacitive and constant phase element suggested that the polymer film serves the purpose of a variable capacitor.

4. Hybrid polymer/inorganic layer

In this set of experiments, a polymer film was formed using 5 or 10 cycles of an applied potential ramp to the platinum substrate and the resulting organic layer was dip-coated with a sol-gel solution for 1 or 5 minutes. The resulting polymer/inorganic hybrid has the following suggested structure as indicated in the schematic diagram of figure 23. Several considerations will be taken at this point, thus, the conducting polymeric film (*P*) is relatively thicker than that of the inorganic layer (*I*). The conducting polymer film is porous in nature and less dense compared to the inorganic layer. Figure 22 shows impedance plots for

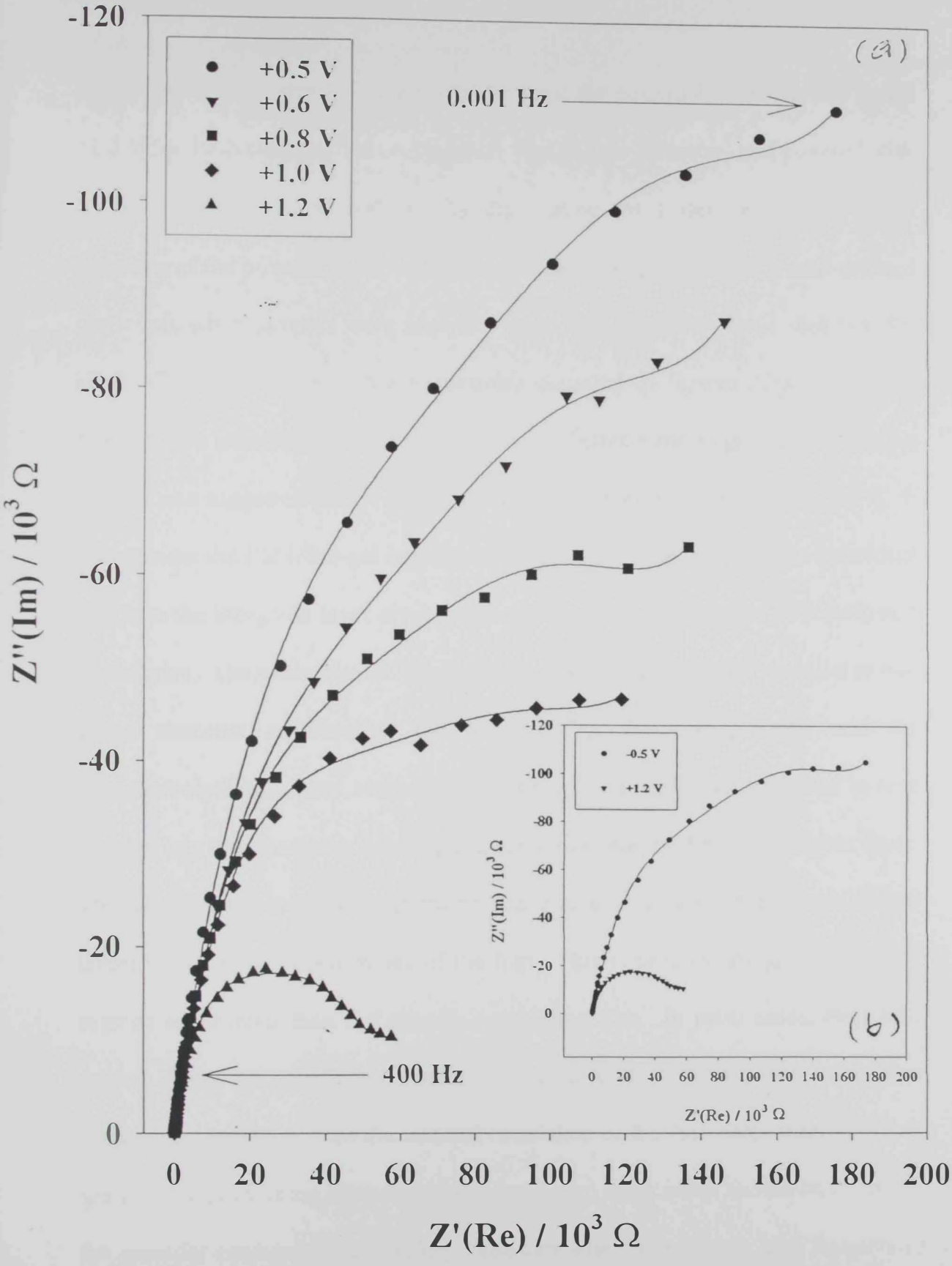
(a)
+0.5 V
+0.6 V
+0.8 V
+1.0 V
+1.2 V
0.001 Hz
400 Hz
-120
-100
-80
-60
-40
-20
0
Z''(Im) / 10^3 Ω
0 20 40 60 80 100 120 140 160 180 200
Z'(Re) / 10^3 Ω
-0.5 V
+1.2 V
(b)

Figure 22

poly(3-methylthiophene) (formed with ramping the potential between -0.5 V and +1.2 V for 10 cycles) grafted on platinum wire (1 mm diameter) and covered with a sol-gel layer (fired at 350 °C) by dip-coating for 1 minute. The Nyquist diagrams of the polymer layer without modification did not display a well-defined semicircle when samples were analyzed up to high frequency limit used (ca. 5.0 kHz). The occurrence of the semicircles depicted in figures 22(a) and 22(b) suggests the possibility of inter- and/or intra-cluster ionic migration. A similar finding was suggested earlier in the literature for other granular systems [133]. If we consider the PMT/Sol-gel interface as a heterogeneous layer, where individual grains in the inorganic layer are in contact with each other at the PMT/inorganic boundaries. Therefore, the a.c. response may be analyzed into two parallel or two series elements representing the intra- and/or the inter-granular and the film/electrolyte interfaces, respectively. The parallel model was assigned in case of relatively thin inorganic coating and the series one for the rather thicker layer. The capacitance associated with the presence of grain boundary regions is always larger than the bulk capacitance of the film. This is because the grain boundary regions are thinner than the organic conducting film. In most cases, migration across grain boundaries is highly restricted and therefore, the inter-grain resistances are larger than the internal resistance of the film despite the fact that grain boundaries being thinner. As expected, two semicircles should be observed for granular containing films [133]. The first one (at relatively high frequency) will be assigned to the bulk capacitance and bulk resistance (intra-film ionic

migration), and the second one expresses the capacitance and resistance associated with the grain boundary regions (inter-cluster ionic migration). Thus, the Nyquist diagrams obtained at room temperature for the organic conducting polymer film hybridized with the inorganic layer were fitted using the $R(RC)(Q)$ or the $R(R/CW)$ equivalent circuit.

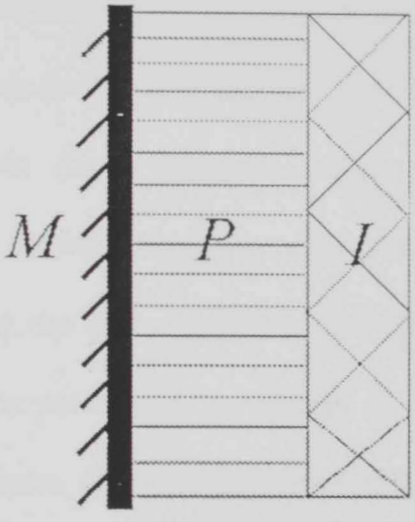

Figure 23. Schematic diagram representing the structure of sol-gel modified conducting polymer over a platinum substrate

R, C, Q and W represent resistance, capacitance, constant phase element, and the Warburg element, respectively. The candidate was not able to model the data by any equivalent circuit that is composed entirely of frequency-independent components. The CPE and W components had to be included in order to explain circular arcs whose centers lay below the real axis. The CPE is generally

expressing the distribution of the current density along the polymer surface as a result of surface non-homogeneity [134]. Tables 13 and 14 show the polarization resistance, R_p, the Warburg element, W, the film capacitance, C_c, and the interfacial resistance, R_u values for platinum/polymer/inorganic system. The results display the effect of changing the thickness of the polymeric layer and the dipping time used to deposit the inorganic film. The following observations could be made from the data of tables 13 and 14: (i) the ohmic resistance, R_u, associated with the modified film/electrolyte interface decreased appreciably when compared to the non-modified film (ca. a difference of one order of magnitude). This behavior indicates that the inter-cluster ionic migration was facilitated. The later observation is because the ionic inclusion increases as the applied potential approaches the oxidation potential of the system. It is also clear that as the applied positive potential decreases, cf. figure 22, the semicircle start to be ill defined, and the separation between inter- and/or intra-cluster ionic migration and electronic conduction could not be identified. In summary, when the inorganic phase was introduced into the polymeric matrix, noticeable changes in impedance behavior (ca. figures 28 and 29) and in film morphology (as will be indicated later) were observed. It could be noticed that the obtained diagrams do not represent perfect semicircles that is generally attributed to the frequency dispersion. They present a capacitive loop that increases in diameter when the applied d.c. potential decreases. This indicates a dramatic change in the conduction mode through the film. The semicircle at the high frequency region starts to be followed by a

Table 13. EIS fitting data of polymer/inorganic layers coated over Pt surface for 10 cycles (polymer)/1 min (inorganic layer) and tested in TBAHFP / AcN

E / V	R_u / Ω.cm^2 x 10^2	R_p / Ω.cm^2 x 10^5	W x 10^{-2} F.cm^2	C_c x 10^{-5} F.cm^2
-0.5	1.990	0.378	3.215	2.858
-0.2	7.151	2.128	3.856	7.804
0.0	6.601	2.529	3.562	5.817
0.2	1.295	5.386	2.765	3.697
0.4	1.474	59.93	2.958	8.480
0.5	2.138	6.429	2.958	84.84
0.6	1.027	5.429	1.958	8.485
0.8	7.302	2.658	1.535	18.02
1.0	1.372	0.398	1.224	11.69
1.2	3.318	0.313	1.171	9.929

Table 14. EIS fitting data of polymer/inorganic layers coated over Pt surface for 10 cycles (polymer)/5 min (inorganic layer) and tested in TBAHFP / AcN

E / V	R_u / Ω.cm^2 X 10^2	R_p / Ω.cm^2 X 10^5	C_f / F.cm^2 x 10^{-6}	CPE / $\Omega^{-1}.s^n$ x 10^{-3}	n
-0.5*	1.098	0.108	1.571	1.264	0.699
-0.2*	1.267	0.170	2.246	1.735	0.731
0.0*	1.401	1.635	4.499	3.256	0.792
0.2	1.385	1.283	5.434	3.229	0.915
0.4	1.329	10.79	3.444	2.830	0.782
0.5	1.146	0.925	1.768	1.367	0.710
0.6	1.098	0.636	1.631	1.281	0.707
0.8	1.069	0.675	1.811	8.532	0.671
1.0	1.131	0.132	1.790	5.926	0.646
1.2	9.483	0.128	1.176	2.522	0.552

change to a straight line for $E_{appl.} < 1.2$ V. In the later case, the contribution of the bulk capacitance associated with the dielectric polarization of the polymer chains caused by the alternating field starts to be realized. At high frequencies, on the other hand, the impedance of the bulk resistance, R_p, and capacitance, C_f or C_c, approach the same magnitude. Both resistance and capacitance of the bulk

contribute significantly to the overall impedance. Therefore, for relatively smaller dipping time (ca. 1 minute) for inorganic film deposition, the equivalent circuit used is that displayed in figure 20b and that of figure 20a will be used to model the film bearing thicker inorganic layer. (ii) At the relatively low frequency ranges C_f/C_c makes a negligible contribution to the impedance and the straight line starts to develop in the complex impedance plane. The low-frequency response carries information on the film-system/electrolyte interface. Moreover, at any point from the start of the development of the straight line (i.e. at the offset of the semi-circle):

$$C_c/C_f = 1/Z''\omega \qquad (7)$$

Where Z" is the value of the imaginary part of the impedance at a frequency ω, R_u is the effective d.c. resistance at the solid/liquid interface and C_f/C_c is the film capacitance. The highest values for R_p, and C_f/C_c were observed in the case of an applied potential of +0.4 V and +0.5 V, respectively. (iii) The effect of changing the thickness of the inorganic layer was reflected slightly on the decrease in the values of R_u, R_p, and C values respectively (cf. tables 13 & 14 and figures 24-27). The data proves that as the thickening time for the deposition of the inorganic layer increases the rate of charge transfer at the film/electrolyte interface increases and the capacitive charging of the film decreases. Many factors would contribute to this finding; the capacitive loop increases as the film thickness decreases as depicted in figures 25 a and 25b, the bulk and film/electrolytic frequency ranges

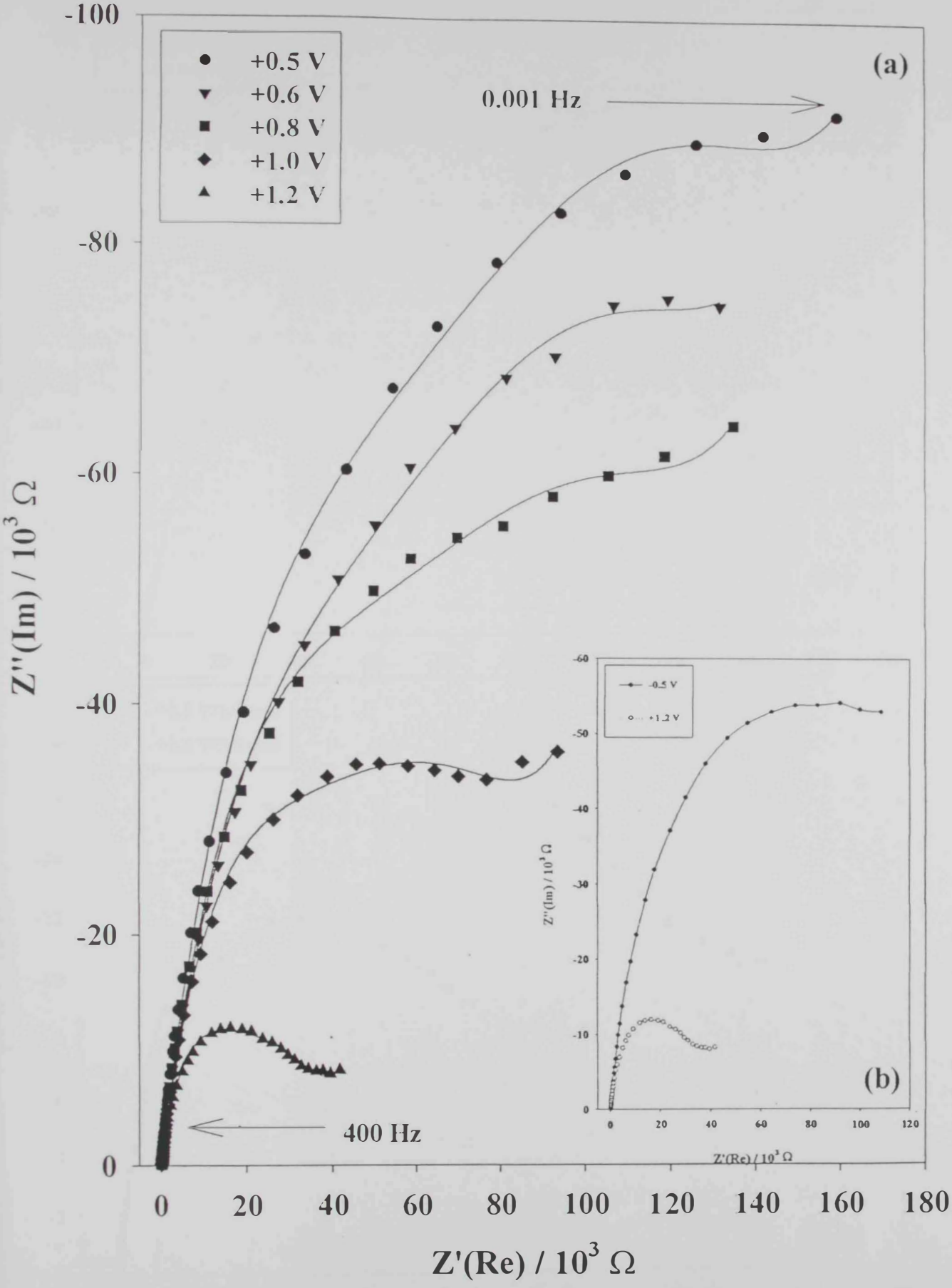
+0.5 V
+0.6 V
+0.8 V
+1.0 V
+1.2 V
(a)
0.001 Hz
400 Hz
-100
-80
-60
-40
-20
0
0
20
40
60
80
100
120
140
160
180
Z''(Im) / 10^3 Ω
Z'(Re) / 10^3 Ω
(b)
-0.5 V
+1.2 V
Z''(Im) / 10^3 Ω
Z'(Re) / 10^3 Ω

Figure 24

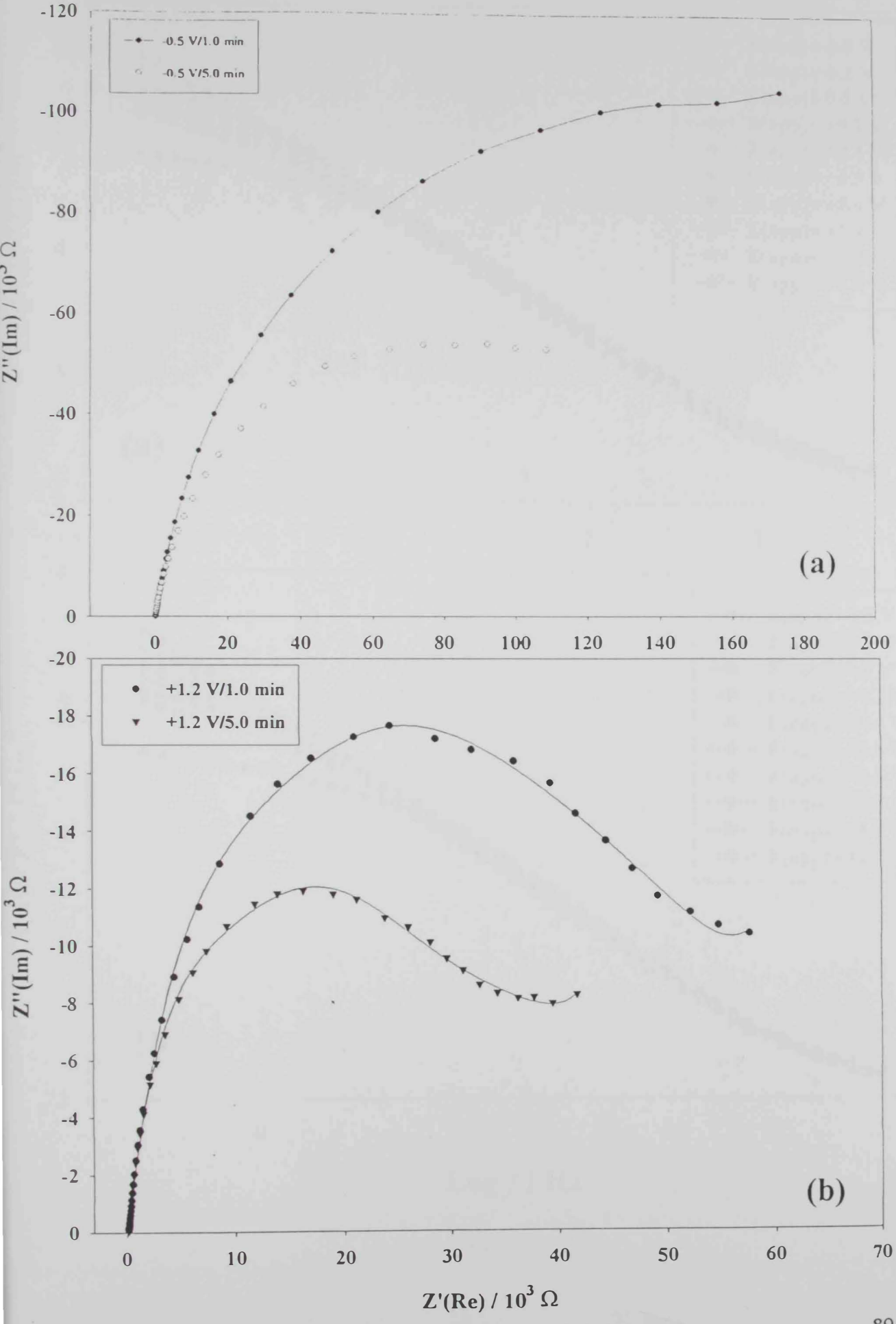

Figure 25

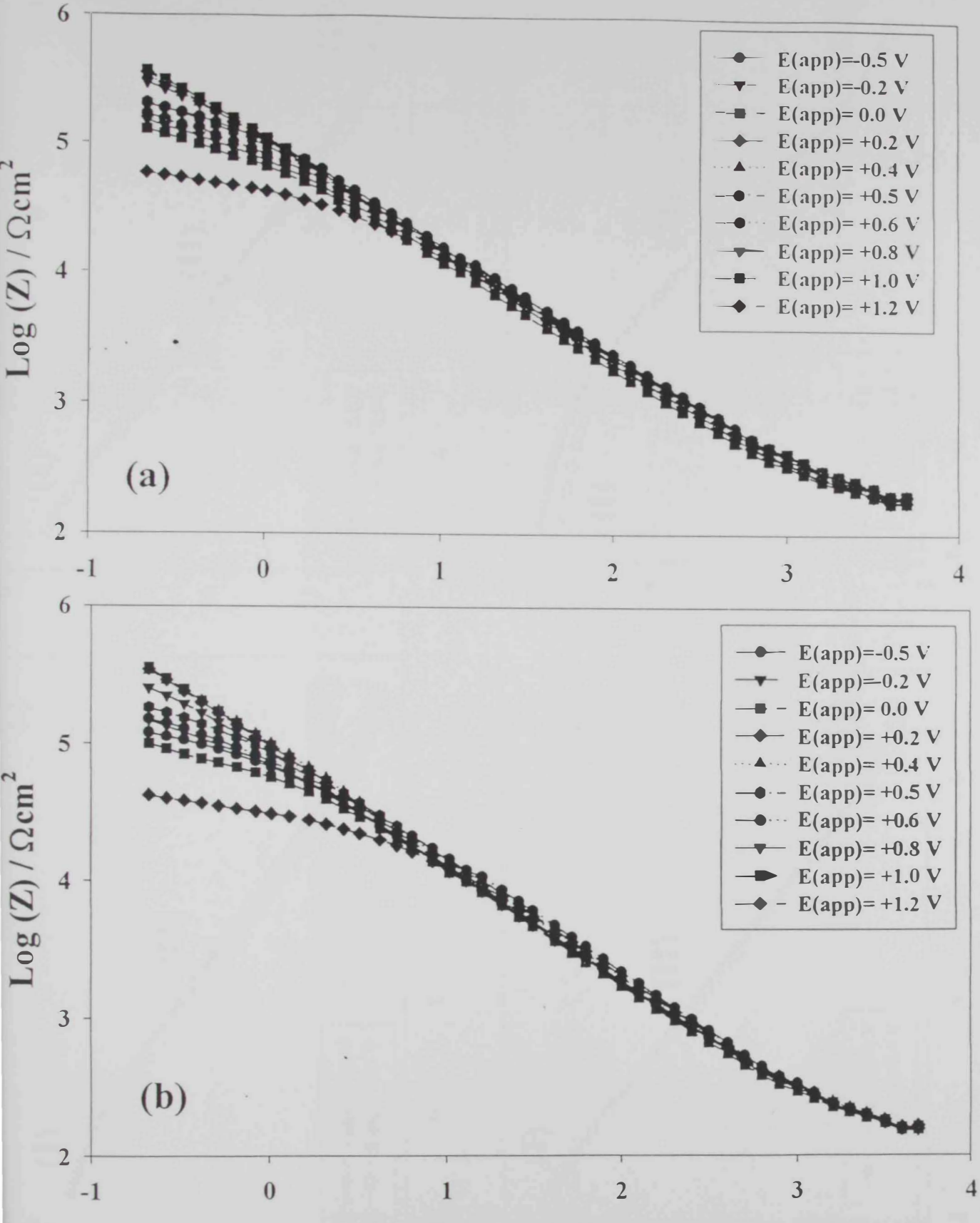
Log (Z) / Ωcm²
E(app)=-0.5 V
E(app)=-0.2 V
E(app)= 0.0 V
E(app)= +0.2 V
E(app)= +0.4 V
E(app)= +0.5 V
E(app)= +0.6 V
E(app)= +0.8 V
E(app)= +1.0 V
E(app)= +1.2 V
(a)
(b)
Log f / Hz

Figure 26

(a)
(b)
(c)
(d)
(I)
(II)
(III)
1 min / -0.5 V
5 min / -0.5 V
1 min / 0.0 V
5 min / 0.0 V
1 min / +0.4 V
5 min / +0.4 V
1 min / +1.2 V
5 min / +1.2 V
Log (Z) / Ωcm²
Log f / Hz

Figure 27

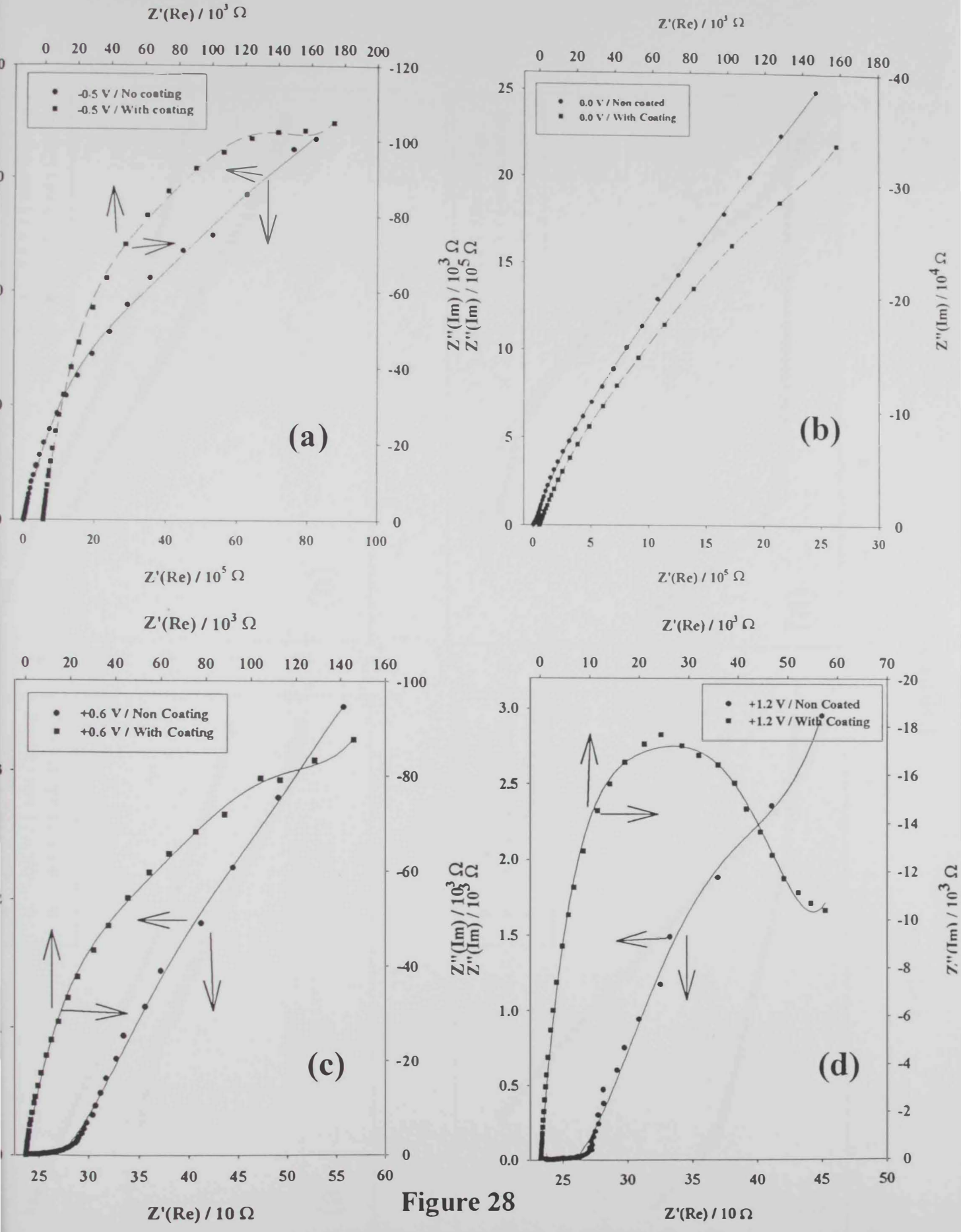
Z'(Re) / 10³ Ω
-0.5 V / No coating
-0.5 V / With coating
(a)
Z'(Re) / 10⁵ Ω
Z'(Re) / 10³ Ω
0.0 V / Non coated
0.0 V / With Coating
Z''(Im) / 10³ Ω
Z''(Im) / 10⁵ Ω
Z''(Im) / 10⁴ Ω
(b)
Z'(Re) / 10⁵ Ω
Z'(Re) / 10³ Ω
+0.6 V / Non Coating
+0.6 V / With Coating
(c)
Z'(Re) / 10 Ω
Z'(Re) / 10³ Ω
+1.2 V / Non Coated
+1.2 V / With Coating
Z''(Im) / 10³ Ω
Z''(Im) / 10³ Ω
(d)
Z'(Re) / 10 Ω

Figure 28

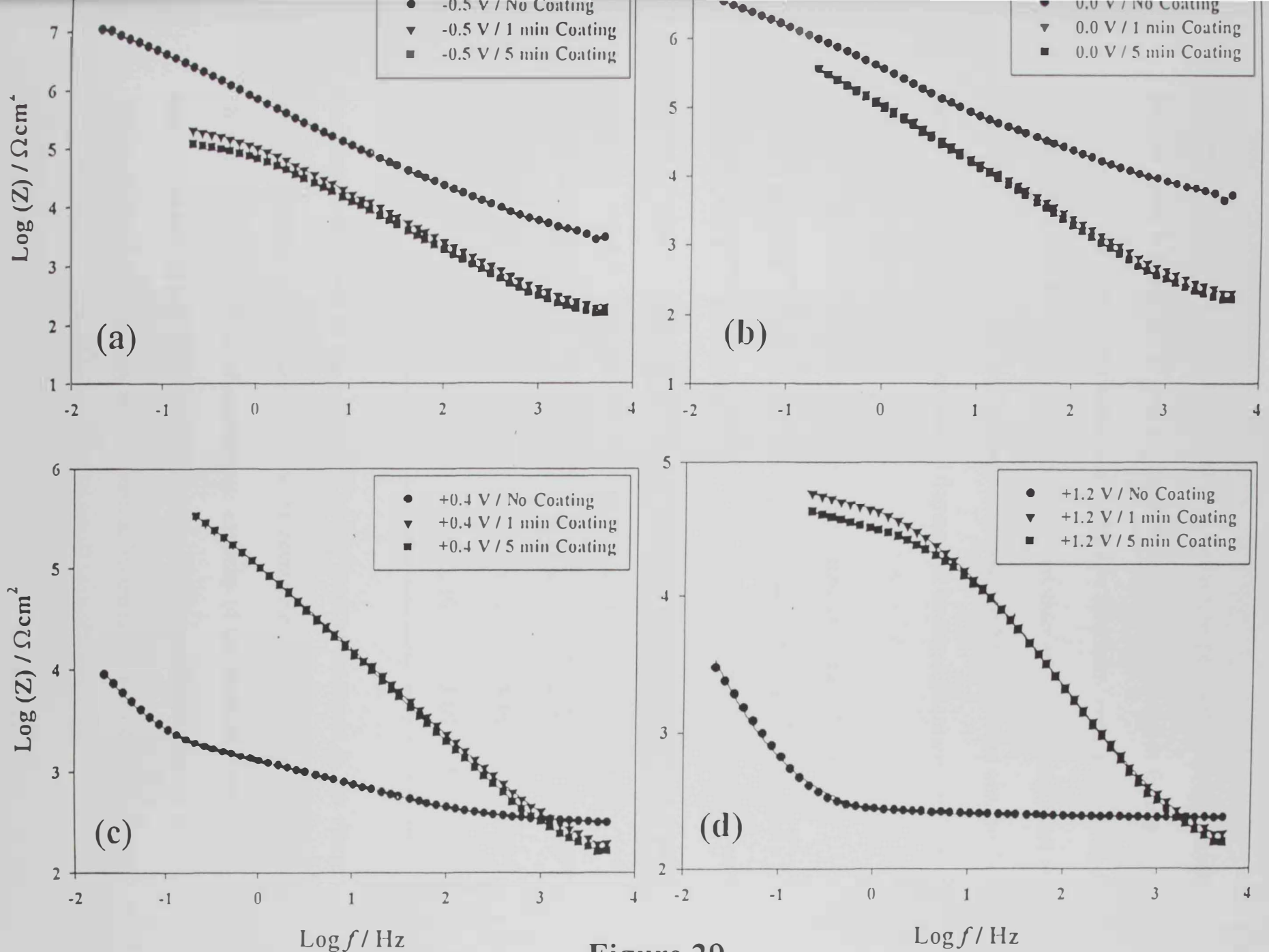
-0.5 V / No Coating
-0.5 V / 1 min Coating
-0.5 V / 5 min Coating
(a)
0.0 V / No Coating
0.0 V / 1 min Coating
0.0 V / 5 min Coating
(b)
+0.4 V / No Coating
+0.4 V / 1 min Coating
+0.4 V / 5 min Coating
(c)
+1.2 V / No Coating
+1.2 V / 1 min Coating
+1.2 V / 5 min Coating
(d)
Log (Z) / Ωcm²
Log f / Hz

Figure 29

(i.e. the relatively large and medium frequency ranges, respectively as indicated by regions I and II in figures 27 a-c) are almost identical as depicted in figures 26a and 26b, and the noticeable change was in the low frequency ends as the charge transfer within the film prevails the process of conduction. It was important to notice that departure from equivalency of impedance behavior was noticed for films subjected to extreme potentials of doping and un-doping as shown in figures 27a and 27d, respectively.

Table 15. Electrochemical data from simulation calculations

Film	E_{appl} / V	CPE / Ω^{-1} s^n	N	Y_o / Ω^{-1} cm^{-2} $s^{0.5}$	B ($s^{0.5}$)	D_i / cm^2 s^{-1}
PMT	-0.2	2.788×10^{-3}	0.6	2.77×10^{-3}	0.97	6.24×10^{-8}
	0.0	4.101×10^{-3}	0.6	3.45×10^{-3}	0.84	3.76×10^{-9}
	+0.6	2.050×10^{-3}	0.9	9.81×10^{-3}	0.80	1.17×10^{-8}
PMT +	-0.2	-	-	2.88×10^{-3}	2.90	1.05×10^{-9}
Inorg.	0.0	-	-	3.50×10^{-3}	3.38	3.66×10^{-10}
Film	+0.6	-	-	3.00×10^{-3}	3.80	1.08×10^{-10}

One important aspect of the utilization of this class of materials is the charge storage capability and the facilitation of the reversible charge/discharge -ability. Thus, the evolution of the charge-storage capacity of the modified films of this class of conducting polymers with the applied potential is shown in figure 30a. A clear increase in this capacity as the potential becomes more anodic is observed.

The charge storage capacity has insignificant values at potentials where the film is in a neutral (i.e. when the film possess a relatively high resistance) state, and at relatively high positive potentials where the film is "highly" oxidized. This variation in the capacity with potential can be explained qualitatively if we take into consideration that the capacitive processes are associated with charge displacements. At cathodic potentials, the PMT film is in relatively low conducting state and is forming polar sites that, prevents the transit of ions across the films. The amount of charge able to move in this medium is low and the resulting capacity is also low. At more anodic potentials the polymeric medium is more polar since the PMT is approaching its oxidized and fully doped state [85], and with anions compensating the positive charges in the polymeric chains. Therefore, the amount of charge able to move in this polar medium is greater and the capacity increases. The evolution of the capacity with potential is similar to that observed on a voltammogram measured in the presence of the supporting electrolyte. Moreover, voltammograms measured with only capacitive charge passages taken into account [102], are in good agreement with the results found in this work. A possible explanation would be that the polymer film behaves as a variable capacitor. The unique shape of the voltammogram would be due to the particular variation of this capacity with the doping level of the polymer that varies with the applied potential. A general increase in the charge storage capacity as the thickness of the film increases was also observed. This can be noticed as displayed in figure 30b. When comparing the polymer film with that modified

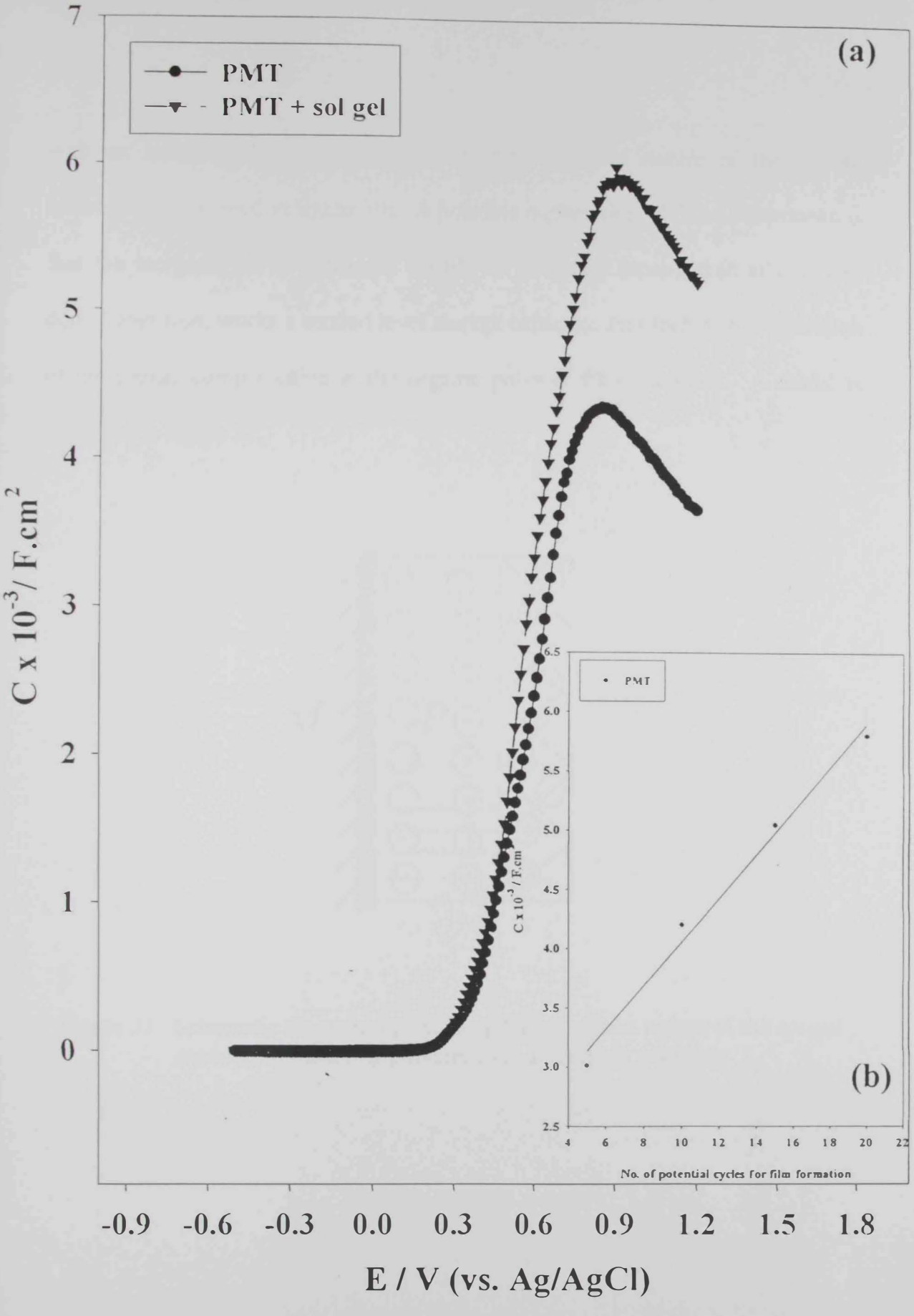
(a)
PMT
PMT + sol gel
C x 10^-3 / F.cm^2
E / V (vs. Ag/AgCl)
(b)
PMT
C x 10^-3 / F.cm
No. of potential cycles for film formation

Figure 30

with an inorganic layer, we found that the capacitive nature of the system increases as indicated in figure 30a. A possible explanation of this phenomenon is that the inorganic layer composed mainly of inorganic cross-linked silicate and doped with iron, works a second level storage capacitor that forbids the saturation of the charge compensation at the organic polymer film boundary. A model is proposed in figure 31.

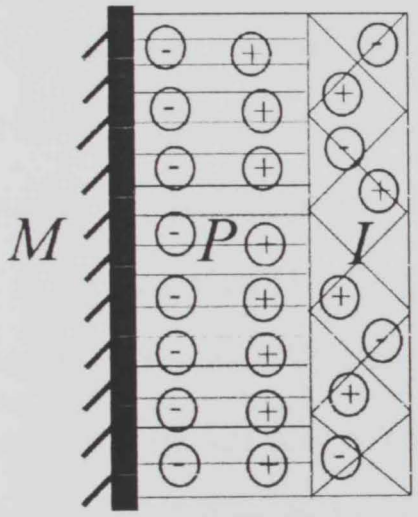

Figure 31. Schematic diagram representing the capacitive nature of the sol-gel modified conducting polymer over a platinum substrate

3.5 Characterization of the inorganic Film material

3.5.1 Thermogravimetric analysis

TG-DTG of the dried gel precursor for the film material carried out in helium and airflow are shown in Fig. 32 and Fig. 33, respectively. The TG curves, exhibited a total weight loss amounts to 39.97 and 41.87% upon heating from room temperature up to 600°C in helium and airflow, respectively. The TGA curve for the analysis carried out in helium shows a group of peaks at 152, 191, 267, and 395°C. The corresponding TGA curve for the analysis carried out in air shows a similar group of peaks at 151, 199, 261, and 352°C, however. The shifting of the DTG peak observed at 267°C (in helium) to 261°C (in air) indicates its association with combustion of organic species. This also reflected from the sharpening of the peak in the case of air (Fig. 33) in comparison to the case of helium (Fig. 32), respectively. The other DTG peaks observed at 152 and 191°C (in helium) or at 151 and 199°C (in air), may be due to the loss of adsorbed (or included) water and organics, see FTIR results below.

Figure 34 shows typical TG-DTG curves for a module film deposited on a glass-slide (used for light microscope) and previously dried for 24 h at 60°C. The TG curves (in air) exhibited a total weight loss amounts to 21.89% upon heating from room temperature up to 600°C. This value is much less than the value observed for the bulk precursor (non-film sample). This observation indicates that effective evaporation of the solvent and /or adsorbed material was achieved during drying of the module film at low temperature (60°C).

TGA curve for the module film shows a large maxima, which starts at 100°C, ends at ~ 280°C, and maximize at 184°C. However, more than 17.12% weight loss (out of 21.89% total weight loss) occurred by the end of this peak. In addition, other minor peaks were recorded at 326 and 419°C, which are associated with hydroxyl group condensation and cross-linking of the module film material. Table 16 shows weight loss % recorded upon heating of portions of the dried gel precursor material from room temperature up to a series of successive temperatures (100, 150, 200, 250, 300, 350, 400, 500, and 600°C). Heating was carried out at 10°C/min up to the desired temperature and then followed by holding at that temperature isothermally for 60 min in flow of helium.

Table 16: weight loss % recorded upon heating of the dried precursor for the film material from room temperature up to a series of successive temperatures.

Temperature, °C	Weight Loss %
100	14.995
150	25.551
200	30.887
250	34.747
350	34.766
400	35.753
500	36.597
600	36.132

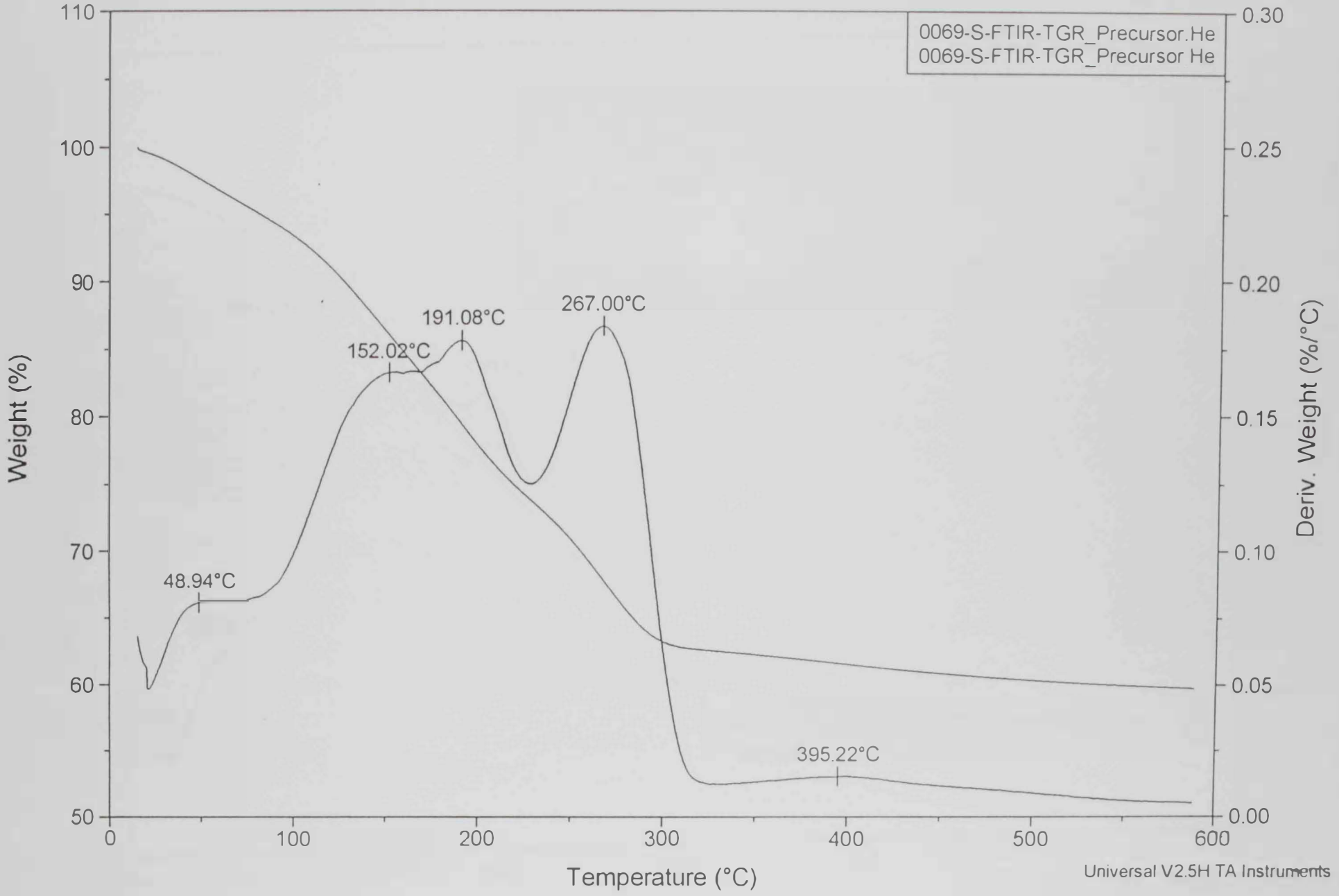
0069-S-FTIR-TGR_Precursor.He
0069-S-FTIR-TGR_Precursor He
Weight (%)
Deriv. Weight (%/°C)
Temperature (°C)
48.94°C
152.02°C
191.08°C
267.00°C
395.22°C
Universal V2.5H TA Instruments

Figure 32

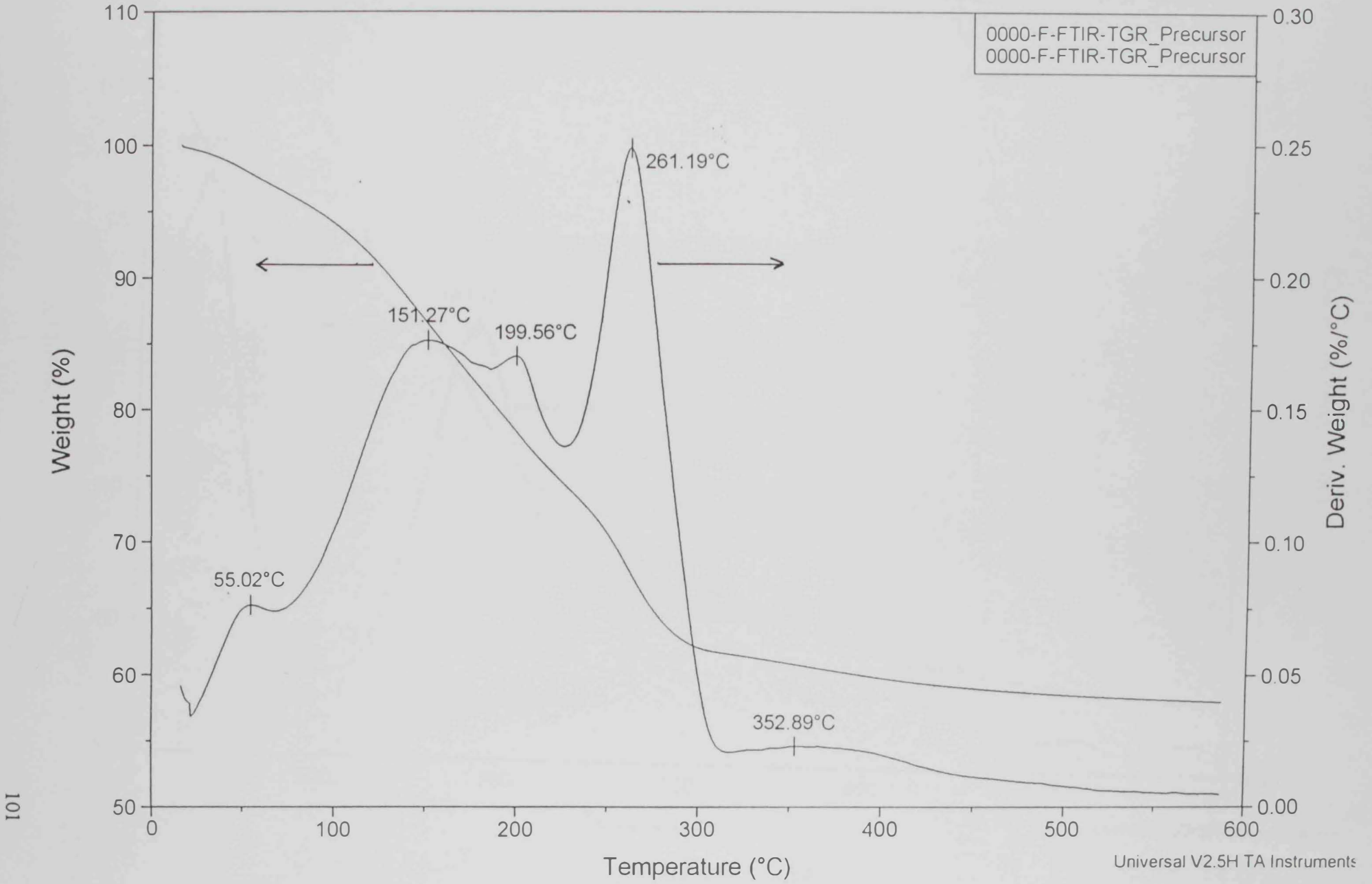
0000-F-FTIR-TGR_Precursor
0000-F-FTIR-TGR_Precursor
261.19°C
151.27°C
199.56°C
55.02°C
352.89°C
Weight (%)
Deriv. Weight (%/°C)
Temperature (°C)
Universal V2.5H TA Instruments
110
100
90
80
70
60
50
0.30
0.25
0.20
0.15
0.10
0.05
0.00
0
100
200
300
400
500
600

Figure 33

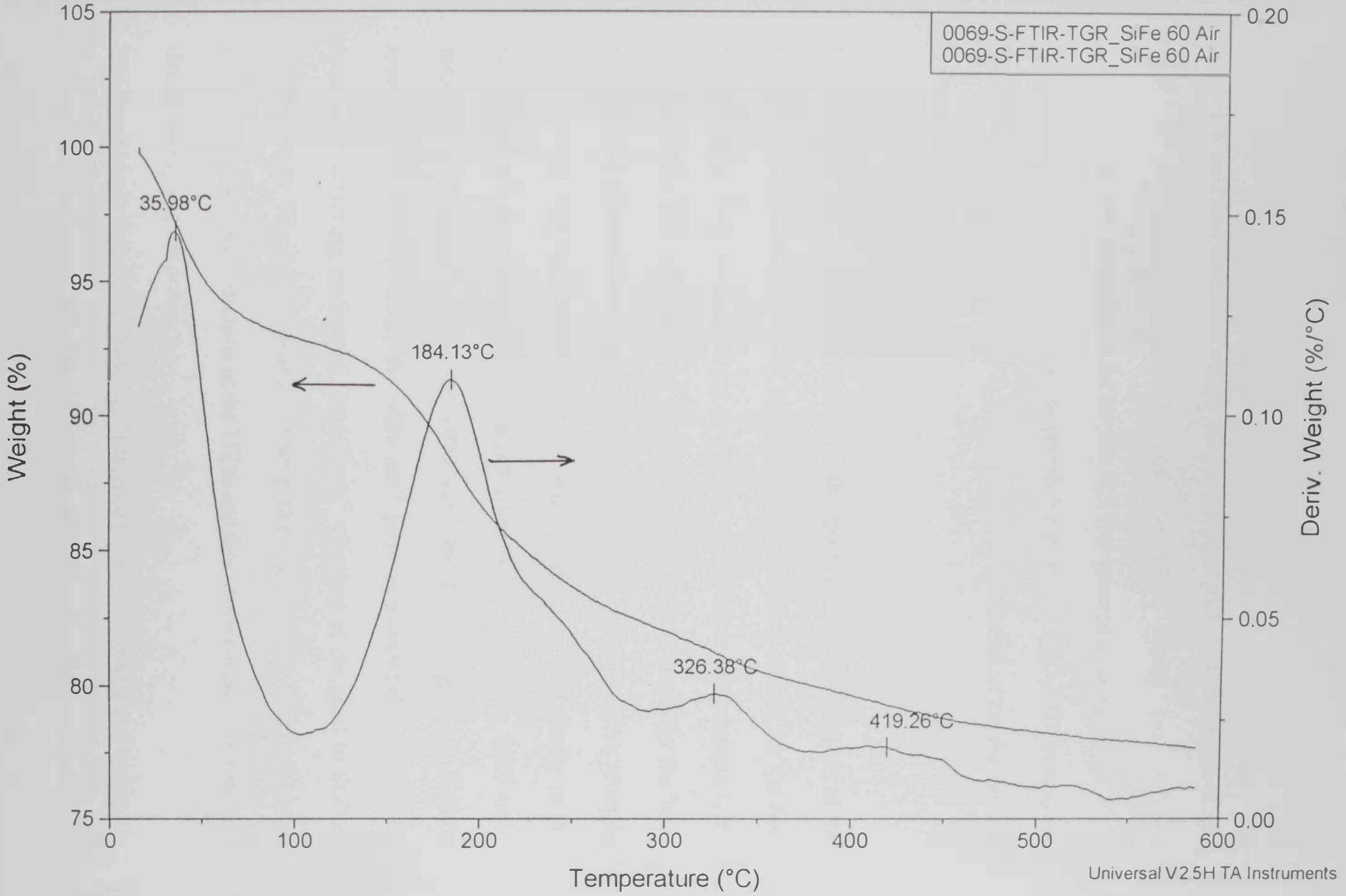
0069-S-FTIR-TGR_SiFe 60 Air
0069-S-FTIR-TGR_SiFe 60 Air
35.98°C
184.13°C
326.38°C
419.26°C
Weight (%)
Deriv. Weight (%/°C)
Temperature (°C)
105
100
95
90
85
80
75
0.20
0.15
0.10
0.05
0.00
0
100
200
300
400
500
600
Universal V2.5H TA Instruments

Figure 34

The table indicates that, most of the recorded weight loss occurred at 300°C. In light of the above TGA results and the FTIR results (see below), 350°C calcinations temperature for the test film was selected as an optimum temperature, which is high enough to permit the proposed Fe_2O_3/SiO_2 composite film formation and mild enough to prevent severe deformation of the conducting polymer layer.

3.5.2 FTIR spectroscopy

Figures 35a and 35b show FTIR results for the solid produced by pyrolysis of the bulk precursor material, obtained by heating of the dried precursor for the film material from room temperature up to a series of successive temperatures (100, 150, 200, 250, 300, 350, 400, and 500°C), as described previously for the TGA analysis. The Spectrum observed for the material heated at 100°C show a group of peaks at 450, 792, and 1070 cm^{-1}, these peaks position are very similar to the peaks reported for completely hydrolyzed silica gel at 460, 800, 1080 cm^{-1}, respectively [135,136]. Thus, the 1070 cm^{-1} band is assigned to Si-O-Si asymmetric stretching mode, the ~800 cm^{-1} peak is associated with Si-O-Si symmetric stretching mode, and the 450 cm^{-1} vibration is assigned to Si-O-Si bending mode. The absence of any distinct peaks in the 2800 – 3000 cm^{-1} region indicate the complete hydrolysis of the TEOS and that re-esterification of silica gel during drying was not occur.

The broad bands cenered at ~3440 cm^{-1} assigned to various isolated and hydrogen-bonded SiO-H stretching vibrations, the 1628 cm^{-1} assigned to the stretching mode

of the molecularly adsorbed H_2O. Other peaks observed at 1388, 1691 cm^{-1} are assigned to adsorbed nitrate and formamide species, respectively.

Upon heating, the adsorbed nitrate and formamide species are effectively desorbed as low as 250°C, see Fig 35a, note that formamide boiling point is 210°C. Samples heated at >250°C indicted complete desorption of the nitrate and organic species. No much changes were observed upon heating the precursor material at 300°C and up to 500°C, see Fig 35b.

3.5.3 SEM microscopy

SEM micrograph of the dried module film obtained on glass substrate is shown in Fig. 36. In spite of the observed cracking, due to the thickness of the module film, it was cohesive and well adhesive to the substrate. Coherent area as wide as 20 – 30 μm was observed. The film thickness was observed by tilting of the sample holder by 45° angle, Fig. 37, under the electron beam, a thickness of 3 - 4 μm was estimated. SEM micrograph of a module film calcined at 350°C for 60 min, Fig. 38, showed the development of some porosity and the evolution of micro grain boundaries.

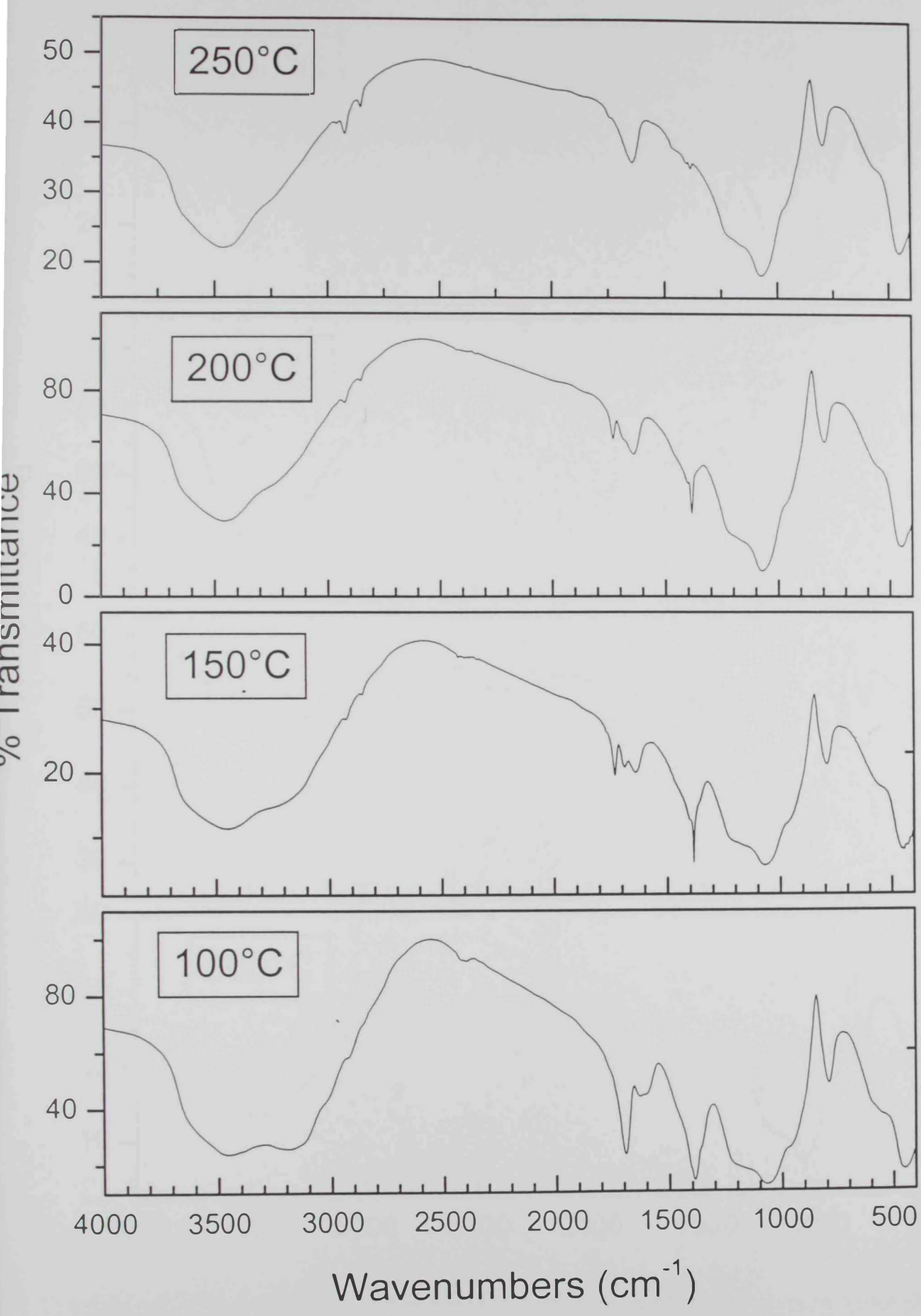
250°C
200°C
150°C
100°C
% Transmittance
Wavenumbers (cm-1)
4000
3500
3000
2500
2000
1500
1000
500

Figure 35a

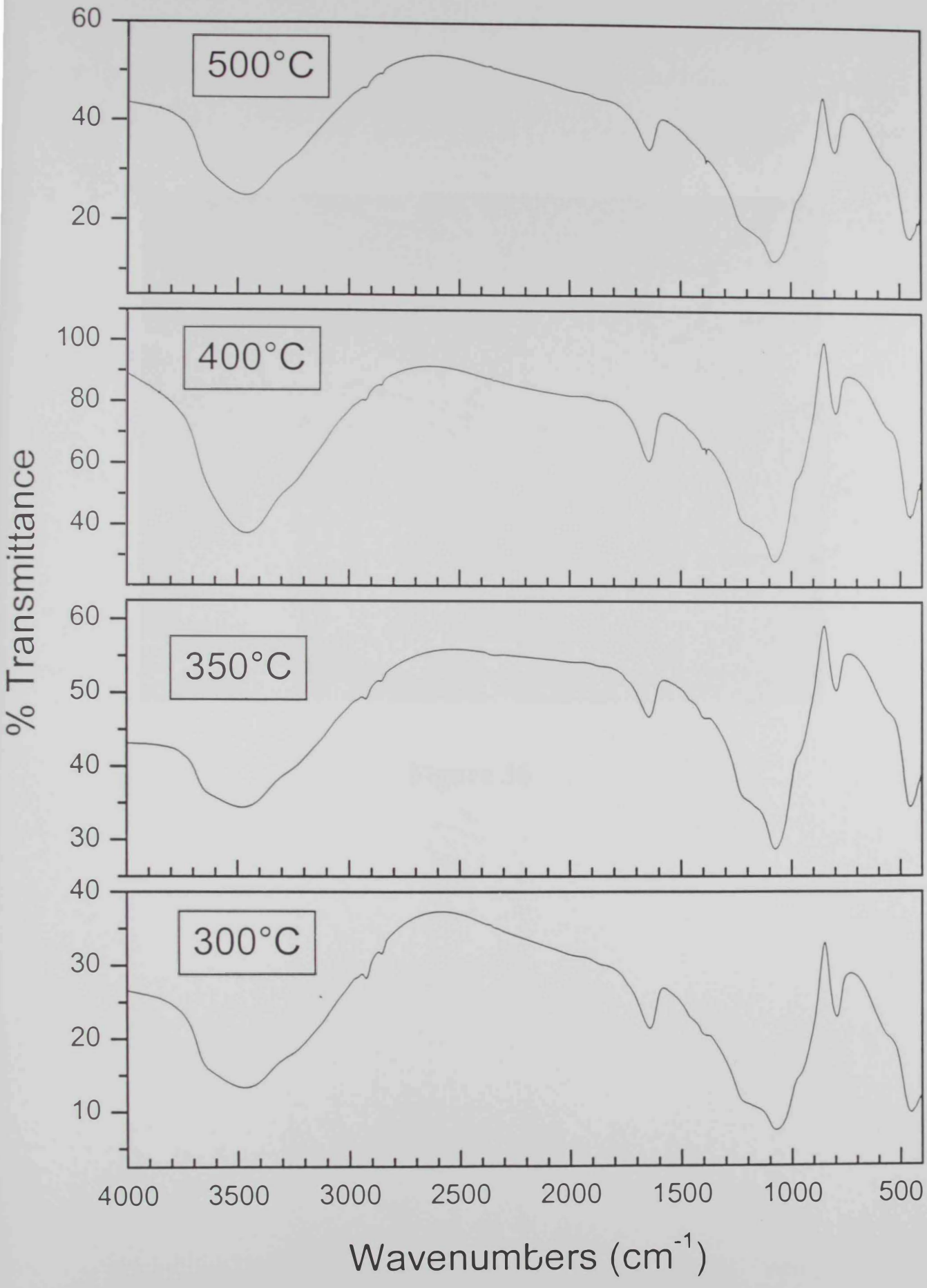
500°C
400°C
350°C
300°C
% Transmittance
Wavenumbers (cm-1)
4000
3500
3000
2500
2000
1500
1000
500

Figure 35b

Figure 36

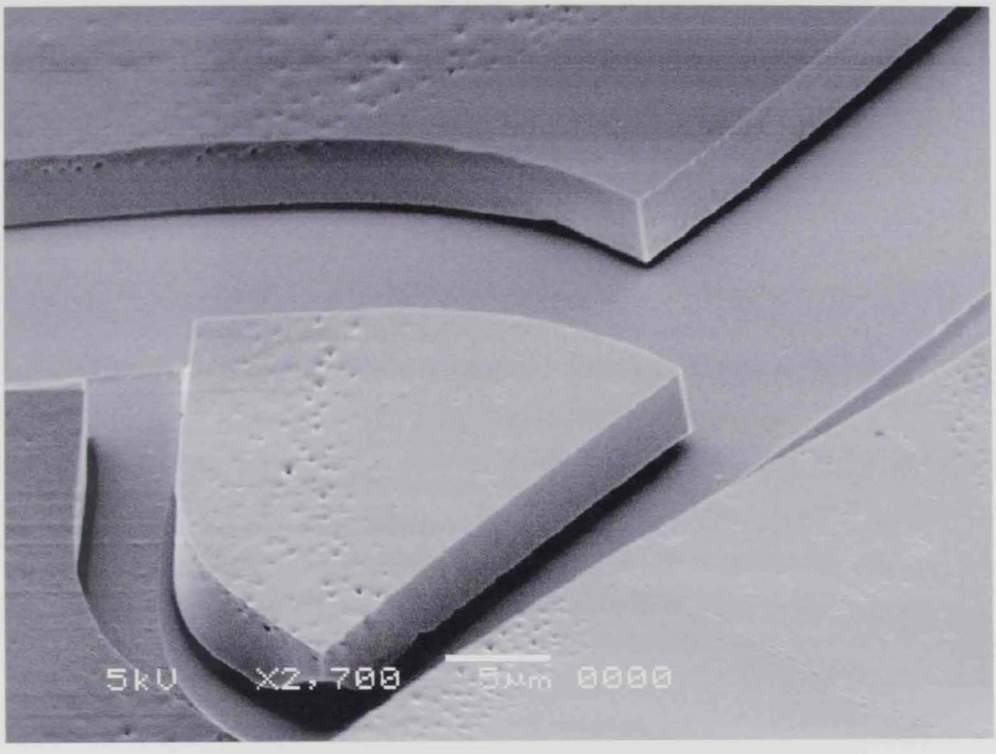

Figure 37

Figure 38

3.6 Surface, spectroscopic, and thermal characterization of the polymer/inorganic hybrid films

In order to ascertain the aforementioned suggestions regarding synthesized film behavior and characteristics, surface investigations were inevitable in order to gather further information of the structural aspects of the film. Three important measurements were performed on the as-grown films, namely scanning electron microscopy (SEM), energy dispersive X-ray analysis (EDXA), and Fourier transform infrared spectroscopy (FTIR).

3.6.1 Scanning electron microscopy of PMT and polymer/inorganic hybrid

Scanning electron micrographs of PMT thin films showed that the surface is regular and homogeneous and does not show the spheroid-like defects of other conducting polymers [137]. Figure 39a depicts the SEM of a PMT formed upon scanning the applied potential between –0.2 V and +1.75 V (vs. Ag/AgCl) for 20 cycles. The film is expected to have a thickness of about 40 μm, however, it showed a relative homogeneous structure with well-defined defects after heating at 350 °C for 15 minutes. A porous structure was also expected for relatively thick films as was found earlier with similar polymeric classes [138]. For the sake of comparison, the candidate prepared three samples; for the first, a polymer layer was deposited at platinum substrate and its SEM picture is depicted in figure 39a, for the second an inorganic layer was deposited at a platinum substrate and the coating process took 1 minute (cf. figure 40a), the third was a polymer layer coated with the inorganic layer and its SEM picture is shown in figure 41a. All samples were heated according to the following scheme: the film was first washed

thoroughly with de-ionized water and then subjected to drying in oven at 60 °C for 30 minutes, then was "fired" at 350 °C for 15 minutes. The samples were then desiccated and presented for the surface measurements. As could be noticed for the inorganic layer-covered platinum (cf. figure 40a), the film is mainly formed of a cracked silicon layer forming platelets of average dimension of about 5-20 μm. The cracking of the film is mainly due to the incompatibility between the thermal coefficients of the film and the substrate. The film is mainly composed of oxygen, silicon, and iron with elemental composition of 18.34%, 8.29%, and 1.42%, respectively (and the rest composition is platinum). It is obvious at this stage that, the film contains iron-doped silicon oxide. EDXA diagram for this film is given in figure 40b. The morphology of the resulting film after modifying the polymer with the inorganic hybrid depended on the thickness of the organic layer substrate and the time of deposition of the inorganic layer. Thus, as shown in figure 41a for 20 cycles organic polymer/1 minute inorganic layer, a one-minute coating resulted in nicely dispersed particles of diameters ranging from 20 – 100 nm. The majority of the particles though are in the range of 20 nm. The near perfect distribution of the particles indicates that the nucleation of the inorganic particles takes place at some specific active centers at the polymer surface. This finding is of prime importance, namely for the field of surface catalysis. The structure of the film as revealed by the EDXA analysis (cf. figure 41b) showed the incorporation of the inorganic particles with identical composition as that depicted in figure 40b. The

film composition is: oxygen (34.54%), carbon (19.31%), silicon (11.29%), sulfur (7.85%), iron (1.36%) and the rest composition is platinum. Large deposition time (ca. 10 minutes) resulted in an irregular inorganic film that showed accumulation of the particles in the form of chunky plates as shown in figures 42a and 42b. Average time of deposition (ca. 5 minutes) resulted in inorganic particle well imbedded in the polymer film as depicted in figure 43a. It is obvious that the phases of the film are distinctly different in the three cases displayed in figures 41a – 43a. Thus, while a two phase discrimination are identified in SEM micrograph of figure 41a for the polymer and the inorganic particles, a thick layer of non-defined phase separation was found for the long period dipping in the inorganic coating electrolyte (cf. figures 42a and 42b), and a unique half-submerged inorganic particles of silica doped with iron in the organic polymer melt matrix as shown in figure 43a. It could be explained at this stage that the electrical properties described in the previous sections of the polymer/inorganic "hybrid" are in good agreement with the findings of the SEM experiments. For instance, the small time of deposition resulted in the "distinct" phase separation between the organic film/inorganic particles that was manifested in the relatively higher polarization resistance, R_p, and capacitance, C_c, and the use of the modeling circuit that employed a "Warburg" component that expresses the charge diffusion across the electrolyte/film interface. The relative increase in phase homogeneity as shown in figure 43a between the organic polymer phase and inorganic phase resulted in a relative decrease in both R_p and C_c values.

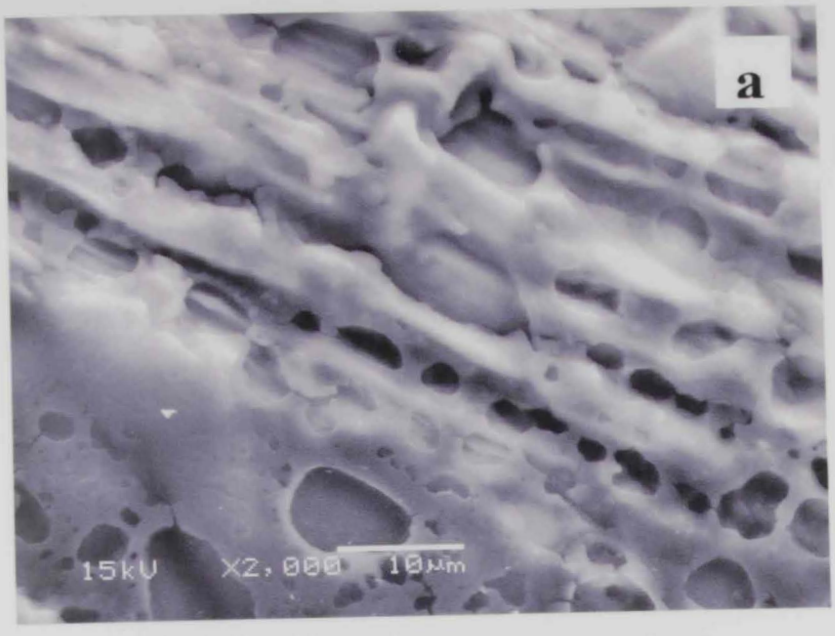
a
15kV X2,000 10µm

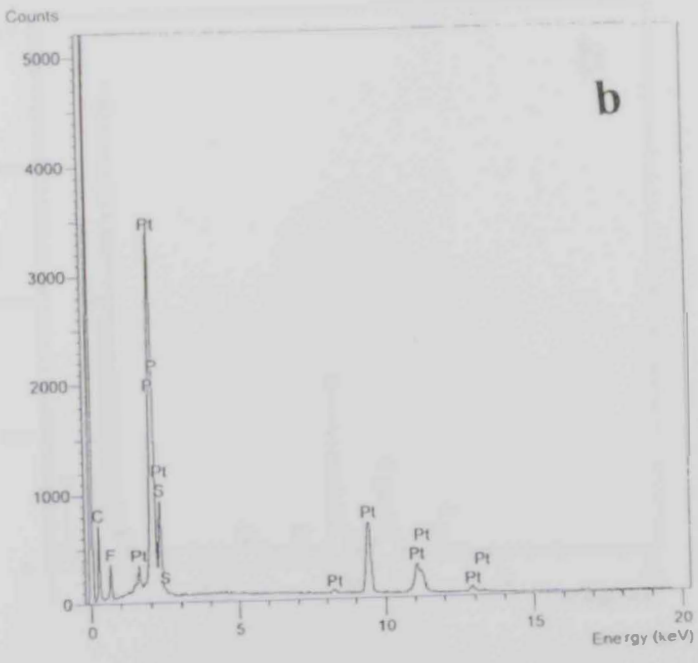
b
Counts
5000
4000
3000
2000
1000
0
Pt
C
F
Pt
Pt
S
Pt
Pt
Pt
Pt
Pt
0
5
10
15
20
Energy (keV)

Figure 39

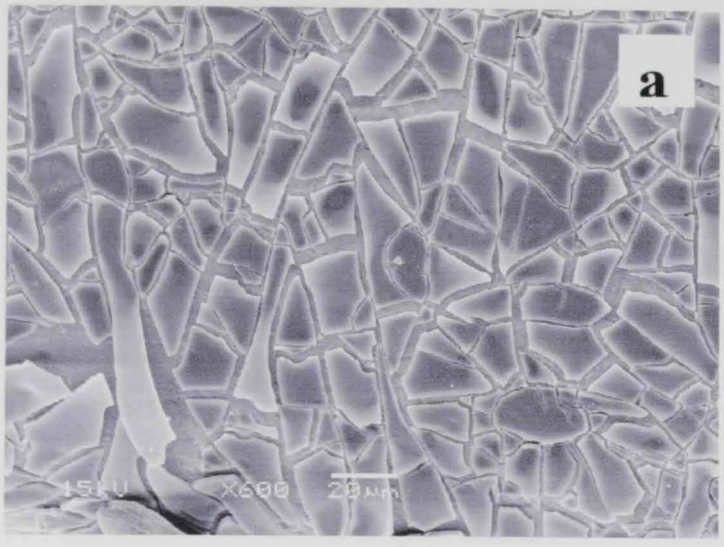
a

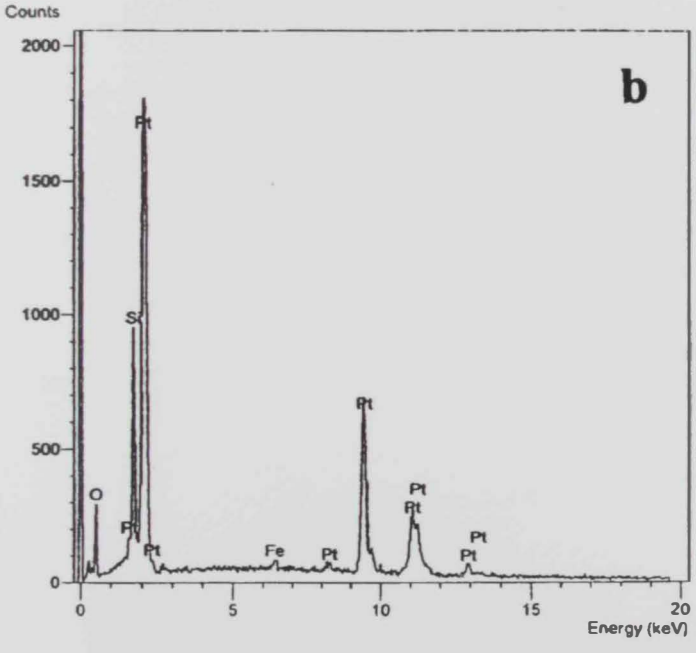
Counts
2000
1500
1000
500
0
b
Pt
Si
O
Pt
Pt
Fe
Pt
Pt
Pt
Pt
Pt
Pt
0
5
10
15
20
Energy (keV)

Figure 40

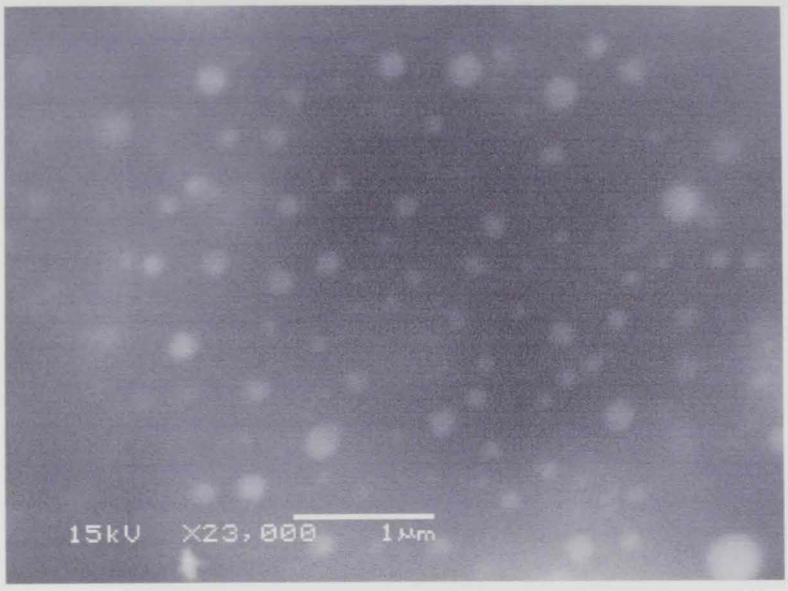
15kV X23,000 1μm

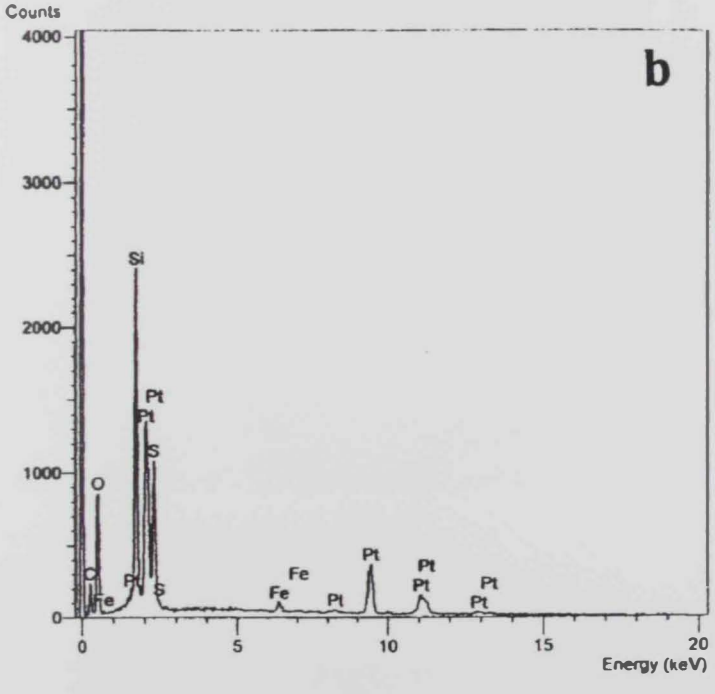
Counts
4000
3000
2000
1000
0
b
Si
Pt
Pt
S
O
C
Fe
Pt
S
Fe
Fe
Pt
Pt
Pt
Pt
Pt
0
5
10
15
20
Energy (keV)

Figure 41

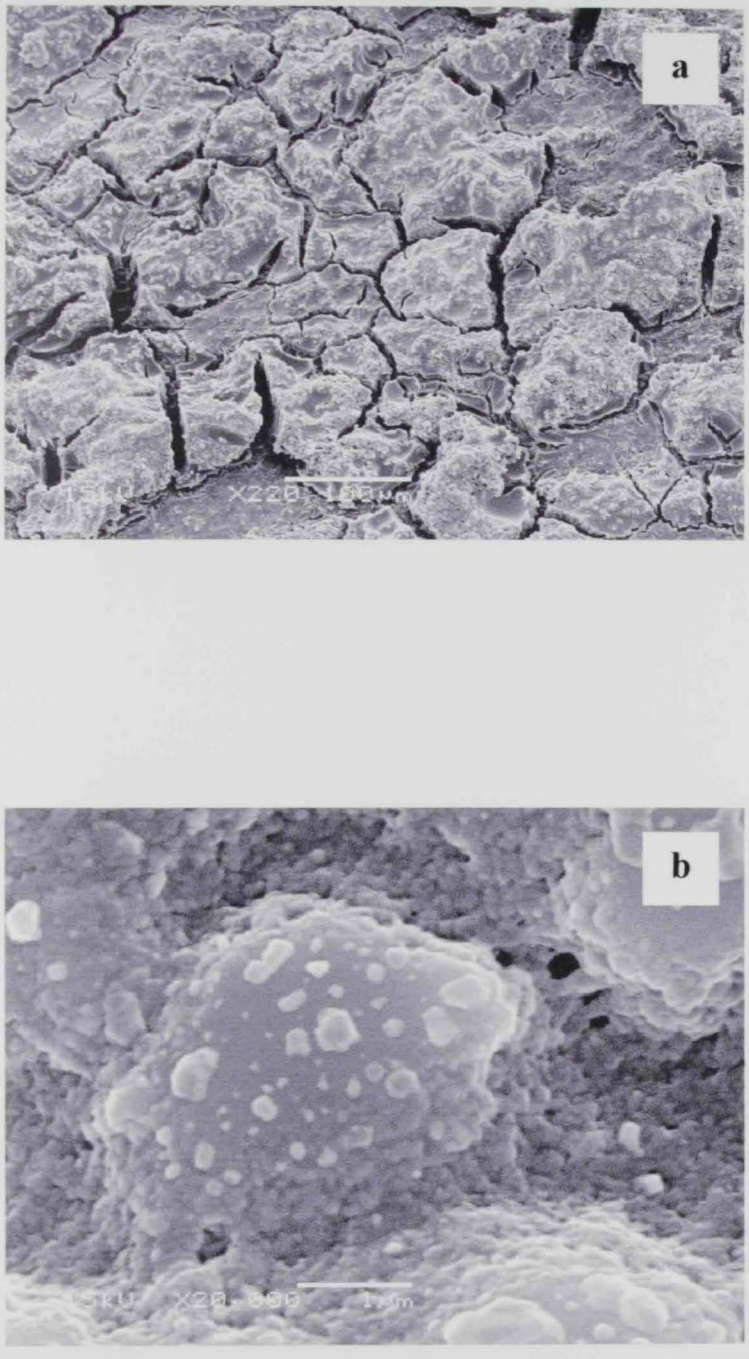

Figure 42

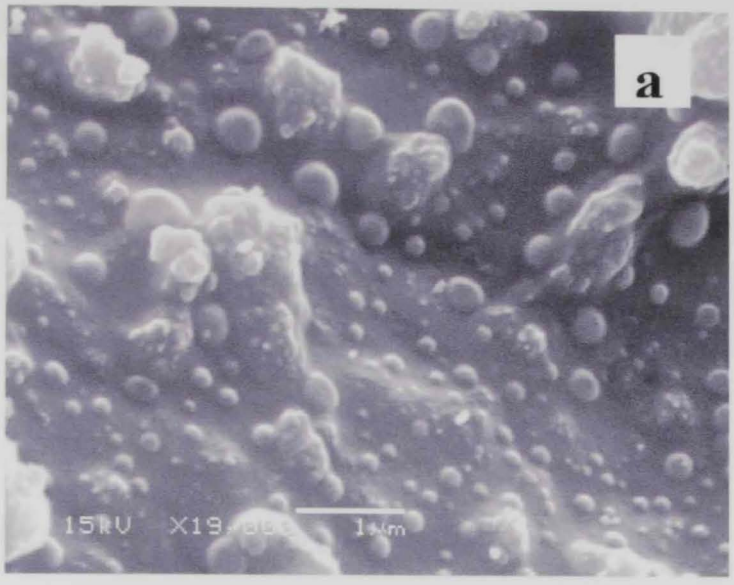
a
15kV X19,000 1μm

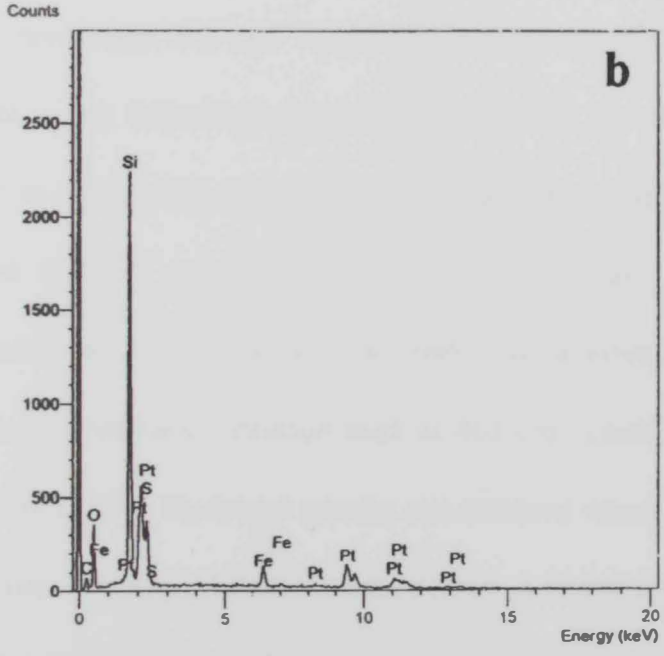
b
Counts
2500
2000
1500
1000
500
0
Si
Pt
O
Fe
Fe
Fe
Pt
Pt
Pt
Pt
Pt
Pt
Pt
0
5
10
15
20
Energy (keV)

Figure 43

3.6.2 Fourier transform infrared spectroscopy of PMT and polymer/inorganic hybrid

The current infrared investigations were aimed to provide molecular-scale information about the polymer film before and after modification. The inorganic layer was prepared from the silicate precursor, TEOS, using an acid-catalyzed process with a large excess of water in the present work. Therefore, it would be advisable to be guided by the assigned framework vibrations cited by Bertoluzza [139], Thorpe [140], and Galeener [141]. The major features of the IR bands were thus observed at 460, 800, 1080, and 1220 cm^{-1}, for the silicate precursor, TEOS. Figures 44a and 44b display the FTIR spectra of KBr pressed pellets of un-modified PMT and hybrid PMT/inorganic films, respectively. The number of scans collected at a resolution of 2 cm^{-1} and with an accuracy of 0.004 cm^{-1}, was 48 for both samples. The following conclusions could be withdrawn from the spectrum displayed in figure 44b; the sharp (and relatively broad) band at 1084 cm^{-1} is assigned to Si-O-Si asymmetric stretching mode, and the 819 cm^{-1} vibration is associated with symmetric Si-O-Si stretching or vibrational modes of ring structures. The well-defined vibration peak at 463 cm^{-1} could be assigned to Si-O-Si bending mode [139]. Hydroxyl groups are eminent when correlating the bands at 974 cm^{-1} that is assigned to Si-OH stretching, a broad band centered at 3304 cm^{-1} that is assigned to isolated hydrogen-bonded SiO-H stretching vibrations and hydrogen-bonded water. We can still notice in the same spectrum of figure 44b shoulders superimposed on the broad band namely at ~3200 cm^{-1} and

~3500 cm^{-1}, respectively. The assignments of the principal absorption bands are: the group of bands between 856 cm^{-1} and 633 cm^{-1} are characteristics of the C-H out-of-plane vibrations, the absorption band at ~840 cm^{-1} is attributed to the ring C-H out-of-plane bending vibration, which is specific for the 2,5-disubstituted thiophene rings, the peak appearing at 1470 cm^{-1} is attributed to the stretching vibration of the 2,3,5-trisubstituted thiophene rings, and the band at 1387 cm^{-1} can be attributed to the deformation vibration of the methyl group. The previous results are in good agreement with those mentioned earlier in the literature [142]. The important observation is the sharpening of the following peaks in the case of the organic/inorganic hybrid film: 1327 cm^{-1}, 1385 cm^{-1}, and 1686 cm^{-1}, respectively. At this stage no further explanation can be given to explain the appearance of these sharp peaks, however, local Fe-Si oxide formation (Fe being the dopant used during the synthesis step), and the presence of the absorption peak at ~530 cm^{-1} is due to the FeO vibration as indicated earlier [143]. Size effects of the nano- to micro-scale particles hybridized within the polymer matrix would have also an effect on the sharpness of these peaks.

3.6.3 Thermal gravimetric analyses for the unmodified and modified polymer films

Thermal analyses were necessary to investigate the changes imparted to the as-grown polymer films and the hybrid samples. Figures 45a and 45b display the thermal gravimetric analysis (TGA) and differential thermal gravimetric (DTG) data for the unmodified and modified polymer films, respectively. TGA curves

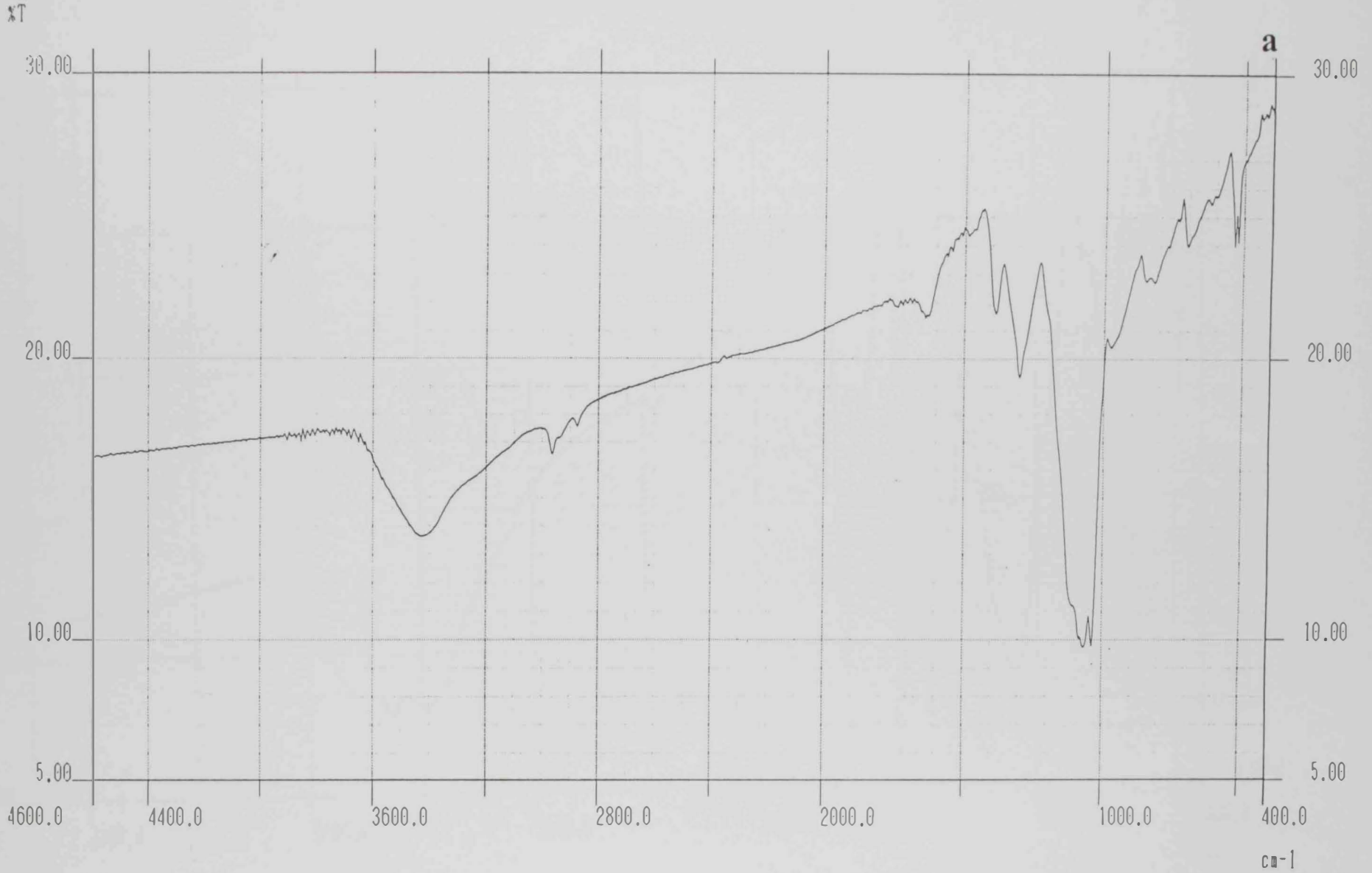
%T
a
30.00
20.00
10.00
5.00
4600.0
4400.0
3600.0
2800.0
2000.0
1000.0
400.0
cm-1

Figure 44

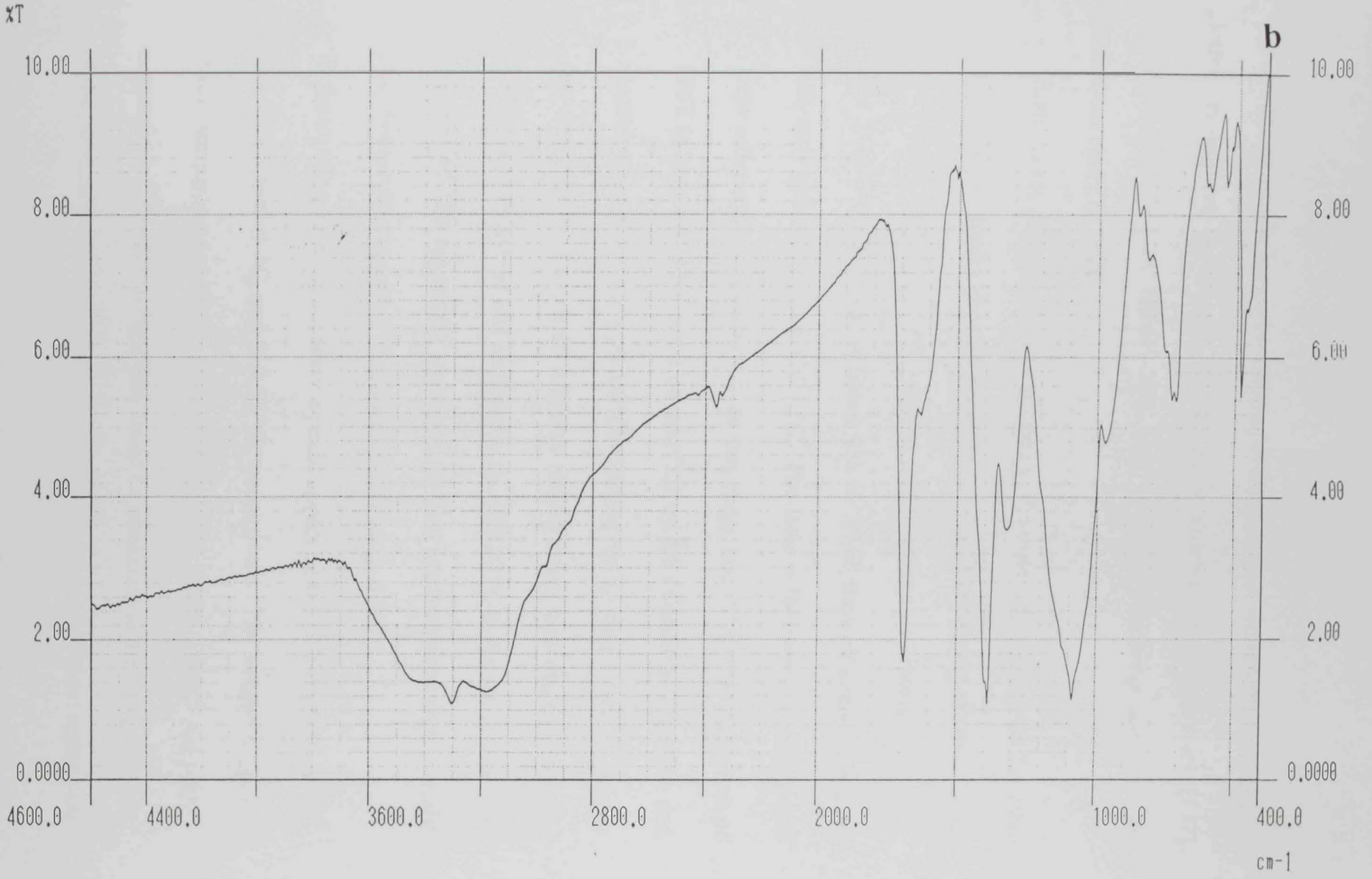
%T
b
10.00
8.00
6.00
4.00
2.00
0.0000
4600.0
4400.0
3600.0
2800.0
2000.0
1000.0
400.0
cm-1

Figure 44

were plotted as weight losses as function of temperature, while DTG curves were plotted as the rate of weight change as a function of temperature [142]. Comparing the data of figures 45a and 45b, the following analyses and conclusions could be withdrawn:

- Both curves did not display a plateau at the onset of heating. On the other hand, both samples showed however, weight loss regions afterwards and the thermal behavior of both samples differs noticeably onward.
- The TGA/DTG behavior of figure 45a for PMT showed a relatively small and early inflection at ca. 38.24 °C. The later is followed by a sharp and large inflection at ca. 92.93 °C. At this stage, about 18% of weight loss of PMT is noticed. This could be justified by the considerable solvent and electrolyte uptake of the polymer film during the synthesis step. A similar one-step peak of inflection at which similar trend was observed for the PMT/Inorganic hybrid was recorded at ca. 133.20 °C as shown in 46b. The silica-based film apparently stabilized the first (solvent/electrolyte) weight loss that resulted in such a temperature shift of ca. 40 °C.
- In figure 45a a series of successive peaks appeared at 169.71 °C, 208.66 °C, 335.82 °C, 596.05 °C, and 818.26 °C, respectively. The weight losses for these temperature transitions are: 25%, 38%, 50%, 80%, and 96%, respectively. The first weight loss could be attributed to the reorganization of the polymer chains that resulted in the decomposition of short superficial

chains The sharp inflection at ca. 335 82 °C is due to the full phase transition of the PMT films to a glassy state. After this temperature an increase in the polymer film volume is expected and accompanied with decomposition This is noticed with a ca 80% of weight loss that reaches near completion (98.15%) at 818.26°C.

- In figure 45b different thermal behavior of the polymer/inorganic hybrid could be noticed at temperatures higher than 133 20 °C. First, the rate of weight loss is slower compared to the case of PMT Second, the stabilization of the polymer phase change and degradation continues with the presence of the inorganic phase. A full degradation was still observed, however, as the temperature of ca. 818.26 °C was reached. At this temperature, a total weight loss of 50.25% was reached and the formation of Si and Fe oxides is expected at this stage (cf. thermal behavior of pure inorganic phase).

The shifts in the temperature of inflections when comparing both figures is attributed to the phase interchange between the organic and inorganic layers. Chain mobility would also be expected to be restricted in the case of modified polymer layers with the coating of the inorganic phase. Two diffusion trends would also be suggested, thus, as two-dimensional chain migration and reconstruction is expected for the organic polymeric layers, an inward three-

dimensional diffusion of the inorganic layer within the polymer layer is likely to take place.

3.6.4 X-ray diffraction analyses

XRD experiments were performed on the organic conducting polymer and on that modified with inorganic iron-doped silica based films. XRD data for the organic polymer film did not display any recognized feature for the presence of a semi-crystalline or metallic feature within the film. Figure 46 depicts XRD data of an iron-doped silica based conducting polymer film. Five distinct peaks at ca. 36.065°, 37.130°, 39.565°, 42.840°, 45.940°, and 46.735° were observed. These relatively strong lines were matched with the tetragonal systems of "cristobalite", stishovite SiO_2, and "clinoferrosilite" $FeSiO_3$ minerals diffraction patterns [144]. The 2-theta and the d-values spacing comparison pointed to (hkl) values of (112), (201), (011), (211), and (111). The fact that the peak width of the relatively high intense line ranges in the order of 0.280 (°2θ) indicates the nano-scale dimension of the inorganic particles.

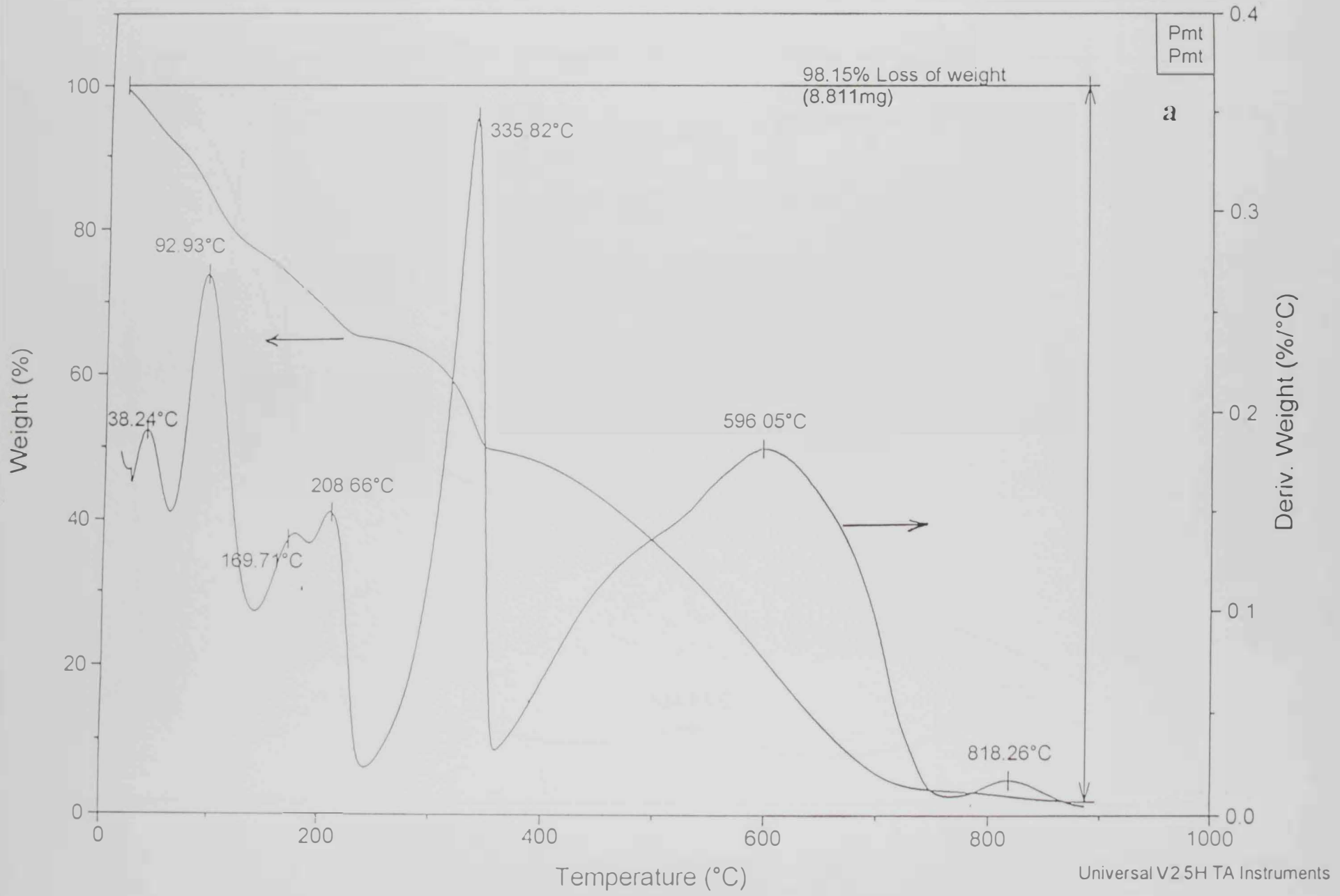
Pmt
Pmt
98.15% Loss of weight
(8.811mg)
a
335 82°C
92.93°C
38.24°C
208 66°C
169.71°C
596 05°C
818.26°C
Weight (%)
Deriv. Weight (%/°C)
Temperature (°C)
Universal V2 5H TA Instruments

Figure 45

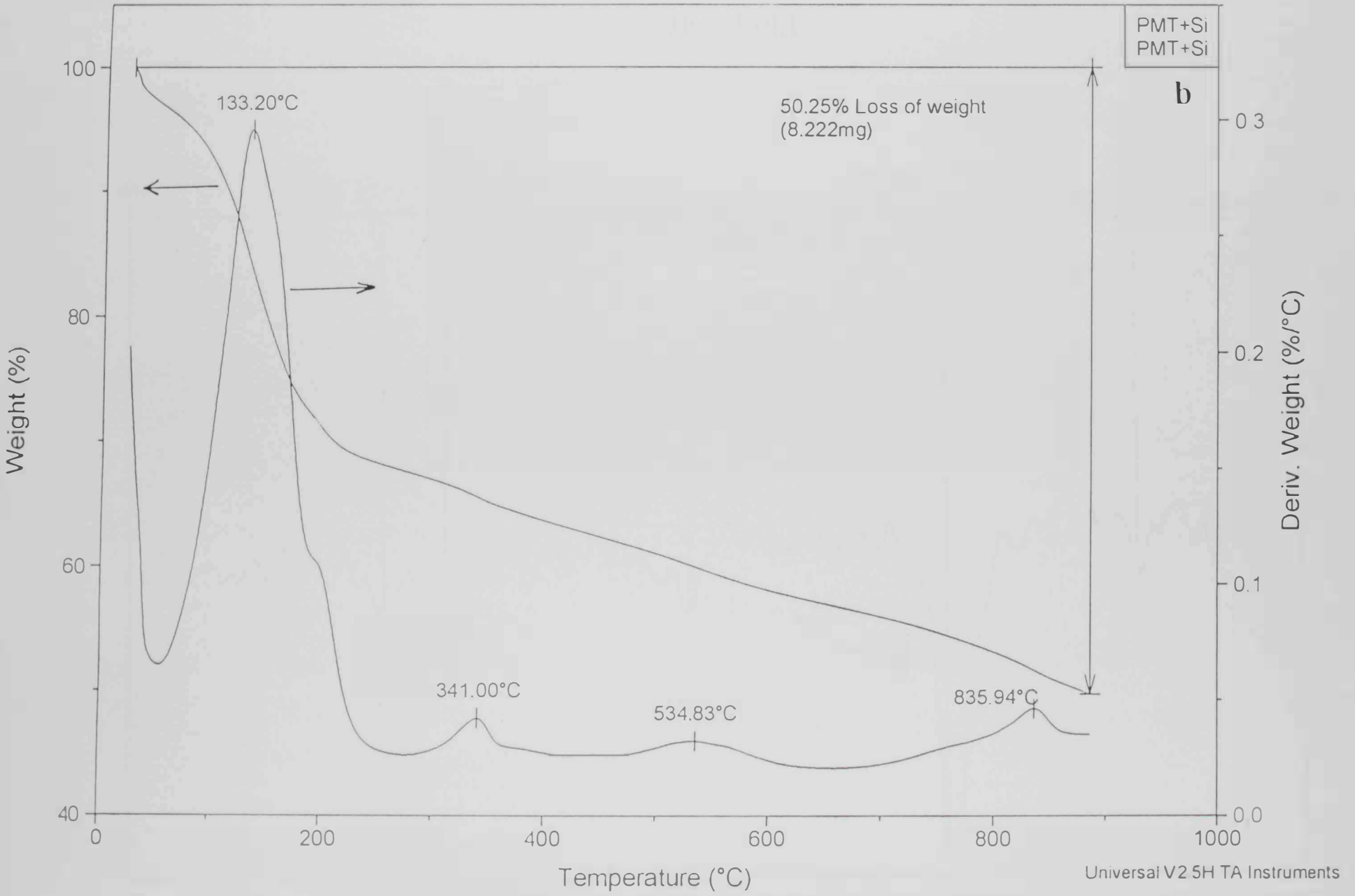
PMT+Si
PMT+Si
b
133.20°C
50.25% Loss of weight
(8.222mg)
341.00°C
534.83°C
835.94°C
Weight (%)
Deriv. Weight (%/°C)
Temperature (°C)
100
80
60
40
0
200
400
600
800
1000
0.3
0.2
0.1
0.0
Universal V2.5H TA Instruments

Figure 45

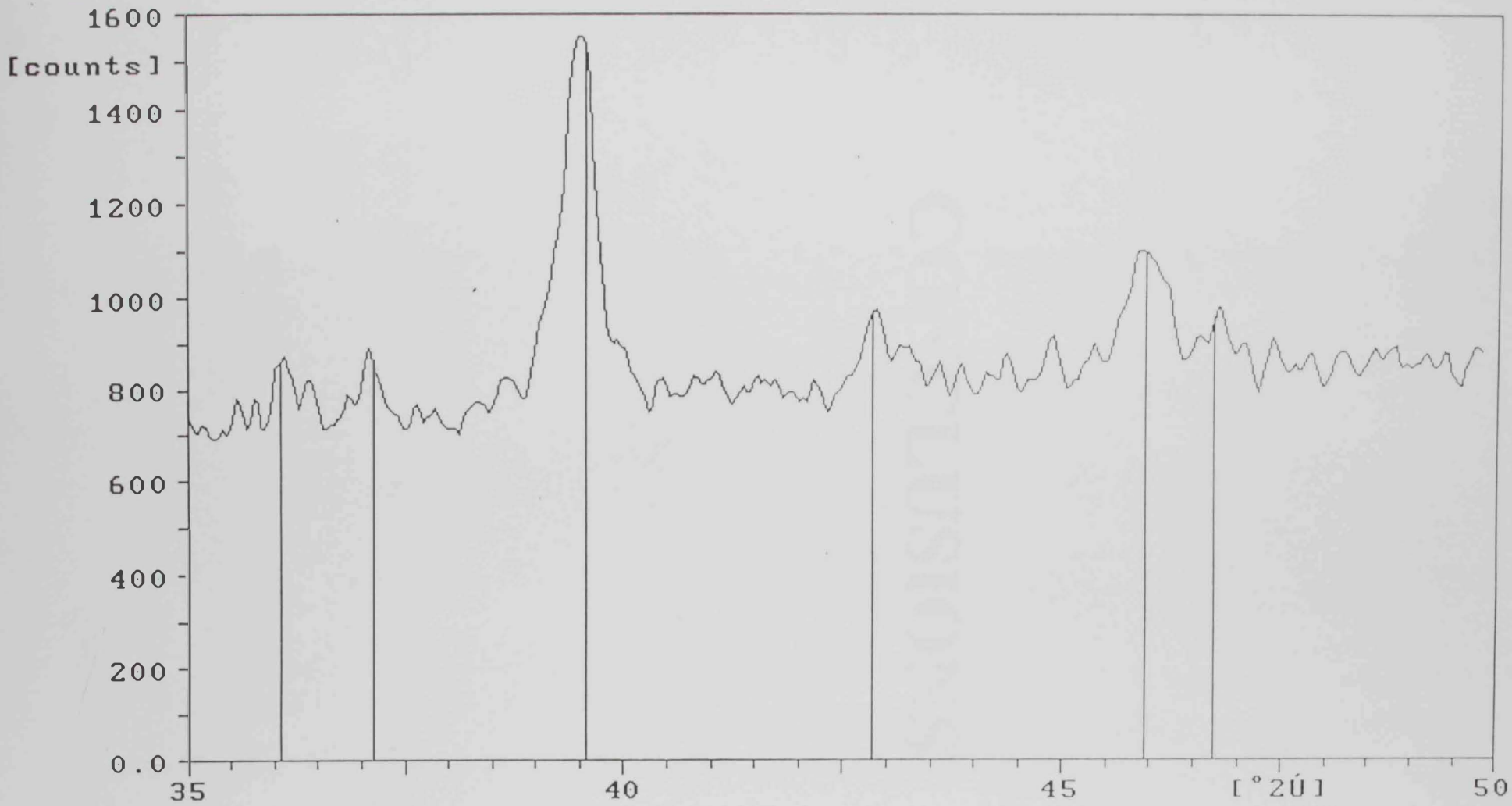

Figure 46

CONCLUSIONS

In this thesis, the candidate were able to electrochemically synthesize poly(3-methylthiophene). The electro-polymerization was possible in presence of TBAHFP/AcN. The thickness of the deposited polymer layer was controlled by the amount of charge passing through the electrolytic cell. EIS measurements proved that the electrical properties of the film depended on the applied "bias" potential. Thus, a mixed ionic/electronic conductance starts to predominate as the polymer film approaches its oxidation (doped) state. Moreover, the diffusion part that is usually represented by a 45° straight line in the Nyquist plots and is due to the charge transport is not identified when the film is oxidized. On the other hand, the influence of the film thickness on the impedance spectrum was pronounced. The changes found in the resistance and capacitance of the film was attributed to the changes in the morphological aspects of the film. Thus, the merging of the film towards pure capacitive behaviors took place at the transition frequency where the semicircular shape of the impedance curve changes to a linear part of 90° phase angle. It was found that as the film thickness increases, the transition frequency shifts towards lower values and the 45° line is enlarged. This behavior was explained in terms of the increase of the finite diffusion length and was assigned to the homogeneous model. Testing the film in different electrolytes showed dramatic differences. For instance, the hydrophobic nature of the polymer film did not favor ionic diffusion through the chains that increased the film resistance and lowered the intrinsic capacitance of the film. The experimental data were compared and modeled using "electrical equivalent circuits". The results

nicely fitted simulation with modified Randles circuits. A constant phase element or a Warburg element was used to simulate the diffusion component.

Upon modification of the organic polymer film with the inorganic layer, the intrinsic capacitance changed remarkably. A model was proposed to describe the charge accumulation at the polymer/inorganic layer interface. The concept was better visualized from the SEM pictures that revealed the inclusion of nano-particles into the polymer matrix. The formation of a hybrid organic/inorganic layer was therefore possible in this work frame. The type of bonding between the two phases cannot be concluded at this stage of the present work. However, FTIR measurements showed the presence of Si-O and Fe-O bonding along with the featured polymer film vibrations. Moreover, TGA proved that the inorganic layer (with metal doping) resulted in more stabilization in the film thermal properties.

REFERENCES

References

1. Arnold, Jr., F. E.; Arnold, F. E. *Adv. Poly. Sci. 117,* 257(**1994).**

2. Vogel, H.; Marvel, C. S. *J. Poly. Sci. L,* 511 **(1961).**

3. Techagumpuch, A.; Nalwa, H. S.; Miyata, S. Promising Applications of Conducting Polymers. In *Electroresponsive Molecular and Polymeric Systems,* Vol. 2; Marcel Dekker: New York, **(1988).**

4. Neuse, E. W. *Adv. Poly. Sci. 47,* 1 **(1982).**

5. Yu, L.; Chen, M.; Dalton, L. R. *Chem. Mater. 2,* 649 **(1990).**

6. Miller, J. S. *Adv. Mater. 5,* 671 **(1993).**

7. Skotheim, T., Ed.; *Handbook of Conducting Polymers;* volume 1, 2 Marcel Dekker: New York, **(1986).**

8. Osaheni, J. A.; Jenekhe, S. A. *Chem. Mater. 4,* 1282 **(1992).**

9. Roberts, M. F.; Jenekhe, S. A. *Chem. Mater. 6,* 135 **(1994).**

10. Dotrong, M.; Meheta, R.; Balchin, G. A.; Tomlinson, R. C.; Sinksky, M.; Lee, C. Y.-C.; Evers, R. C. *J. Poly. Sci. Part A, 31,* 723, **(1993).**

11. Osaheni, J. A.; Jenekhe, S. A. *Macromol. 28,* 1172 **(1995).**

12. Wolfe, J. F.; Sybert, P. D.; Sybert, J. R. U.S. Patents 4,533,692, 4,533,693, 4,533,724, **(1988).**

13. Wolfe, J. F. In *Encyclopedia of Polymer Science and Engineering,* Vol. 11; Wiley: New York, **(1986).**

14. Wolfe, J. F.; Arnold, F. E. *Macromol. 14,* 909 **(1981).**

15. Wolfe, J. F.; Loo, B. H.; Arnold, F. E. *Macromol. 14,* 915 **(1981).**

16. Frommer, J. E.; Chance, R. R. In *Encyclopedia of Polymer Science and Engineering*, Vol. 5; Wiley: New York, (**1986**).

17. Ito, T.; Shirakawa, H.; Ikeda, S. *J. Polym. Sci. Chem. Ed.*, *12*, 11 (**1974**)

18. Chiang, C. K.; Park, Y. W.; Heeger, A. J.; Shirakawa, H.; Louis, E. J.; MacDiarmid, A. G. *Phys. Rev. Lett. 39*, 1098 (**1977**).

19. Roncali, J. *Chem. Rev. 92*, 711 (**1992**).

20. Wilbourn, K.; Murray, R. W. *J. Phys. Chem. 92*, 3642 (**1988**).

21. Heinze, J. Electronically Conducting Polymers. In *Topics in Current Chemistry*, Vol. 152; Springer-Verlag: Berlin, (**1990**).

22. Chung, T. C.; Kaufman, J. H.; Heeger, A. J.; Wudl, F. *Phys. Rev. B*, *30*, 702 (**1984**).

23. Brédas, J.; Chance, R.; Silbey, R. *Phys. Rev. B*, *26*, 5843 (**1982**).

24. Murray, R. W. *Electroanal. Chem.*, *13*, 191 (**1984**).

25. Kaneko, M.; Wöhrle, D. *Adv. Polym. Sci.*, *84*, 141 (**1988**).

26. Abruña, H. D. *Coord. Chem. Rev.*, *86*, 135 (**1988**).

27. Arana, C.; Keshavarz, M.; Potts, K. T.; Abruña, H. D. *Inorg. Chim. Acta*, *225*, 285 (**1994**).

28. Guadalupe, A. R.; Usifer, D. A.; Potts, K. T.; Hurrell, H. C.; Mogstad, A.-F.; Abruña, H. D. *J. Am. Chem. Soc.*, *110*, 3462 (**1988**).

29. Hurrell, H. C.; Mogstad, A.-L.; Usifer, D. A.; Potts, K. T.; Abruña, H. D. *Inorg. Chem.*, *28*, 1080 (**1989**).

30. Youssoufi, H. K.; Hmyene, M.; Yassar, A.; Garnier, F. *J. Electroanal. Chem.*, *406*, 187 (**1996**).

31. Ren, X.; Pickup, P. G. *J. Electroanal. Chem.*, *365*, 289 (**1994**).

32. Kaufman, F. B.; Engler, M. B. *J. Am. Chem. Soc.*, *101*, 547 (**1979**).

33. Deronzier, A.; Moutet, J.-C. *Coord. Chem. Rev.*, *147*, 339 (**1996**).

34. Ochmanska, J.; Pickup, P. G. *J. Electroanal. Chem.*, *271*, 83 (**1989**).

35. Cameron, C. G.; Pickup, P. G. *J. Chem. Soc. Chem. Commun.*, 303 (**1997**).

36. Cameron, C. G.; Pickup, P. G. *J. Am. Chem. Soc.*, *121*, 7710 (**1999**).

37. Cameron, C. G.; Pickup, P. G. *J. Am. Chem. Soc.*, *121*, 11773 (**1999**).

38. Maclean, B. J.; Pickup, P. G. *J. Chem. Soc. Chem. Commun.* (**1999**), 2471.

39. Gangopadhyay, R.; and De, A., *Chem. Mater.*, *12(3)*, 608-622, (**2000**).

40. P. Fiordiporti and G. Pistoia, Electrochemi. Acta, 34, 215(**1989**).

41. C. Gabrielli and M. Keddam, Electrochemi. Acta, 41, 957(**1996**).

42. E. Brillas, G. Anton, T. Otero and J. Carrasco, J. Electroanal. Chem., 445, 125(**1998**).

43. B. Feldman, P. Burgmayer and R. Murray, J. Am. Chem. Soc., 107, 872(**1985**).

44. M. Sluijs, A. Underhill and B. Zaba, J.Phys.D: Appl. Phys., 20, 1411(**1987**).

45. A. Nekrasov, V. Ivanov and A. Vannikov, J. electroanal. Chem., 482,11(**2000**).

46. E. Cordruwisch, G. Popkirov, E. Turk, J. Theiner and G. Nauer, Electrochimi. Acta, 41, 1369(**1996**).

47. M. Pinto, H. Mishima and B. Mishima, j. Appl. Electrochemistry, 27, 831(**1997**).

48. A. Sargent and O. Sadik, Electrochimi. Acta, 44, 4667**(1999)**.

49. D. Bloor, Electrical Conductivity, London, UK, pp.698-699 **(1986)**.

50. G. Tourillon and F. Garnier, J. Electroanal. Chem., 135, 173 **(1982)**.

51. Y. Teragishi and K. Aoki, J. Electroanal. Chem., 473, 132 **(1999)**.

52. C. Arbizzani, M. Gastragostino, L. Meneghello, M. Morselli and A. Zanelli, J. Appl. Electrochemistry, 26, 121**(1996)**.

53. S. Panero, P. Prosperi, S. Passerini, and B. scrosati, J. Electrochem. Soc., 12, 136, 3729 **(1989)**.

54. K. Gurunathan, A. Murugan, R. Marimuthu, U. mulik, and D. Amalnerkar, Materials Chem.Phys., 61, 173 **(1999)**.

55. R. Bull, F. Fan and A. Bard, J. electrochem. Soc., 129,5, 1009 **(1982)**.

56. (a) A. Athawale, B. Deore, and V. Chabukswar, Materials chem. Phys., 58, 94**(1999)**, (b) B. A. Athawale, B. Deore and M. Kulkarni, Materials chem. Phys, 60, 262 **(1999)**.

57. C. Chidsey and R. Murray, J. Phys. Chem., 90, 1479 **(1986)**.

58. A. Kelaidopoulou, E. Abelidou and G. Kokkinidis, J. Appl. Electrochemistry, 29, 1255 **(1999)**.

59. S. Vico, V. Carlier and C. Herman, J. Electroanal. Chem., 475,1**(1999)**.

60. H. Lee, S. Cui and S. Park, J. Electrochem. Soc., 148, D139 **(2001)**.

61. S. Feldberg, J. Am. Chem. Soc., 106,4671 **(1984)**.

62. D. Crow, Principles and Applications of Electrochemistry, New York, ed4, pp.225-226 **(1994)**.

63. W. Su and J. Iroh, Electrochimi. Acta, 44, 4655 **(1999)**.

64. G. Inzett, Electrochimi. Acta, 34, 2, 83 **(1989)**.

65. C. Andieux, J. Bouchiat and J. Saveart, J. Electroanal. Chem., 131, 1 **(1982)**.

66. J. Sibilia, A Guid to Materials Charecterization and Chemical Analysis, New York, pp. 5-6 **(1996)**.

67. J. Tanguy, J. Baudoin, F. Chao and M. Costa, Electrochimi. Acta, 8, 37, 14179 **(1992)**.

68. P. Nunziante and G. Pistoia, Electrochimi. Acta, 34, 2, 223 **(1989)**.

69. O. Clot, M. Wolf, and B. Patrick, J. Am. Chem. Soc., 123,9963 **(2001)**.

70. A. laforgue, P. Simon, J. Fauvarque, J. Sarrau and P. Lailler, J. Electrochem. Soc., 148(10) A1139 **(2001)**.

71. A. Walcarius, *Chem. Mater.*, 3351-3372, *13(10)*,(**2001**).

72. (a) Wilkes, G. L.; Orler, B.; and Huang, H., *Polym. Prepr.*, *26*, 300, **1985**, (b) Wen, J.; and Wilkes, G. L., *Chem. Mater.*, *8*, 1667, **(1996)**.

73. (a) Wei, Y.; Yeh, J.-M.; Wang, W.; and Jang, G. –W., US Pate. 5,868,966, **(1996)**, (b) Wei, Y., *Encyclopedia of Materials: Science and Technology*, Elsevier Science Ltd., **(2001)**.

74. Neves, S.; Fonseca, C.P.; Zoppi, R.A.; and de Torresi, S.I.C., *J. Solid State Electrochem.*, 412-418, *5(6)*, **(2001)**.

75. Verghese, M.M.; Ramanathan, K.; Ashraf, S.M.; Kamalasanan, M.N.; and Malhotra, B.D., *Chem. Mat.*, 822-824, *8(4)*, **(1996)**.

76. Onoda, M.; Matsuda, T.; and Nakayama, H., *Jpn. J. Appl. Phys. Part 1 - Regul. Pap. Short Notes Rev. Pap.*, 294-298, *35(1A)*, **(1996)**.

77. Lee, Y.; Kim, J.; and Son, Y., *Polym. –Korea,* 443-449, *23(3), (***1999**).

78. Lee, Y.; and Kim, J., *Mol. Cryst. Liquid Cryst. Sect. A Mol. Cryst. Liq.*, 213-216, *337*, **(1999)**.

79. Tess, M.E.; and Cox, J.A., *J. Pharm. Biomed. Anal.*, 55-68, *19(12)*,**(1999)**.

80. Walcarius, A., *Electroanalysis*, 701-718, *13(8-9)*, **(2001)**.

81. Riddick, J.A.; Bunger, W.B.; and Sakano, T.D., "*Organic solvents: physical properties and methods of purification*," 4th edition, Wiley, New York, **(1986)**.

82. Mehrotra, R.C.; and Singh, A., *Progr. Inorg. Chem.*, *46*, 239, **(1997)**.

83. J.R. Macdonald, in "Impedance Spectroscopy; Emphasizing Solid Materials and Systems," Wiley Interscience, NY., **(1987)**.

84. Roncali, J., *Chem. Rev.*, *97*, 173-205, **(1997)**.

85. Abdo, A., "Preparation, characterization and applications of some poly(heteroarylenes)," Ph.D. Thesis, Cincinnati, Oh., USA, **(1991)**.

86. Brédas, J.L.; and Street, G.B., *Acc. Chem. Res.*, *18*, 309, **(1985)**.

87. Chung, T.C.; Kaufman, J.H.; Heeger, A.J.; and Wudl, F., *Phys. Rev. B: Condens. Matt.*, *30*, 702, **(1984)**.

88. Zotti, G; and Schiavon, G, *Synth. Met.*, *31*, 347, **(1989)**.

89. Kaneto, K.; Hayashi, S.; Ura, S.; and Yoshino, K., *J. Phys. Soc. Jpn.*, *54*, 1146, **(1985)**.

90. Fosset, B.; Amatore, C.A.; Bartelt, J.E.; Michael, A.C.; and Wightman, R.M., *Anal. Chem.*, *63*, 306, **(1991)**.

91. Ren, X; and Pickup, P.G., *J. Phys. Chem.*, *97*, 5336, **(1993)**.

92. Pickup, P.G., *J. Chem. Soc. Faraday Trans.*, *86*, 3631, **(1990)**.

93. Kankare, J.; and Kupila, E.-L., *J. Electroanal. Chem.*, *322*, 167, **(1992)**.

94. Buttry, D.A.; and Ward, M.D., *Chem. Rev.*, *92*, 1355, **(1992)**.

95. Mulder, W.H.; and Sluyters, J.H., *Electrochim. Acta*, *33*, 303, **(1988)**.

96. Mermilliod, N.; Tanguy, J.; and Petiot, F., *J. Electrochem. Soc.*, *133*, 1073, **(1986)**.

97. Jüttner, K.; Schmitz, R.H.J.; and Hudson, A., *Electrochim. Acta*, *44*, 4177-4187, **(1999)**.

98. Tanguy, J.; Baudoin, J. L.; Chao, F.; and Costa, M., *Electrochim. Acta*, *37(8)*, 1417-1428, **(1992)**.

99. Jow, T.R.; and Shacklette L.W, *J. Electrochem. Soc.*, *135*, 541, **(1988)**.

100. Otero, T.F.; and Angulo, E., *Synth. Met.*, *51*, 87, **(1992)**.

101. Fletscher, S., *J. Chem. Soc. Faraday Trans.*, *89*, 311, **(1998)**.

102. Tanguy, J.; Slama, M.; Hoclet, M.; and Baudouin, J.L., *Synth. Met.*, 28, 145, **(1989)**.

103. Genz, O.; Lohrengel, M.M.; and Schultze, J.W., *Electrochim. Acta*, *39*, 179, **(1994)**.

104. Sathiyanarayanan, S.; and Balakrishnan, K., *Electrochim. Acta*, *39*, 831, **(1994)**.

105. Sato, M.; Tanaka, S.; and Kaeriyama, K., *Synth. Met.*, *14*, 279, **(1986)**.

106. Marque, P.; Roncalli, J.; and Garnier, F., *J. Electroanal. Chem.*, *218*, 107, **(1987)**.

107. Cunningham, D.D.; Galal, A.; Pham, C.V.; Lewis, E.T.; Burkhardt, A.; Davidson-Laguren, L.; Nkansah, A.; Ataman, O.Y.; Zimmer, H.; and Mark,Jr., H.B., *J. Electrochem. Soc.*, *135* (11), 2750-2754, **(1988)**.

108. Helfferich, F., "*Ion-exchange*," *Vol. 1*, Grundlagen, Chemie, Weinheim, pp. 77, McGraw-Hill, New York, **(1962)**.

109. Andrieux, C.P.; Haas, O.; and Savéant, J.M., *J. Am. Chem. Soc.*, *108*, 8175, **(1986)**.

110. Andrieux, C.P.; and Savéant, J.M., *J. Phys. Chem.*, *92*, 6761, **(1988)**.

111. Huang, W.-S.; Humphrey, B.D.; and MacDiarmid, A.G., *J. Chem. Soc. Faraday Trans. 1, 82*, 2385, **(1986)**.

112. Wegner, G.; and Rühe, J., *Faraday Discuss. Chem. Soc., 88*, 333, **(1989)**.

113. Peover, M.E. in Bard, A.J. (ed.), *Electroanalytical Chemistry, Vol. 2*, Marcel Dekker, New York, p. 1., **(1967)**.

114. Penner, R.M.; and Martin, C.R., *J. Phys. Chem., 93*, 984, **(1989)**.

115. Albery, W.J.; Chen, Z.; Horrocks, B.R.; Mount, A.R.; Wilson, P.J.; Bloor, D.; Monkman, A.T.; and Elliott, C.M., *Faraday Discuss. Chem. Soc., 88*, 247, **(1989)**.

116. Fiordiponti, P.; and Pistoia, G., *Electrochim. Act., 34(2)*, 215-221, **(1989)**.

117. From the "Gamry Instruments, Inc., CMS 300, Framework Software, Operator's Manual, Revision 2.1," pp. (1-1)-(2-31), **(1994)**.

118. Mulder, W., *J. Electroanal. Chem., 326*, 231, **(1992)**.

119. Skinner, N.G.; and Hall, E.A.H., *Synth. Met., 63*, 133, **(1994)**.

120. Sandi, G.; and Vanysek, P., *Synth. Met., 64*, 1, **(1994)**.

121. CMS300 Software, version 2.4a, Gamry Instruments, Inc., USA, **(1996)**.

122. Johnson, B.W.; Read, D.C.; Christensen, P.; Hammett, A.; and R. D. Armstrong, *J. Electroanal. Chem., 364*, 103, **(1994)**.

123. Tanguy, N.; Mermilliod, N.; and Hoclet, M.; *J. Electrochem. Soc., 134*, 795, **(1987)**.

124. Scheider, W., *J. Phys. Chem., 79*, 127, **(1975)**.

125. Armstrong, R. D.; and Burnhem, R. A., *J. Electroanal. Chem.*, *72*, 257, **(1976)**.

126. Stoynov, Z., *Electrochim. Acta*, *35*, 1493, **(1990)**.

127. Tanguy, J.; Baudoin, J. L.; Chao, F.; and Costa, M., *Electrochim. Acta*, *37*, 1417, **(1992)**.

128. Bard, A. J.; and Faulkner, L. R., "*Electrochemical methods: Fundamentals and applications*," 2nd ed., pp. 115-132, John Wiley & Sons, New York, **(2001)**.

129. André, M; Brédas, J. L.; Delhalk, J.; Ladik, J.; Leroy, G.; and Moser, C., "*Recent advances in the quantum theory of polymer*," Vol. 113 of lectures notes in physics, Springer, Berlin, (1980).

130. Albery, W. J.; and Mount, A. R., *J. Electroanal. Chem.*, *305*, 3, **(1991)**.

131. Boukamp, B. A., *Solid State Ionics*, *20*, 31, **(1986)**.

132. Vorotynsev, M. A.; Daikhin, L. I.; and Levi, M. D., *J. Electroanal. Chem.*, *364*, 37, **(1994)**.

133. Bruce, P. G.; and West, A. R., *J. Electrochem. Soc.*, *130*, 662, **(1983)**.

134. Brug, G. J.; Van Den Eeden; A. L. G.; Sluyters-Rehbach, M.; and Sluyters, J. H., *J. Electroanal. Chem.*, *176*, 275, **(1984)**.

135. Brinker, C. J.; and Scherer, G. W., "*Sol-Gel Science, The Physics and Chemistry of Sol-Gel Processing*", Academic Press, New York, pp. 581-582, **(1989)**.

136. Khalil, K. M. S., Elsamahy, A.; and Elanany, *J. Colloidal & Interfacial Sci.*, *249*, 359, **(2002)**.

137. Tourillon, G.; and Garnier, F., *J. Electroanal. Chem.*, *135*, 173, **(1982)**.

138. van de Leur, R. H. M., *Synth. Met.*, *51*, 69, **(1992)**.

139. Bertoluzza, A; Fagnano, C.; Morelli, M. A.; Gottardi, V.; and Guglielmi, M., *J. Non-Cryst. Solids*, *48*, 117, **(1982)**.

140. Sen, P. N.; and Thorpe, M. F., *Phys. Rev.*, *B15*, 4030, **(1977)**.

141. Galeener, F. L., *Phys. Rev.*, *B19*, 4292, **(1979)**.

142. Galal, A., J. Solid State Electrochem., 2, 7, **(1998)**.

143. Suzuki, N.; Kimura, S.; Nakada, T.; Kaito, C.; Saito, Y.; and Koike, C., *Meteor. & Plan. Sc.*, *35*, 1269, **(2000)**.

144. Schroder, E.; Muller, G.; and Arndt, K. F., "Polymer Characterization," Hanser, Munich, **(1989)**.

ملخص الأطروحة:

تحظى البوليمرات الموصلة باهتمام علمي بالغ، وذلك لما لهذه المواد من تطبيقات تكنولوجية عديدة مثل استخدامها في البطاريات الكهربية، والأجهزة الإلكترونية، والمكثفات الكهربائية، والمجسات الكهروكيميائية، وكمصادر كهربائية وميضية، وفي التخلص من النفايات، وتثبيط التآكل، وما شابه ذلك من التطبيقات.

ونظرا لأن المواد الكيميائية المستخدمة فى تحضير هذه البوليمرات مثل مادة الثيوفين والبيرول والأنيلين ومشتقاتها لها جهود أكسدة تكوين منخفضه نسبيا. فان طريقة تحضير هذه البوليمرات تعتمد على عملية الأكسدة وذلك إما بطريقة كيميائية أو كهروكيميائية. وتعتبر الطرق الكهروكيميائية هي الأكثر إستخداما فى مجال تحضير هذه المواد. وذلك لما لها من ميزات عديدة أهمها :

- البساطة، حيث تتم عملية التحضير من خلال خطوة واحدة.
- البوليمرات الناتجة ذاتية التوصيل ولا تحتاج الى عملية تنقية.
- غير مكلفة إذا تم مقارنتها بالطرق الكيميائية الأخرى.

وغالبا ما يتم تحضير هذه البوليمرات فى خلايا كهروكيميائية وترسيب طبقات منها على أسطح صلبة مثل الجرافيت والذهب والبلاتين.

ولقد قامت الطالبة، في هذة الرسالة، بتحضير أحد فصائل هذه المواد المتقدمة ودراسة العوامل التى تؤثر على خواص البوليمرات الناتجة مثل طبيعة الوسط المستخدم أثناء عملية التحضير، طبيعة الإضافات المستخدمة، الخ...، هذا وقد قامت الطالبة أيضا بتعديل الخواص السطحية لهذه البوليمرات عن طريق ترسيب طبقة غير عضوية على طبقة البوليمر فنتج عن ذلك طبقة "مهجنة" (عضوية وغير عضوية). وكذلك درست الطالبة تأثير ذلك التعديل على خواص المادة المهجنة الناتجة. وقد استخدمت الطالبة العديد من الطرق والتقنيات المعملية القياسية فى دراسة هذه الخواص منها الطرق الكهروكيميائية، والطيفية، والميكروسكوبية، وطرق التحليل الوزني الحراري. وقد أثبتت نتائج القياسات وتحليلها أن المواد الجديدة التى تم تحضيرها تمتاز بخواص كهربائية فريدة مما يقترح استخدامها في مجالات البطاريات التي يمكن إعادة شحنها والأجهزة الضوئية والإلكترونية.

تحضير وتوصيف وتطبيقات بعض البلمرات الموصلة

أطروحة مقدمة إلى
عمادة الدراسات العليا
جامعة الإمارات العربية المتحدة

فاطمـــة يوســف محمـــد بالحاي

لمتطلبات الحصول على درجة الماجستير

في

علوم وهندسة المواد

٢٠٠٢